CIS-SPECIFIC BINDING PARTNERS ARE ESSENTIAL FOR IDENTIFYING CRITICAL MOLECULAR MECHANISMS THAT ARE PROMINENT IN BIOLOGICAL DEVELOPMENT AND DISEASE

A Dissertation

Presented to the Faculty of the Graduate School

of Cornell University

In Partial Fulfillment of the Requirements for the Degree of

Doctor of Philosophy

by

Josephine Maria Gonzales

December 2020

CIS-SPECIFIC BINDING PARTNERS ARE ESSENTIAL FOR IDENTIFYING CRITICAL MOLECULAR MECHANISMS THAT ARE PROMINENT IN BIOLOGICAL DEVELOPMENT AND DISEASE

Josephine Maria Gonzales, Ph. D.

Cornell University 2020

A growing body of literature recognizes the *cis/trans* isomerization of the peptidyl-prolyl bond as playing key roles in processes that are important for development and disease in humans and plants. The atomically identical cis and trans isomers are structurally distinct and may have different binding partners, thereby cis/trans isomerization can serve as a molecular switch. In this work, the impact of *cis* isomers in two different biological systems is investigated.

In the first system, *Oryza sativa* (Asian rice) utilizes the phytohormone auxin to regulate the proteasomal degradation of a family of transcription repressors, the auxin/indoleacetic acid (Aux/IAA) proteins. The *cis* isomer of a well-conserved Trp-Pro peptide bond in Aux/IAA proteins is selectively recognized by the corresponding E3 ligase only in the presence of auxin. This leads to an auxin-dependent, *cis*-specific degradation of the transcription repressor and activation of its regulated genes including its own. One family member, OsIAA11, interacts with the peptidyl prolyl isomerase (PPIase) LRT2, an enzyme shown to be essential for lateral root initiation. Quantitative studies *in vivo* of the rate of auxin-induced degradation of OsIAA11 and the dependence of this rate on LRT2 are necessary to mathematically model the auxin circuit. Levels of OsIAA11 and LRT2 were quantified using fluorescent protein tags and confocal microscopy. We found that detection of the degradation rate of OsIAA11 *in vivo* is

dependent on both temperature and the elapsed time post-transfection. These studies confirm that the degradation rate of OsIAA11 is already optimally tuned by endogenous LRT2, and the results are consistent with a potential role of Hsp90 in the rice auxin circuit. Overall, these findings suggest a mechanism by which additional factors such as Hsp90 and co-chaperone SGT1 might be involved in LRT2-dependent proteasomal degradation of OsIAA11.

In Alzheimer's disease (AD), the amyloid precursor protein (APP) is cleaved at the β-site by APP Cleaving Enzyme-1 (BACE1). Cleavage is necessary for the amyloidogenic pathway to produce amyloid-beta (Aβ) peptides found in senile plaques. The cytoplasmic tail of APP contains a *cis* isomer of the phospho-Thr668-Pro669 motif correlated with an increase in amyloidogenic processing of AβPP and the production of Aβ. A novel *cis*-locked cyclic dipeptide pCDP-DB mimics the cis isomer of the prolyl peptide bond and is known to inhibit the generation of Aβ and secretion of the large BACE1-generated APP fragment sAPPβ. Here we have utilized H4 neuroglioma cell lines overexpressing APP695 (WT7) or BACE1 (B18) and confocal microscopy. We found that the treatment with pCDP-DB treatment does not alter colocalization of APP and BACE1. Importantly, treatment does not block the endocytosis of APP. Additionally, treatment reduces the colocalization of APP and BACE1 to early endosomes. Although point mutations made within the APP cytoplasmic tail significantly impacted the proteolytic processing, these mutations did not inhibit endocytosis. We performed proteomics to identify potential pCDP-DB interacting proteins and gain insight on the mechanism of pCDP-DB bioactivity. These findings point to a hypothesized mechanism by which pCDP-DB enhances the lysosomal

targeting of endosomes containing APP and BACE1, resulting in the lysosomal degradation of sAPPβ and Aβ.

BIOGRAPHICAL SKETCH

Josephine Maria Gonzales was born in Oklahoma City, Oklahoma, raised in San Diego, California with her parents, Louie and Bicky Gonzales, and her younger sister, Selina Gonzales. Josephine grew up running cross country, and playing soccer and the clarinet, while helping others through her ten years as a Girl Scout. At a young age Josephine was diagnosed with Grave's disease, an autoimmune disorder that negatively affects thyroid function. After leaving the doctor's office, Josephine had many questions about the thyroid hormone. Josephine's questions were fueled by her curiosity, which in turn were only answered by science.

In 2009, Josephine attended California State University of San Marcos (CSUSM) and found her passion for math in science while attending an Immunology seminar at CSUSM. In Josephine's junior year at CSUSM she was accepted to the Minorities Advancing Research and Conductivity (MARC) program, where she became involved with the Office of Training Research and Education through the Science (OTRES) program. Through OTRES she was mentored in scientific research by Dr. Keith Trujillo, Dr. Victor Rocha, Dr. Angelica Rocha, Dr. Susan Hizer, Dr. Garcia, Dr. Stephen Tsui, Debbie DeRoma, and Perla Rivera. During Josephine's undergraduate career, Dr. Julie Jameson saw great potential in Josephine as both a scientist and role model and encouraged her to apply to graduate school. In May 2015, Josephine graduated cum laude from California State University of San Marcos, where she received her B.S. in Biology with a concentration in Molecular and Cellular Biology and minored in Chemistry and Visual Arts.

Josephine joined the Biochemistry, Molecular, and Cellular Biology program

in the department of Molecular Biology & Genetics at Cornell University in 2015. She was awarded an Alfred P. Sloan Graduate Research Fellowship in 2016 to fund her research at Cornell. In 2016, Josephine re-established and was the President for the Society for Advancement of Chicanos and Native Americans in the Sciences (SACNAS) chapter at Cornell University. Her goal for this chapter was to bridge the knowledge gap of what it is like to be a graduate student by connecting with undergraduate students of color. As a Mexican American graduate student, Josephine finds motivation from her mentee's and peer's by remembering her family's history of working in the fields. Her life's passion is to further promote diversity in her quest to become a lifelong learner of the world.

This dissertation is dedicated to my family, Louie, Bicky, Selina and Sasank for all of their love, encouragement, and support throughout this journey.

ACKNOWLEDGMENTS

During my first semester at Cornell, I met Dr. Linda Nicholson as my instructor for the course on Protein Structure and Function. Linda was the first faculty member in my department whom I felt showed empathy for the graduate students as people rather than just worker bees. Linda has a good heart, and it shows every day with the many things she does to mentor and help the students at Cornell. She is the strongest proponent for diversity in the department, and I am grateful to have worked in her lab. I would like to thank my committee members Dr. Chris Fromme and Dr. Dave Holowka for their support, input, and attention. For all of my committee members, I have the deepest respect for them as people and scientists.

I would like to thank the Nicholson Lab: Dr. Ross Resnick, Nathan Korson, Kenenni Wiegand, who made the lab an enjoyable work environment. And thank you to the past Nicholson lab members especially Andrea Acevedo, who had major contributions to starting these projects. Thank you to Dr. Ross Resnick who was my partner and mentor on each of these projects. Thank you for blasting “oldies” music in the lab on the weekends, making it easier to come into work. This work would not have been possible without your dedication to science, thank you.

During my PhD program, I became a part of many communities at Cornell that would then support me throughout my graduate school years. I would like to give a special thank you to the Cornell Graduate School, specifically Dean Jan Allen, Dean Sara Xayarath Hernandez, and Anitra Douglas-McCarthy for all the work they do to help graduate students succeed at Cornell, and for always making the time to meet with me. I would like to thank the Diversity Programs in Engineering (DPE) and

Alfred P. Sloan programs, specifically Jami Joyner, Mark Lewis, and Cindy Mosqueda, without the supportive environment and community that they give to graduate students this journey would have seemed more overwhelming. I would like to thank all my Sloan friends, especially Johana Uribe, Jessica Elmore, and Monet Roberts, for being my supportive friends and writing buddies, especially when we were all in quarantine. Thank you to all the graduate student programs and the friends that I have made in these programs: Society for Advancement for Chicanos and Native American in the Science (SACNAS), Latin Graduate Student Coalition (LGSC), and the Graduate Student Ambassadors programs, for helping me fulfill my passion of helping first generation students incoming or present throughout the Cornell community. Thank you to the community that I built at Cornell (alphabetical order): Aaron Joiner, Andrea Acevedo, Gwen Beacham, Azul Barros, DPE community, Irma Fernandez, Jessica Elmore, Johana Uribe, Mariela Santos, Marysol Luna, OISE community. Oriana Pumar, Sasank Vemulapati, Steve Halaby, Tanner Pearson.

I would like to give my sincere thanks to my dissertation writing coaches Dr. Wendy Carter-Veale and Dr. Katy Peplin to whom without the constant advice, nagging, encouragement, and support this PhD journey. This journey would not have had such a strong finish without your guidance. Also, I would like to thank Ms. Cathy Kinder and Dr. Nadia Abdo for their thoughtfulness and personal conversations, which helped me grow as a person and continue to pursue this journey. To these women, I am sincerely grateful for their advice, and to whom I would not have learned the tools that I needed to succeed in life.

Thank you to my family, Louie, Bicky, and Selina Gonzales. Thank you to my father for his strong work ethic. Thank you to my mother for teaching me how to persevere. Thank you to my sister for her encouragement. The last few years at Cornell were dedicated to the love of my life Sasank Vemulapati. I am grateful to have met and fell in love with you at Cornell. Thank you for being my best friend; for challenging me, supporting me, and giving my daily life a "much-needed work-life balance". Thank you to my whole family, because without your love and support, I would not have been able to get through the challenging and difficult times of being a woman in science.

Lastly, thank you to my late grandmother Josephine Cruz, who exemplifies a strong independent woman. Because of the sacrifices she made and the challenges that her generation of Mexican Americans faced; she was instrumental in promoting education into our family values. Her perspective changed the future generation of our family. Therefore, I had the courage to continue this mindset and break down barriers in order to obtain a PhD.

TABLE OF CONTENTS

CIS-SPECIFIC BINDING PARTNERS ARE ESSENTIAL FOR IDENTIFYING CRITICAL MOLECULAR MECHANISMS THAT ARE PROMINENT IN BIOLOGICAL DEVELOPMENT AND DISEASE

CHAPTER 1

INTRODUCTION

The X-pro peptide bond plays a pivotal role in cis/trans isomerization (1). A proline (Pro) directed phosphorylation is a central cellular signaling mechanism often used to recognize a proline switch (molecular switch) (2). However, the cell contains different regulatory mechanisms of phosphorylation of cis-specific proteins. There is a growing body of literature that recognizes the cis/trans isomerization of the peptidyl-prolyl bonds involved in processes that are important for development and disease. In this dissertation, we investigate the impact of *cis* specific proteins involved in two different regulatory systems.

The first system involves a peptidyl-prolyl isomerase (PPIase), Lateral Rootless 2 (cyp2/LRT2), known to be essential for lateral root development in rice(3-5). The purpose of this quantitative in vivo protoplast study is to examine the role of LRT2 catalysis of the Trp-Pro motif in Oryza Sativa (rice) Indole-3-Acetic-Acid protein (OsIAA), a specific prolyl cis-trans isomerization switch in the auxin-responsive negative feedback circuit that controls the initiation of lateral root development in rice (6).

In the second system (further discussed in Chapter 4), I have investigated the impact of a novel small molecule phosphor-Thr-Pro Cyclic dipeptide-dibenzyl, referred

to as pCDP-DB, on endocytosis of the Amyloid Precursor Protein (APP) and on the intracellular localization of APP, BACE1 and other proteins of interest. The pCDP-DB, a small molecule, was designed as a 100% "*cis*-locked" molecular mimic of a phosphor-Serine/Threonine-Proline motif (S/TP) (7). In the literature, the phosphor-T668-P669 has been shown to be increased in Alzheimer's disease (AD) (8). The aim of this investigation is to understand how the *cis*-locked small molecule pCDP-DB affects APP trafficking in H4 Neuroglioma cells.

Proline

Fundamental life on earth is dependent on amino acids, which are the essential building blocks of proteins. A distinctive amino acid, proline has a unique dipeptide backbone containing an amino and carboxylic acid group and a pyrrolidine slide chain (9). Proline is a notable amino acid because of its unique structure, containing a ring that cyclizes back on to the amide backbone, which causes restriction, bulkiness, and the inability to act as a hydrogen bond donor (1). The unique structure of proline is key to understanding its potential contributions in biological pathways and disease. The conformation of this backbone causes restriction as it is only able to form a small angle which is approximately -65 degrees. Proline's backbone contains an N-CH2 group, which causes bulkiness and restriction on the conformation, thus disfavoring the alpha-helix conformation. Lastly, Proline is unable to act as a hydrogen bond donor because the CH2 group replaces the amide proton (1). Many peptides and proteins contain proline's distinctive amide bond as part of their backbone (10). These key structural features are what makes proline unique compared to other essential amino acids (11).

Many protein–protein interactions involve amino acid sequences that contain proline-rich motifs and even poly-proline stretches (12). Several proteins contain proline-rich regions (PRRs), understanding these regions that contain repetitive proline sequences or multiple tandem repeats between repeated sequences, play an important role in understanding their binding interactions as well as an (XP) bond, where X is any amino acid (1,13-17). The fact that proline-rich polypeptides have a lack of mobility and therefore relatively low entropy gives the protein strength of the binding derives from the PRRs even before binding to another protein (1).

In 1948 Linus Pauling, was the first scientist to discuss the amide bond resonance (cis and trans isomers). The cis isoform is indicated when two substituents X and Y are on the same side of the molecule. The trans isoform is indicated when the X and Y substituents are on opposite sides of the configuration (18,19). The cis/trans isomer of proline rotates about the C–N bond and is closely related to amide bond resonance (20). The energy needed to overcome the imide bond interconversion barrier between cis and trans is 14-24 kcal/mol (2). Proline isomerization is different from covalent modification or global unfolding, because there is an intrinsic conformational exchange process that is able to control protein activity within the native state of the protein (2).

Scientists found that proline is the only naturally occurring amino acid thermodynamically achievable in both cis and trans peptide bond conformations (21). The energy barrier between the cis and trans states is largely uncatalyzed by the exchange between these isomerization state, which occurs on a time scale of tens of minutes (2). The X-Pro peptide bonds are able to bring the cis and trans isomers of the

peptide bond much closer in free energy. Because the cis and trans states are structurally distinct, meaning they can have different functions and binding partners(1,19). Therefore, a prolyl isomerase (proline isomerization) may be crucial for appropriate folding and stability of proteins in vivo and in vitro (10,22,23). The universal method for direct detection of prolyl isomerization in native proteins and peptides is NMR spectroscopy (24-27). Methods to directly detect peptidyl-prolyl cis/trans isomerization within short peptides can be achieved by NMR spectroscopy and ultraviolet (UV) absorbance (2). However, the majority of protein heterogeneity structures are now solved by X-ray crystallography (2) Protein–protein interactions regulate a diverse array of cellular processes, including growth and differentiation, motility and enzyme function (12). Therefore, the proline isomerization itself may play an important functional role where rates can be controlled by a specific action of the peptidyl-prolyl isomerases (PPIase). It is possible, the more cellular pathways involving prolines involved rate limiting connection between the different biological pathways that are controlled by a specific PPIase.

Peptidyl-Prolyl Isomerase (PPIase)

Enzymes are essential to understanding protein sequence, structure, dynamics, and function. PPIases, originally called “foldases”, are enzymes known to assist protein folding, regulate stability, and accelerate isomerization of specific sequences, as well as unfavorable cis/trans isomerization of a peptide bond preceding a proline, including conformational changes in target proteins (28-31). In 1984, Gunter Fischers and colleagues discovered that PPIases were enzymes capable of catalyzing the isomerization between the cis and trans isoforms of a peptide bond indicated by the

presence of an amino acid proline (X-Pro) bond. This isomerization then allows for 180° rotation about the prolyl bond (28,30). Concluding that PPIase are able to catalyze the isomerization between the cis and trans isoforms of peptide bonds and the protein proline has found to have a pivotal role in cis-specific binding partners

PPIases are a major area of interest within the field, specifically how they are found to play an important role in biology. In theory, the isomerization rate can be controlled by a specific peptidyl-prolyl isomerase (PPIase) and the corresponding activation barrier. PPIase are able to regulate molecular interactions and enzymatic reactions as well as act to reversibly shift between two or more stable states, thus creating a molecular switch in various biological processes. Therefore, the cis-trans equilibrium can operate as a binary molecular switch where the cis-trans isomerization of an X-Pro peptide bond (where X is any residue) can reduce the time from micro to milliseconds (10,31,32). PPIases are able to accelerate cis-trans isomerization of peptide bonds by controlling upstream signaling pathways that can regulate gene-specific transcription during development, hormone response, and environmental stressors (30). Overall, PPIases are enzymes that are characterized as both proteins that play a major part in electrophilic assistance and as a biological catalyst (11). Recently, researchers have shown an increased interest in cis-trans equilibrium operating as a binary molecular switch, because these studies can provide a key rate limiting connection between different biological pathways, which are controlled by a specific PPIase (33,34). Central to the entire disciple of cis-trans equilibrium of a PPIase is the concept of the enzyme operating as a binary molecular switch providing key rate-limiting connections to prolines found in all proteins.

It is now well established that there are three PPIase families, the FKBPs, the parvulins, and the cyclophilins (Cyps) (11,18,29,30,34,35). FKBPs and Cyps are recognized as being similar in function but not in sequence and belonging to the immunophilin family (20,36). A given organism typically has multiple family members. For example, in yeast, *Saccharomyces cerevisiae,* there are 8 Cyps and 4 FKBPs, and in humans there are 18 Cyps and 16 FKBPs (34). Similarly, the rice genome has 27 cyclophilin genes and 29 FKPBs (37,38). The existence of PPIases across a broad array of organisms, from bacteria to humans, indicates a fundamentally critical function that is evolutionarily conserved (30). Moreover, the high number of family members within a given organism suggests a diversification into perhaps highly specific roles that are not well understood.

The Cyps are an established family of PPIase's containing a common domain of approximately 109 amino acids with known roles in many processes including protein folding, signaling, chaperoning and gene regulation (30,39-41). In plants, cyclophilins are abundant proteins that are found in all subcellular compartments (18). In Sekhon 2013, the first study done in plants, the structure of an enzymatically active plant cyclophilin was proposed, with further work suggesting that many plant cyclophilins (OsCyp-19, ZmCyp, PtCyp, and AtCyp-19) have diverged from the non-plant members of the family (BmCyp, Cyp40, PfCyp, MtCyp, TRIMCyp and hCypA) (42). The 27 cyclophilin genes in the rice genome are, with the exception of OsCyp17, homologous to *Arabidopsis* cyclophilins (38,42). All of the rice cyclophilins were predicted to be catalytically active, except OsCyp19 (42). An important question is why there are so many cyclophilins in a given plant species, which has particular

relevance for the project here that focuses on the unique role of a single cyclophilin, OsCyp2, that is essential for lateral root development. In this dissertation, the term Lateral Rootless2 (LRT2) will be used when referring to OsCyp2.

While prolyl isomerization is well studied *in vitro* (33,39), specific *in vivo* functions of this class of molecular switches have only recently come to light (22,30). For example, the Aux/IAA class of transcription regulators in plants that control developmental processes is the Aux/IAA repressor protein family have a sequence motif known to undergo prolyl isomerization, which is central to an auxin responsive negative feedback circuit (43). Therefore, this feedback inhibition circuit known as the Auxin Circuit can be used to study PPIase activity *in vivo*. In the next section, I will discuss the plant hormone Auxin and its features as well as the negative feedback circuit, called the Auxin Circuit.

Auxin the Hormone

The auxin hormone, indole-3-acetic acid (IAA) is a class of phytohormones that regulates essentially all developmental processes in plants (Fig. 1). Auxin is one of the five classes of plant hormones that are conserved in all plant species (35,44-47). Auxin regulates gene expression in developmental processes through the well-studied Auxin Circuit (4). In plants, hormone gradients act as a nervous system to convey information from one part of the plant to another. An important factor to consider is the plant's sensitivity to auxin, or

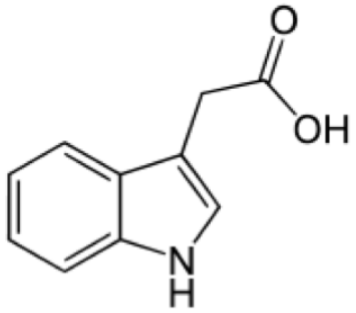

Figure 1: **Auxin Indole-3 Acetic Acid (IAA).** The most commonly naturally-occurring auxin indole-3 acetic acid (IAA), which is used in this dissertation.

responsiveness, which is tissue-specific and involves the presence of specific receptors and signal-transduction pathway components. Overall, auxin has been shown to be required in a number of processes such as tropic responses, apical dominance, cambial cell divisions, differentiation of vascular tissues and lateral root development (47-50). Later on, in this Chapter, I will discuss the significance of lateral root development in rice.

In the early1940s, IAA was isolated from higher plants in straight growth experiments (34). However, IAA was first isolated from human urine, yeast, and Rhizopus suinus (45). There have been several other native auxins found in plants, but I will be focusing on IAA in this work. Throughout the life of a plant, levels of auxin change in response to the changing environment and developmental conditions. This phenomenon is known as "auxin homeostasis" where auxin levels are regulated and maintained in biosynthesis, inactivation, transport, and interconversion pathways (51). Most of the auxin research done today is on the model organism *Arabidopsis thaliana*, which is commonly used for plant molecular biology (45). In the work presented in Chapters 2 and 3, IAA is used as a 'trigger' that enables time-dependent characteristics of the auxin circuit to be quantified using fluorescent protein tags and confocal fluorescence microscopy to gain quantitative insights on the role of cis-trans isomerization in the growth and development of rice plants.

The Auxin Factors

In the past ten years, auxin homeostasis has been discovered to be a highly interactive network of redundant pathways (51). The amount of auxin regulated in the plant is dependent on biosynthesis, degradation, and conjugation pathways, and the location of

auxin in the plant is affected by movement or transport of the hormone. For example, in growing pea plants auxin was shown to be transported downward, or basipetally, to growing zones of the stem and root (52). In the plant, all of the natural auxins are free acid and in conjugated forms. The indole-3-pyruvic acid pathway is now considered the "main" auxin biosynthetic pathway (45). The most commonly studied natural auxin, indole-3-acetic acid (IAA, or heteroauxin) is used in this thesis (51).

Throughout plant growth and development, auxin is able to exert pleiotropic effects by regulating the expression of early auxin-responsive genes, including auxin/indole acetic acid (Aux/IAA), small auxin-up RNAs (SAURs), and GH3 classes of genes (53). This regulation is achieved through the well-studied Auxin Circuit, in which the Aux/IAA protein family members play central roles as auxin-sensitive transcription repressors (35,44,54). To date, several studies have investigated auxin-modulated transcription factors, in particular those in the Aux/IAA and Auxin Response Factor (ARF) genes, which are mostly 'primary-response genes' (45,46,55). Most research identifying Aux/IAA genes has been carried out using biochemical and molecular genetic analysis of several gain-of-function and loss-of-function mutants in *Arabidopsis Thaliana* (56).

Previous studies have indicated that a certain ARF acts as a transcription activator or repressor for a set of genes through its recognition of a specific cis-acting promoter element known as an auxin-response element (AuxRE). This specificity of ARF-DNA interactions has been found to be mediated by an amino-terminal DNA-binding domain (DBD) in ARF (57). Guilfoyle 1998 and Liscum 2002 propose that the Aux/IAA proteins regulate transcription by modifying ARF activity (49,56).

However, it is also known that different cells in the plant may also exhibit differential responses to auxin as various subsets of ARFs, Aux/IAAs, and/or other tissue-specific factors may interact with regulators(56-58).

In *Oryza Sativa*, there are 31 Aux/IAA genes and 25 ARF genes (59). Similarly, in the model organism *Arabidopsis Thaliana*, there are 29 AUX/IAA and 23 ARF genes with tissue-specific expression and interactions(35,60). Since most of the Aux/IAA literature focuses on studies in *Arabidopsis Thaliana*, these studies will be included in this dissertation for comparison. The existing body of research indicates that Aux/IAA genes play a critical role in plant growth and development, photomorphogenesis, and auxin signaling (60).

In Jain 2006, the group identified and analyzed early auxin-responsive Aux/IAA gene families from rice (*Oryza sativa*) (60). Using real-time polymerase chain reaction (PCR) they analyzed rice Aux/IAA genes that were expressed in various organs/tissues grown in light or dark and their sensitivity to auxin treatment. Results indicate that Aux/IAA in different cells/tissues may perform specific as well as redundant functions in different areas of the plant. Similar to the model organism *Arabidopsis Thaliana*, the preferential retention throughout evolution of the duplicated Aux/IAA genes in rice could reflect critical relationships with interacting proteins such as ARFs to preserve the specific targeting of genes through their cis-regulatory elements (61).

The Paterson et al. (2004) group investigated the structural analysis of genomic duplication in rice, investigating the timing of the duplication event and explored its impact on cereal comparative genomics (62). Of the nine nonoverlapping duplicated

blocks four occurred between chromosomes 1 and 5 (OsIAA1 and 15, OsIAA2 and 16, OsIAA3 and 17, OsIAA5 and 19, OsIAA6 and 18), 2 and 6 (OsIAA9 and 20), 3 and 7 (OsIAA14 and 24), and 3 and 12 (OsIAA12 and 31; OsIAA11 and 30), which gave rise to Aux/IAA gene duplications. Results showed that on 10 of the 12 chromosomes the 31 rice Aux/IAA genes were distributed (62).

In 1995, Abel used a progressive deletion analysis and site-directed mutagenesis in pea (*Pisum sativa*) to report the identification of the nuclear localization signals (NLS) in PS-IAA4 and PS-IAA6 (58). PS-IAA6 was shown to serve as a dominant transferable degradation signal and had an in vivo half-life of 13.5 min in transgenic *Arabidopsis Thaliana* seedlings. To date, several studies have indicated that the rapid degradation of Aux/IAA proteins is necessary for a normal auxin response (46,47,60,63,64).

The Auxin Circuit

As mentioned above, rapid degradation of Aux/IAA proteins is essential for a normal auxin response at the cellular level, and for normal phenotypes at the organism level. The auxin circuit is now understood to be the mechanism for this link between auxin levels, Aux/IAA protein degradation rate, and phenotype (Fig. 2). Briefly, the repression of auxin-regulated genes is achieved through binding of an Aux/IAA transcriptional repressor protein to an activating ARF transcription factor on the ARE of the promoter. In the presence of auxin, Aux/IAA releases from ARF and binds to auxin and the TIR1 component of the SCF^{TIR1} E3 ubiquitin ligase complex (54,65,66). The Aux/IAA protein is subsequently ubiquitylated and irreversibly degraded via the proteasome(64). The release of Aux/IAA from ARF activates transcription of the

auxin-responsive genes, including the gene encoding the Aux/IAA protein itself. Hence, as Aux/IAA is degraded, expression of its gene is activated, which leads again to repression as new Aux/IAA binds to ARF on the promoter (48,56,67,68), thereby generating a classic negative feedback circuit.

Structural studies have shown that auxin binds directly to TIR1 in concert with the Aux/IAA protein substrate (69). Prior to the work of Tan et al. (2007), how AUX/IAA proteins bound to TIR1 was largely unknown. That work shows that natural auxin IAA binds to the base of the TIR1 pocket via two important functional moieties: the side-chain carboxyl group and the indole ring (69). On top of auxin, the Aux/IAA substrate cooperatively binds via its conserved GWPPV motif that represents the hallmark of the Aux/IAA degron sequence. Remarkably, the GWPPV motif binds exclusively in the *cis* conformation of the W-P peptide bind, imparting strict isomer specificity to this interaction. Auxin functions as a 'molecular glue' that fills a hydrophobic cavity on the protein interface which enhances the TIR1-Aux/IAA interaction. Unexpectedly, the group also found that the leucine-rich repeat domain of TIR1 contains an inositol hexakisphosphate co-factor. This structural work demonstrated that the auxin dependence of Aux/IAA protein degradation is mediated through the ubiquitin-ligase complex, SCFTIR1, which promotes ubiquitin-dependent proteolysis(69). It is now well established that auxin regulates SCFTIR1 activity by directly promoting the interactions between TIR1 and its polypeptide substrates.

In Zhu et al. (2012), a rice Aux/IAA family member was isolated from a rice mutant defective in lateral root development known as OsIAA11 (LOC_Os03g43400)(70). In an investigation into OsIAA11, Zhu et al (2012)

constructed transgenic plants harboring the mutated gene Osiaa11 driven by the promoter of OsIAA11, which displayed a decrease in lateral root number (71). However, the results also displayed an increase in resistance to exogenous auxin treatment, suggesting that other Aux/IAA genes have overlapping functions with OsIAA11. These results identified a difference between AtIAA14 and OsIAA11, which until this point has been highly conserved in higher plants. Thus, rice lateral root primordium is different from *Arabidopsis Thaliana* in that it is initiated from both pericycle cells at the phloem pole and endodermis (70). In Arabidopsis, the lateral root primordium is initiated from pericycle cells adjacent to the protoxylem (72). It is known that auxin transport facilitators auxin efflux carriers PINs play a key role in maintaining an auxin gradient at the root tip (70). Zhu et al. (2012), results may provide insight into the different auxin signaling regulation mediated by Aux/IAAs for lateral root primordium formation between rice and Arabidopsis.

The Aux/IAA protein family contains four highly conserved domains, I-IV, and family members are short-lived nuclear proteins (58). Domain I is known to be a transcriptional repressor while Domain II is has been shown to be responsible for the rapid degradation of Aux/IAA proteins (73). Domain III has been found to contain an amphipathic βαα-DNA recognition motif, but its role in DNA binding has not been shown. This motif has been discovered to be the same β ribbon DNA binding domain of prokaryotic repressors such as MetJ and Arc (58). More recently, the structure of Domains III-IV reveals a single structural domain, PB1, that mediates interactions between Aux/IAA proteins and ARFs (74,75). Domains II and IV are known to contain nuclear localization signals (NLSs) as well as facilitate homo- and hetero-

dimerization among the Aux/IAA proteins and auxin response factors (ARFs) (46,58,76). Jain 2006 states that mutants of Aux/IAA genes have illustrated how Aux/IAA proteins perform a central role in managing plant growth and development (45,60,68,77).

Overall, auxin responses are coordinated by two separate pathways: the TRANSPORT INHIBITOR RESPONSE1/AUXIN SIGNALING F-BOX (TIR1/AFB) auxin response pathway and the AUXIN BINDING PROTEIN1 (ABP1) auxin response pathway. For this thesis, the experiments focus on the TIR1 pathway, which involves the auxin circuit and is well studied (78). Since the discovery of auxin, it has been found to be involved in a broad range of regulation activities in many aspects of plant growth and development. It has been undoubtedly concluded that the fine-tuning of this hormone may be achieved through cross-talk potentially involving ARFs and other Aux/IAA proteins and possibly other protein interactions like PPIases (78,79). In Kang 2013, characterization of *Oryza sativa* rice plants with mutations in a cyclophilin gene (LRT2) displayed the lateral rootless phenotype and defects in auxin responses, demonstrating a critical role of a cyclophilin in the auxin circuit that regulates lateral root development (3).

The Importance of Prolyl Peptidyl Isomerases in the Auxin Circuit

This dissertation aims to investigate the relationships between LRT2 and the rate of Aux/IAA protein degradation, two essential components in the Auxin Circuit that governs lateral root development in rice (Fig. 2). Studies in *Arabidopsis thaliana* and yeast provide experimental support for Aux/IAA degradation rate, which is essential to the Auxin Circuit dynamics (5,6,80). However, quantitative characterizations of the

impact of specific cis-trans isomerization rates on biological processes in living cells, and relationships to the resulting phenotypes have not yet been elucidated (44,67,81,82).

Recent trends in plant biology have led to a proliferation of studies that focus on Aux/IAA proteins involved with cyclophilins, which are a novel component of auxin signaling pathways in higher plants such as tomatoes and rice. A single domain tomato cyclophilin DIAGEOTROPICA (DGT) has been previously observed to affect auxin-induced transcription (83). This is evidence that cyclophilin plays a central role in regulating the degradation of Aux/IAA proteins. Utilizing a cyclophilin, the Aux/IAA proteins have the ability to release the repression of ARFs concluding in an ARF-dependent transcription (83). Previous research has demonstrated that a DGT mutant displays a lateral-rootless and auxin-resistant phenotype (84) concluding that this is a highly conserved regulatory mechanism in dicots and monocots as well as in lower plants (85).

In the rice genome 27 cyclophilin-like genes were annotated, and the other cyclophilin-like proteins share relative sequence similarities with LRT2 (5,38). Kang et al. (2013) investigated two LRT2 mutants that displayed defective lateral root development such as reduced shoot length, decreased fertility, and a delayed heading stage (3). Utilizing gain-of-function mutations in domain II of Aux/IAAs proteins they were able to remove the TIR1–Aux/IAA interaction causing an auxin-resistant phenotype. Studies of LRT2 show the importance of a PPIase in a stress protection role possibly by participating in a protein folding reaction of stress-driven aggregated proteins (4). The existing body of research on plant cyclophilins, including LRT2

genes, suggests that under abiotic and biotic stresses cyclophilins act as molecular chaperones and are involved in other metabolic processes.

In rice, LRT2 has been shown to catalyze OsIAA11 (6). As an Aux/IAA protein, OsIAA11 is a transcription repressor that has an irreversible cis-specific degradation and is an essential component of the Auxin Circuit that regulates lateral root development (6,70,86). The cyclophilin LRT2 and the Aux/IAA protein OsIAA11, each independently linked to the lateral rootless phenotype in *Oryza Sativa*, were recently shown to be an enzyme/substrate pair that regulates lateral root development through LRT2-mediated regulation of OsIAA11 stability (6). Their NMR data show that LRT2 is capable of catalyzing conformational exchanges of the OsIAA11 peptide, and they propose that LRT2 mediates the cis/trans isomerization of the Aux/IAA transcriptional repressors, thereby facilitating their proteasomal degradation (6). Jing et al (2015) propose that the cyclophilin-catalyzed isomerization of the Aux/IAA transcriptional repressors could be a general mechanism in regulating auxin signaling in the plant kingdom (6). This system provides an opportunity to perform quantitative characterizations of a specific cis-trans molecular switch in vivo, and to measure the impact of isomerization kinetics on auxin circuit dynamics in living cells.

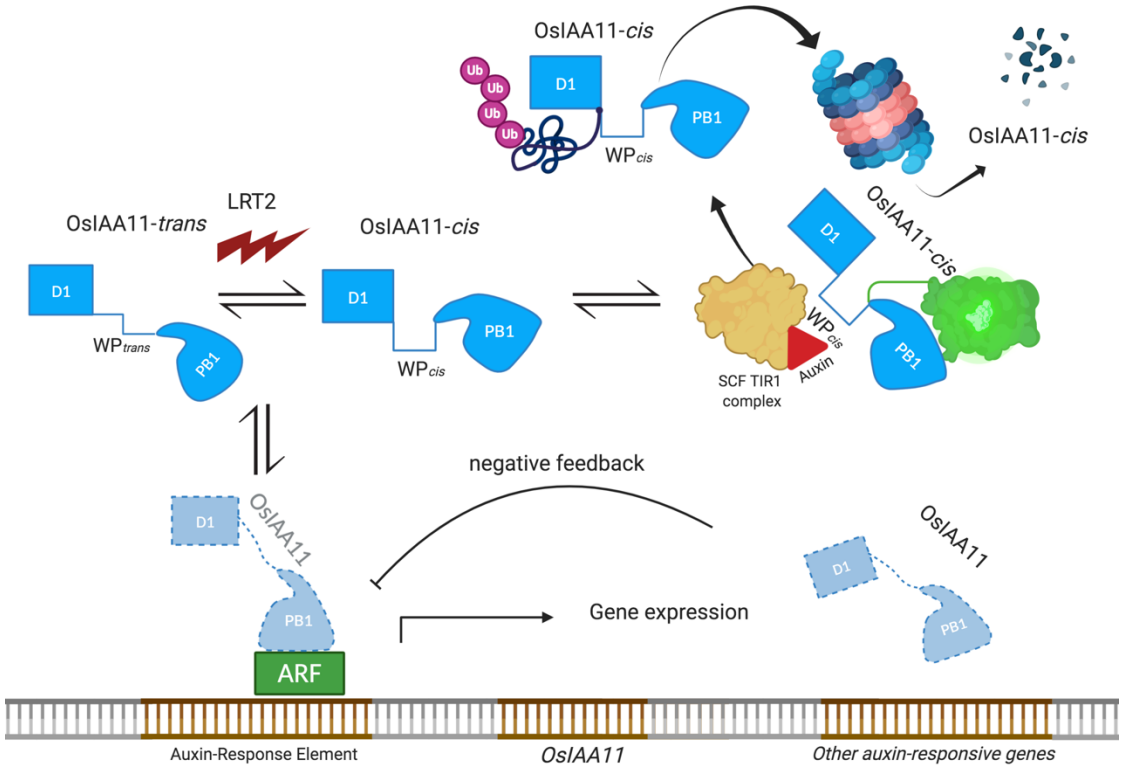

Figure 2: A prolyl isomerization reaction rate can potentially regulate a biological circuit called the Auxin Circuit. The Auxin Circuit in the "on" state, where the increase in auxin concentration shifts the equilibrium to favor the cis-specific proteasomal degradation of OsIAA11 (see main text).

Lateral Root development

Auxin, the phytohormone, plays an important role in regulating several plant responses including cell elongation, cell division, root initiation, apical dominance, and tropic responses. The International Rice Research Institute in the Philippians has concluded by studying the evolution of the plant that in order to have a deep root system it is important to have a well-developed system of lateral roots. A review by Scott 1972 concluded that IAA is synthesized through tryptophan (Trp)-independent and Trp-dependent pathways (45,75). In rice, Nakamura et al. (2006) were the first to identify an Aux/IAA protein OsIAA3 (LOC_Os12g40900, now named OsIAA31), which played a role in lateral root development (70). Nakamura et al. (2006) utilized

transgenic rice plants overexpressing the OsIAA3 (Osiaa3) gene (70). This gene displayed auxin insensitivity in abnormal shoot and root gravitropism, and a deficiency in lateral root initiation. Zhu et al. (2012) isolated a rice Aux/IAA family member from a rice mutant defective in lateral root development known as OsIAA11 (LOC_Os03g43400) (70). This gain-of-function mutation in the domain II of OsIAA11 strictly blocks the initiation of lateral root primordia but does not interfere with the crown root development. Zhu et al. (2012) concluded that OsIAA11is involved in auxin signaling in root caps (70). However, overexpression of OsIAA1 in rice (87) displayed reduced inhibition of root elongation in response to exogenous auxin, which also decreased plant height. In a study on OsIAA genes, Jain et al., 2006 showed that there are various overlapping organ-specific expression patterns in light- and dark-grown seedling/plants (60). Overall, the results indicated that OsIAA3 and OsIAA1 have pleiotropic effects on plant growth and development as well as lateral root development.

Evidence suggests that other factors also regulate the auxin circuit. Kang et al. (2013) identified that LRT2 interacted with co-chaperone OsSGT1, which promoted the degradation of AUX/IAA (Fig. 3)(3). An article from Yamamoto et.al, 2004 analyzed tissues in rice expressing OsSGT1, showing that it is required for degradation (88). The results showed that the expression levels are low in shoots but high in roots. Lastly, Kadota et al., 2008 showed that OsSGT1 required a co-chaperone heat shock protein HSP90 as a requirement for innate immunity in plants (89). Heat shock protein, HsP90, is able to regulate the temperature-dependent seedling growth of *Arabidopsis Thaliana* by stabilizing the auxin co-receptor F-box

protein of TIR1 (90). This existing body of research on *Arabidopsis Thaliana* has established that the OsSGT1 protein is important in lateral root development (3,55). Overall, studies have concluded that LRT2 conducts auxin regulation in the plant by interacting with the co-chaperone OsSGT1, and HSP90, both are involved in the Auxin Circuit and may be required for degradation (Fig. 3) (34,43,91).

In addition to OsSGT1, evidence indicates that a zinc finger protein, OsZFP, may also positively promote lateral root development in rice(43). In Cui et al. 2017, they used RNA interference technology (RNAi) to induce post-transcriptional silencing of LRT2 in rice (*Oryza sativa* L. cv. Aichi-ashahi) in order to induce a defective lateral root phenotype (87). Surprisingly, LRT2 interacted with a C2HC-type zinc finger protein (OsZFP, Os01g0252900), which is located in the rice nucleus (87). Upon IAA treatment, the expression of the OsIAA8, 11, 23 and 31 genes showed significant up-regulation/down-regulation in the LRT2-OE/RNAi plants. They concluded that in rice the IAA pathway involves a zinc finger protein interacting with LRT2 to positively affect lateral root development (Fig. 3) (87).

Similarly, there are other lines of evidence that suggest proteins negatively impact lateral root development in response to auxin response like a rice inositol phosphate kinase (OsIPK2) (43,86). In Chen et al. 2017, OsIPK2, a rice (*Oryza sativa*) inositol polyphosphate kinase has been shown to directly interact with OsIAA11 to repress its auxin-induced proteasomal degradation (Fig. 3) (86). Another study found that the overexpression of OsIPK2 causes auxin-insensitivity and failure to develop lateral roots (86). However, OsIPK2 has been shown to stabilize OsIAA11 protein through interaction with its Domains II and III. Notably, Domain II is where the

degron motif is located. To date, little is known about the functional interaction between OsIPK2 and OsIAA11, but it may be an important factor in regulating the turnover of OsIAA11 in response to cellular signals like auxin.

It has been previously observed in eukaryotic cells that Ras and Rho subfamilies of the Ras superfamily of small GTPases function with molecular switches in various signaling cascades in order to regulate growth (92). However, plants do not have Ras proteins but do contain Rho-like small G proteins called RACs or ROPs. Few studies have investigated the mechanisms between RAC/ROP GTPases and auxin signaling(92). In Wu (2011), experimental evidence suggested that auxin-RAC/ROP GTPases may cross-talk in order to form regulatory feedback loops as well as form auxin gradients regulating cell polarity (93). To date, limited research has been done on how RAC-ROP may mediate the regulation of auxin-responsive gene expression pathways (65,66,78,93).

In order to look at the role of auxin perception and signaling, Hayashi et al (2018) designed small molecules to be auxin agonists and antagonists (34,94). These small molecules were specific to TIR1-mediated events in *Arabidopsis Thaliana* by analyzing the impact of auxin on gene regulation and expression relative to the *Arabidopsis Thaliana* F-box protein TIR1 (34). The results indicated that a small molecule could inhibit the F-box protein-substrate recruitment, suggesting that there may be other small molecules in the cell which could inhibit substrate recognition and subsequent ubiquitination of SCF-type ubiquitin ligases, which is the necessary

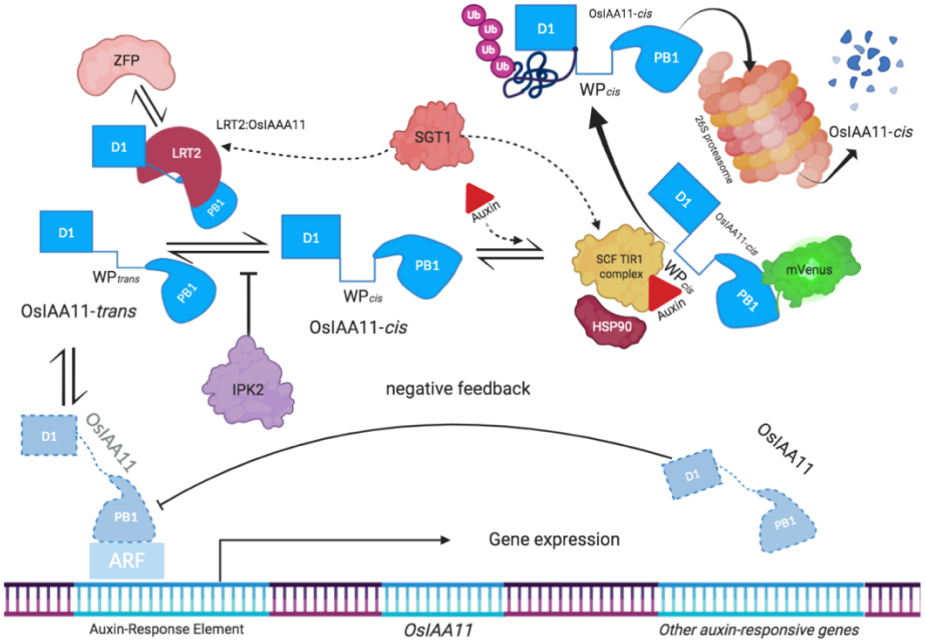

Figure 3: An updated auxin circuit model regarding OsIAA11's role in lateral root development. This is an updated model of the Auxin Circuit based finding in the literature portraying the "on" state, where the increase in auxin concentration shifts the equilibrium to favor the cis-specific proteasomal degradation of OsIAA11 (see main text).

interaction for the degradation of IAA proteins.

The Experimental Approach

Traditionally, Aux/IAA proteins have been assessed *in vitro* by measuring protein levels. Recent advances in protoplast (plant cells without cell walls) methods have facilitated investigation of Aux/IAA proteins *in vivo*. Many researchers have utilized protoplasts to measure *in vivo* characteristics of plant cells (95-99). A key study that observed LRT2-GFP transiently expressed in rice protoplasts by confocal microscopy indicated that LRT2 was localized to the cytosol and nucleus(3). In the literature, plant cyclophilins have been known to be localized in the cytosol, suggesting that even

though the LRT2 protein has no distinctive signal peptide for organelle localization that the LRT2 is localized at the cytosol and the nucleus (3,5,38). Zheng (2013) characterized the subcellular localization of LRT2, using a GFP fusion protein in tobacco leaves driven by the LRT2 promoter (5). This method is particularly useful when visualizing protein within a single protoplast (95). A major advantage of using protoplasts is that fluorescent proteins are able to be transiently transfected into live plant cells (100). In work described in chapters 2 and 3, protoplast was transiently transfected with our protein of interest fused to fluorescent reporter proteins in order to quantitatively monitor protein levels to enable mathematical modeling of the Auxin Circuit. All of the work was carried out by confocal microscopy in order to visualize the fluorescent proteins.

Conclusions

In this investigation, the aim was to quantify the cis-specific degradation rate of OsIAA11 in rice protoplasts, and to investigate the effects of LRT2 on this rate. In Chapter 2, I describe the optimization of protocols to extract and transfect protoplasts for study by confocal fluorescence microscopy. In Chapter 3, our goal was to use rice shoot protoplast experiments to quantitatively monitor key Auxin Circuit components, such as the degradation of OsIAA11. Performing cycloheximide chase studies of an Auxin/IAA protein like OsIAA11 would provide the field with knowledge on the degradation rate of this IAA protein as well as give a key essential parameter for modeling the Auxin Circuit. Overall, the long-term goal is tuning of the LRT2 catalytic activity in plants and quantifying the resulting circuit dynamics of endogenous protein levels in vivo.

REFERENCES:

1. Williamson, M. P. (1994) The structure and function of proline-rich regions in proteins. *Biochem J* **297 (Pt 2)**, 249-260
2. Andreotti, A. H. (2003) Native state proline isomerization: an intrinsic molecular switch. *Biochemistry* **42**, 9515-9524
3. Kang, B., Zhang, Z., Wang, L., Zheng, L., Mao, W., Li, M., Wu, Y., Wu, P., and Mo, X. (2013) OsCYP2, a chaperone involved in degradation of auxin-responsive proteins, plays crucial roles in rice lateral root initiation. *Plant J* **74**, 86-97
4. Kumari, S., Singh, P., Singla-Pareek, S. L., and Pareek, A. (2009) Heterologous expression of a salinity and developmentally regulated rice cyclophilin gene (OsCyp2) in E. coli and S. cerevisiae confers tolerance towards multiple abiotic stresses. *Mol Biotechnol* **42**, 195-204
5. Zheng, H., Li, S., Ren, B., Zhang, J., Ichii, M., Taketa, S., Tao, Y., Zuo, J., and Wang, H. (2013) LATERAL ROOTLESS2, a cyclophilin protein, regulates lateral root initiation and auxin signaling pathway in rice. *Mol Plant* **6**, 1719-1721
6. Jing, H., Yang, X., Zhang, J., Liu, X., Zheng, H., Dong, G., Nian, J., Feng, J., Xia, B., Qian, Q., Li, J., and Zuo, J. (2015) Peptidyl-prolyl isomerization targets rice Aux/IAAs for proteasomal degradation during auxin signalling. *Nat Commun* **6**, 7395
7. Fisher, C. L., Resnick, R. J., De, S., Acevedo, L. A., Lu, K. P., Schroeder, F. C., and Nicholson, L. K. (2017) Cyclic cis-Locked Phospho-Dipeptides Reduce Entry of AβPP into Amyloidogenic Processing Pathway. *J Alzheimers Dis* **55**, 391-410
8. Lee, M. S., Kao, S. C., Lemere, C. A., Xia, W., Tseng, H. C., Zhou, Y., Neve, R., Ahlijanian, M. K., and Tsai, L. H. (2003) APP processing is regulated by cytoplasmic phosphorylation. *J Cell Biol* **163**, 83-95
9. Halling, P. J. (1995) Proteins: Structures and molecular properties (2nd edition). by Thomas E. Creighton, W. H. Freeman, New York, 1992, xiii + 512 pp, price £22.95. ISBN 0-7167-7030-X. *Journal of Chemical Technology & Biotechnology* **62**, 105-105
10. Fischer, G., Bang, H., and Mech, C. (1984) Determination of enzymatic catalysis for the cis-trans-isomerization of peptide binding in proline-containing peptides. *Biomedica biochimica acta* **43**, 1101-1111
11. Fischer, G. (2000) Chemical aspects of peptide bond isomerisation. *Chemical Society Reviews* **29**, 119-127
12. Kanelis, V., Donaldson, L., Muhandiram, D., Rotin, D., Forman-Kay, J. D., and Kay, L. E. (2000) Sequential assignment of proline-rich regions in proteins: application to modular binding domain complexes. *Journal of biomolecular NMR* **16**, 253-259
13. Siligardi, G., and Drake, A. F. (1995) The importance of extended conformations and, in particular, the PII conformation for the molecular recognition of peptides. *Biopolymers* **37**, 281-292

14. Yu, H., Chen, J. K., Feng, S., Dalgarno, D. C., Brauer, A. W., and Schrelber, S. L. (1994) Structural basis for the binding of proline-rich peptides to SH3 domains. *Cell* **76**, 933-945
15. Carl, U. D., Pollmann, M., Orr, E., Gertler, F. B., Chakraborty, T., and Wehland, J. (1999) Aromatic and basic residues within the EVH1 domain of VASP specify its interaction with proline-rich ligands. *Current biology* **9**, 715-S714
16. Musacchio, A., Saraste, M., and Wilmanns, M. (1994) High-resolution crystal structures of tyrosine kinase SH3 domains complexed with proline-rich peptides. *Nature structural biology* **1**, 546-551
17. Nguyen, J. T., Turck, C. W., Cohen, F. E., Zuckermann, R. N., and Lim, W. A. (1998) Exploiting the basis of proline recognition by SH3 and WW domains: design of N-substituted inhibitors. *Science* **282**, 2088-2092
18. Galat, A., and Riviére, S. (1998) *Peptidyl-prolyl Cis/trans Isomerases*, Oxford University Press
19. Wedemeyer, W. J., Welker, E., and Scheraga, H. A. (2002) Proline Cis–Trans Isomerization and Protein Folding. *Biochemistry* **41**, 14637-14644
20. Fischer, G., and Aumüller, T. (2004) Regulation of peptide bond cis/trans isomerization by enzyme catalysis and its implication in physiological processes. in *Reviews of Physiology, Biochemistry and Pharmacology*, Springer Berlin Heidelberg, Berlin, Heidelberg. pp 105-150
21. Pál, C., Papp, B., and Lercher, M. J. (2006) An integrated view of protein evolution. *Nature Reviews Genetics* **7**, 337-348
22. Perrucci, G. L., Gowran, A., Zanobini, M., Capogrossi, M. C., Pompilio, G., and Nigro, P. (2015) Peptidyl-prolyl isomerases: a full cast of critical actors in cardiovascular diseases. *Cardiovascular Research* **106**, 353-364
23. Gething, M.-J., and Sambrook, J. (1992) Protein folding in the cell. *Nature* **355**, 33-45
24. Greenwood, A. I., Rogals, M. J., De, S., Lu, K. P., Kovrigin, E. L., and Nicholson, L. K. (2011) Complete determination of the Pin1 catalytic domain thermodynamic cycle by NMR lineshape analysis. *J Biomol NMR* **51**, 21-34
25. Ramelot, T. A., Gentile, L. N., and Nicholson, L. K. (2000) Transient Structure of the Amyloid Precursor Protein Cytoplasmic Tail Indicates Preordering of Structure for Binding to Cytosolic Factors. *Biochemistry* **39**, 2714-2725
26. Ramelot, T. A., and Nicholson, L. K. (2001) Phosphorylation-induced structural changes in the amyloid precursor protein cytoplasmic tail detected by NMR. *J Mol Biol* **307**, 871-884
27. Dawson, J. E., and Nicholson, L. K. (2008) Folding kinetics and thermodynamics of Pseudomonas syringae effector protein AvrPto provide insight into translocation via the type III secretion system. *Protein Sci* **17**, 1109-1119
28. Hani, J., Schelbert, B., Bernhardt, A., Domdey, H., Fischer, G., Wiebauer, K., and Rahfeld, J. U. (1999) Mutations in a peptidylprolyl-cis/trans-isomerase gene lead to a defect in 3'-end formation of a pre-mRNA in Saccharomyces cerevisiae. *J Biol Chem* **274**, 108-116

29. Wang, W.-X., Wilfred, B. R., Madathil, S. K., Tang, G., Hu, Y., Dimayuga, J., Stromberg, A. J., Huang, Q., Saatman, K. E., and Nelson, P. T. (2010) miR-107 regulates granulin/progranulin with implications for traumatic brain injury and neurodegenerative disease. *Am J Pathol* **177**, 334-345
30. Hanes, S. D. (2015) Prolyl isomerases in gene transcription. *Biochim Biophys Acta* **1850**, 2017-2034
31. Nicholson, L. K., and De, S. (2011) Structural biology: The twist in Crk signaling revealed. *Nat Chem Biol* **7**, 5-6
32. Wang, P., and Heitman, J. (2005) The cyclophilins. *Genome Biol* **6**, 226-226
33. Howard, B. R., Vajdos, F. F., Li, S., Sundquist, W. I., and Hill, C. P. (2003) Structural insights into the catalytic mechanism of cyclophilin A. *Nature Structural & Molecular Biology* **10**, 475-481
34. Luo, J., Zhou, J.-J., and Zhang, J.-Z. (2018) Aux/IAA gene family in plants: Molecular structure, regulation, and function. *International journal of molecular sciences* **19**, 259
35. Dinesh, D. C., Villalobos, L. I. A. C., and Abel, S. (2016) Structural Biology of Nuclear Auxin Action. *Trends in Plant Science* **21**, 302-316
36. Fanghänel, J., and Fischer, G. (2004) Insights into the catalytic mechanism of peptidyl prolyl cis/trans isomerases. *Front Biosci* **9**, 3453-3478
37. Gollan, P. J., and Bhave, M. (2009) Genome-wide analysis of genes encoding FK506-binding proteins in rice. *Plant Molecular Biology* **72**, 1
38. Ahn, J. C., Kim, D.-W., You, Y. N., Seok, M. S., Park, J. M., Hwang, H., Kim, B.-G., Luan, S., Park, H.-S., and Cho, H. S. (2010) Classification of rice (Oryza satival. japonica nipponbare) immunophilins (FKBPs, CYPs) and expression patterns under water stress. *BMC Plant Biology* **10**, 253
39. Christoforides, E., Dimou, M., Katinakis, P., Bethanis, K., and Karpusas, M. (2012) Structure of a bacterial cytoplasmic cyclophilin A in complex with a tetrapeptide. *Acta Crystallogr Sect F Struct Biol Cryst Commun* **68**, 259-264
40. Dilworth, D., Gudavicius, G., Leung, A., and Nelson, C. J. (2012) The roles of peptidyl-proline isomerases in gene regulation. *Biochem Cell Biol* **90**, 55-69
41. Thapar, R. (2015) Roles of prolyl isomerases in RNA-mediated gene expression. *Biomolecules* **5**, 974-999
42. Sekhon, S. S., Kaur, H., Dutta, T., Singh, K., Kumari, S., Kang, S., Park, S. G., Park, B. C., Jeong, D. G., Pareek, A., Woo, E.-J., Singh, P., and Yoon, T.-S. (2013) Structural and biochemical characterization of the cytosolic wheat cyclophilin TaCypA-1. *Acta Crystallogr D Biol Crystallogr* **69**, 555-563
43. Meng, F., Xiang, D., Zhu, J., Li, Y., and Mao, C. (2019) Molecular mechanisms of root development in rice. *Rice* **12**, 1-10
44. Davis, T. L., Walker, J. R., Campagna-Slater, V., Finerty, P. J., Jr., Paramanathan, R., Bernstein, G., MacKenzie, F., Tempel, W., Ouyang, H., Lee, W. H., Eisenmesser, E. Z., and Dhe-Paganon, S. (2010) Structural and biochemical characterization of the human cyclophilin family of peptidyl-prolyl isomerases. *PLoS Biology* **8**
45. Enders, T. A., and Strader, L. C. (2015) Auxin activity: Past, present, and future. *Am J Bot* **102**, 180-196

46. Abel, S., and Theologis, A. (1996) Early genes and auxin action. *Plant physiology* **111**, 9-17
47. Worley, C. K., Ramos, J., Leyser, O., Theologis, A., Zenser, N., Rouse, D., and Callis, J. (2000) Degradation of Aux/IAA proteins is essential for normal auxin signalling. *The Plant journal* **21**, 553-562
48. Tiwari, S. B., Wang, X.-J., Hagen, G., and Guilfoyle, T. J. (2001) AUX/IAA proteins are active repressors, and their stability and activity are modulated by auxin. *The Plant Cell* **13**, 2809-2822
49. Guilfoyle, T. J., and Key, J. L. (1986) Auxin-regulated gene expression in higher plants. *Critical reviews in plant sciences* **4**, 247-276
50. Went, F. W., and Thimann, K. V. (1937) Phytohormones. *Phytohormones*.
51. Normanly, J., Slovin, J. P., and Cohen, J. D. (1995) Rethinking auxin biosynthesis and metabolism. *Plant Physiology* **107**, 323
52. Davies, P. J. (2010) The plant hormones: their nature, occurrence, and functions. in *Plant hormones*, Springer. pp 1-15
53. Overvoorde, P. J., Okushima, Y., Alonso, J. M., Chan, A., Chang, C., Ecker, J. R., Hughes, B., Liu, A., Onodera, C., Quach, H., Smith, A., Yu, G., and Theologis, A. (2005) Functional genomic analysis of the AUXIN/INDOLE-3-ACETIC ACID gene family members in Arabidopsis thaliana. *The Plant cell* **17**, 3282-3300
54. Tan, X., Calderon-Villalobos, L. I., Sharon, M., Zheng, C., Robinson, C. V., Estelle, M., and Zheng, N. (2007) Mechanism of auxin perception by the TIR1 ubiquitin ligase. *Nature* **446**, 640-645
55. Paponov, I. A., Paponov, M., Teale, W., Menges, M., Chakrabortee, S., Murray, J. A. H., and Palme, K. (2008) Comprehensive Transcriptome Analysis of Auxin Responses in Arabidopsis. *Molecular Plant* **1**, 321-337
56. Liscum, E., and Reed, J. W. (2002) Genetics of Aux/IAA and ARF action in plant growth and development. *Plant Mol Biol* **49**, 387-400
57. Tiwari, S. B., Hagen, G., and Guilfoyle, T. (2003) The roles of auxin response factor domains in auxin-responsive transcription. *The Plant cell* **15**, 533-543
58. Abel, S., and Theologis, A. (1995) A polymorphic bipartite motif signals nuclear targeting of early auxin-inducible proteins related to PS-IAA4 from pea (Pisum sativum). *The Plant journal : for cell and molecular biology* **8 1**, 87-96
59. Wang, D., Pei, K., Fu, Y., Sun, Z., Li, S., Liu, H., Tang, K., Han, B., and Tao, Y. (2007) Genome-wide analysis of the auxin response factors (ARF) gene family in rice (Oryza sativa). *Gene* **394**, 13-24
60. Jain, M., Kaur, N., Garg, R., Thakur, J. K., Tyagi, A. K., and Khurana, J. P. (2006) Structure and expression analysis of early auxin-responsive Aux/IAA gene family in rice (Oryza sativa). *Funct Integr Genomics* **6**, 47-59
61. Cherenkov, P., Novikova, D., Omelyanchuk, N., Levitsky, V., Grosse, I., Weijers, D., and Mironova, V. (2018) Diversity of cis-regulatory elements associated with auxin response in Arabidopsis thaliana. *Journal of experimental botany* **69**, 329-339

62. Paterson, A. H., Bowers, J., and Chapman, B. (2004) Ancient polyploidization predating divergence of the cereals, and its consequences for comparative genomics. *Proceedings of the National Academy of Sciences* **101**, 9903-9908
63. dos Santos Maraschin, F., Memelink, J., and Offringa, R. (2009) Auxin-induced, SCFTIR1-mediated poly-ubiquitination marks AUX/IAA proteins for degradation. *The Plant Journal* **59**, 100-109
64. Ramos, J. A., Zenser, N., Leyser, O., and Callis, J. (2001) Rapid degradation of auxin/indoleacetic acid proteins requires conserved amino acids of domain II and is proteasome dependent. *Plant Cell* **13**, 2349-2360
65. Dharmasiri, N., Dharmasiri, S., Jones, A. M., and Estelle, M. (2003) Auxin action in a cell-free system. *Curr Biol* **13**, 1418-1422
66. Kepinski, S., and Leyser, O. (2005) The Arabidopsis F-box protein TIR1 is an auxin receptor. *Nature* **435**, 446-451
67. Mockaitis, K., and Estelle, M. (2008) Auxin receptors and plant development: a new signaling paradigm. *Annu Rev Cell Dev Biol* **24**, 55-80
68. Reed, J. W. (2001) Roles and activities of Aux/IAA proteins in Arabidopsis. *Trends Plant Sci* **6**, 420-425
69. Tan, X., Calderon-Villalobos, L. I. A., Sharon, M., Zheng, C., Robinson, C. V., Estelle, M., and Zheng, N. (2007) Mechanism of auxin perception by the TIR1 ubiquitin ligase. *Nature* **446**, 640-645
70. Zhu, Z.-X., Liu, Y., Liu, S.-J., Mao, C.-Z., Wu, Y.-R., and Wu, P. (2012) A gain-of-function mutation in OsIAA11 affects lateral root development in rice. *Molecular Plant* **5**, 154-161
71. Zhu, Z. X., Liu, Y., Liu, S. J., Mao, C. Z., Wu, Y. R., and Wu, P. (2012) A gain-of-function mutation in OsIAA11 affects lateral root development in rice. *Mol Plant* **5**, 154-161
72. Privat de Garilhe, M. (1967) *Enzymes in nucleic acid research. Preface by M. Laskowski*, Hermann, Paris
73. Tiwari, S. B., Hagen, G., and Guilfoyle, T. J. (2004) Aux/IAA Proteins Contain a Potent Transcriptional Repression Domain. *The Plant Cell* **16**, 533-543
74. Han, M., Park, Y., Kim, I., Kim, E. H., Yu, T. K., Rhee, S., and Suh, J. Y. (2014) Structural basis for the auxin-induced transcriptional regulation by Aux/IAA17. *Proc Natl Acad Sci U S A* **111**, 18613-18618
75. Korasick, D. A., Enders, T. A., and Strader, L. C. (2013) Auxin biosynthesis and storage forms. *Journal of experimental botany* **64**, 2541-2555
76. Han, M., Park, Y., Kim, I., Kim, E.-H., Yu, T.-K., Rhee, S., and Suh, J.-Y. (2014) Structural basis for the auxin-induced transcriptional regulation by Aux/IAA17. *Proceedings of the National Academy of Sciences* **111**, 18613-18618
77. Rousseau, F., Schymkowitz, J. W. H., Sánchez delPino, M., and Itzhaki, L. S. (1998). *J. Mol. Biol.* **284**, 503
78. Chapman, E. J., and Estelle, M. (2009) Mechanism of auxin-regulated gene expression in plants. *Annual review of genetics* **43**, 265-285

79. Salehin, M., Bagchi, R., and Estelle, M. (2015) SCFTIR1/AFB-based auxin perception: mechanism and role in plant growth and development. *The Plant Cell* **27**, 9-19
80. Gray, W. M., Kepinski, S., Rouse, D., Leyser, O., and Estelle, M. (2001) Auxin regulates SCF(TIR1)-dependent degradation of AUX/IAA proteins. *Nature* **414**, 271-276
81. Middleton, A. M., King, J. R., Bennett, M. J., and Owen, M. R. (2010) Mathematical modelling of the Aux/IAA negative feedback loop. *Bull Math Biol* **72**, 1383-1407
82. Moss, B. L., Mao, H., Guseman, J. M., Hinds, T. R., Hellmuth, A., Kovenock, M., Noorassa, A., Lanctot, A., Villalobos, L. I., Zheng, N., and Nemhauser, J. L. (2015) Rate Motifs Tune Auxin/Indole-3-Acetic Acid Degradation Dynamics. *Plant Physiol* **169**, 803-813
83. Lavy, M., Prigge, M. J., Tigyi, K., and Estelle, M. (2012) The cyclophilin DIAGEOTROPICA has a conserved role in auxin signaling. *Development* **139**, 1115-1124
84. Ivanchenko, M. G., Zhu, J., Wang, B., Medvecká, E., Du, Y., Azzarello, E., Mancuso, S., Megraw, M., Filichkin, S., and Dubrovsky, J. G. (2015) The cyclophilin A DIAGEOTROPICA gene affects auxin transport in both root and shoot to control lateral root formation. *Development* **142**, 712-721
85. Zheng, L., Cedazo-Minguez, A., Hallbeck, M., Jerhammar, F., Marcusson, J., and Terman, A. (2012) Intracellular distribution of amyloid beta peptide and its relationship to the lysosomal system. *Transl. Neurodegener.* **1**, 19
86. Chen, Y., Yang, Q., Sang, S., Wei, Z., and Wang, P. (2017) Rice inositol polyphosphate kinase (OsIPK2) directly interacts with OsIAA11 to regulate lateral root formation. *Plant and Cell Physiology* **58**, 1891-1900
87. Cui, P., Liu, H., Ruan, S., Ali, B., Gill, R. A., Ma, H., Zheng, Z., and Zhou, W. (2017) A zinc finger protein, interacted with cyclophilin, affects root development via IAA pathway in rice. *Journal of integrative plant biology* **59**, 496-505
88. Yamamoto, T., Mori, Y., Ishibashi, T., Uchiyama, Y., Sakaguchi, N., Furukawa, T., Hashimoto, J., Kimura, S., and Sakaguchi, K. (2004) Characterization of Rad6 from a higher plant, rice (Oryza sativa L.) and its interaction with Sgt1, a subunit of the SCF ubiquitin ligase complex. *Biochemical and biophysical research communications* **314**, 434-439
89. Wang, R., Zhang, Y., Kieffer, M., Yu, H., Kepinski, S., and Estelle, M. (2016) HSP90 regulates temperature-dependent seedling growth in Arabidopsis by stabilizing the auxin co-receptor F-box protein TIR1. *Nature Communications* **7**, 10269
90. Wang, R., Zhang, Y., Kieffer, M., Yu, H., Kepinski, S., and Estelle, M. (2016) HSP90 regulates temperature-dependent seedling growth in Arabidopsis by stabilizing the auxin co-receptor F-box protein TIR1. *Nature communications* **7**, 1-11

91. Kadota, Y., Amigues, B., Ducassou, L., Madaoui, H., Ochsenbein, F., Guerois, R., and Shirasu, K. (2008) Structural and functional analysis of SGT1-HSP90 core complex required for innate immunity in plants. *EMBO Rep* **9**, 1209-1215
92. Tao, L.-z., Cheung, A. Y., Nibau, C., and Wu, H.-m. (2005) RAC GTPases in tobacco and Arabidopsis mediate auxin-induced formation of proteolytically active nuclear protein bodies that contain AUX/IAA proteins. *The Plant Cell* **17**, 2369-2383
93. Wu, H.-m., Hazak, O., Cheung, A. Y., and Yalovsky, S. (2011) RAC/ROP GTPases and auxin signaling. *The Plant Cell* **23**, 1208-1218
94. Fendrych, M., Akhmanova, M., Merrin, J., Glanc, M., Hagihara, S., Takahashi, K., Uchida, N., Torii, K. U., and Friml, J. (2018) Rapid and reversible root growth inhibition by TIR1 auxin signalling. *Nature plants* **4**, 453-459
95. Zhang, Y., Su, J., Duan, S., Ao, Y., Dai, J., Liu, J., Wang, P., Li, Y., Liu, B., and Feng, D. (2011) A highly efficient rice green tissue protoplast system for transient gene expression and studying light/chloroplast-related processes. *Plant methods* **7**, 1-14
96. Mathur, J., Koncz, C., and Szabados, L. (1995) A simple method for isolation, liquid culture, transformation and regeneration of Arabidopsis thaliana protoplasts. *Plant Cell Reports* **14**, 221-226
97. Chen, S., Tao, L., Zeng, L., VEGA-SANCHEZ, M. E., Umemura, K., and WANG, G. L. (2006) A highly efficient transient protoplast system for analyzing defence gene expression and protein–protein interactions in rice. *Molecular plant pathology* **7**, 417-427
98. COCKING, E. C. (2013) The enzymatic isolation of plant protoplasts: historical perspective. *Plant Protoplasts: International Review of Cytology, Vol. 16* **16**, 1
99. Datta, K., and Datta, S. K. (1999) Transformation of rice via PEG-mediated DNA uptake into protoplasts. in *Plant Cell Culture Protocols*, Springer. pp 335-347
100. Shen, J., Fu, J., Ma, J., Wang, X., Gao, C., Zhuang, C., Wan, J., and Jiang, L. (2014) Isolation, culture, and transient transformation of plant protoplasts. *Current protocols in cell biology* **63**, 2.8. 1-2.8. 17

CHAPTER 2

MATERIALS AND METHODS

Introduction

To study cis-specific protein interactions *in vivo* that regulate lateral root development in rice, this chapter presents investigations that strived to optimize protocols for obtaining and transfecting live rice plant cells (protoplasts). The procedures for rice shoot protoplast excision and transfection developed in this work have enabled confocal fluorescence microscopy studies of live cells that transiently express given proteins of interest fused to a fluorescent reporter protein. To determine the auxin-induced degradation rate of OsIAA11 and investigate its dependence on LRT2 activity, rice protoplasts isolated from shoots were transiently transfected with a fusion protein, OsIAA11-mVenus, containing OsIAA11 fused to the fluorescent reporter mVenus.

In general, methods for obtaining viable protoplasts have evolved over time. In 1892, Klerck was the first to isolate protoplasts (1). Presently, well-developed protocols for isolating protoplasts from *Arabidopsis thaliana* are available (2). Additionally, plant tissue culture for propagation, conservation, and improvement have been expanding methods for obtaining and utilizing protoplasts (3,4). In the past decade, protocols for isolating and transfecting rice protoplasts have been developed to become a common laboratory method. Many researchers have based their criteria for selection of protoplasts by identifying a round circular plasma membrane, indicating the cell wall had been destroyed (5). A number of techniques have been developed to extract, culture, and transfect protoplasts (6). Importantly, the poly-ethylene-glycol (PEG) based method for transfection with desired plasmid(s) provided a means of obtaining multiple

successfully transfected protoplasts at a low cost (7,8).

In this chapter, we first discuss the troubleshooting techniques that were done to obtain protoplasts from the roots of rice. However, rice root protoplasts were unable to survive transient transfection with our fluorescent proteins of interest. Therefore, the majority of this chapter discusses the modifications that were made to current protoplast isolation and transient transfection methods (9) that enabled their successful application to rice shoot tissues. The pEXSG-eYFP vector (gift from Hanson lab) that contains a p35S promoter was used to introduce the OsIAA11 gene by recombination LR reaction (Invitrogen). This vector was modified to insert each of our fusion proteins and fluorescent proteins of interest (Appendix, Fig 2.1). A vectorpUC57 was purchased from Genscript containing the gene for OsIAA11-Auxin-responsive gene family member (LOC_Os03g43400, Rice Genome Annotation Project, Michigan State University). The *Nipponbare* (*O. sativa, ssp. Japonica*) seeds were a gift from Bogdanove lab and purchased from U.S. National Plant Germplasm System (US NPGS).

A primary objective of this work was to determine the auxin-induced rate of OsIAA11 proteasomal degradation by fusing OsIAA11 to the rapidly folding fluorescent protein Venus. An additional objective of this study was to quantitatively measure the level of the peptidyl-prolyl isomerase (PPIase) lateral rootless 2 (LRT2/cyp2) protein by fusing it with a mCherry fluorescent protein. Previous research has identified that LRT2 is essential for the initiation of lateral root development in rice (10-12). At the end of this chapter, I will discuss the methods used for time-lapse imaging of rice protoplasts using confocal microscopy.

The advantage of rice root protoplasts would be that factors involved in lateral root development should be present. However, there are currently no published reports on rice root protoplasts. In the literature, root protoplasts have only been obtained from legume, corn, maize and *Arabidopsis* (2,13-16). The methodological approach taken in this study to obtain rice root protoplast is mainly based legume and *Arabidopsis* root protoplast methods (2,14,17). However, as described below, although a protocol was developed for isolation of root protoplasts, no attempts at transient transfection yielded viable root protoplasts. Therefore, efforts were shifted to focus on optimizing isolation and transfection protocols for rice shoot protoplasts.

In order to obtain rice shoot protoplast, modifications were made based on *Arabidopsis thaliana, Nicotiana tabacum, Brassica oleracea var. botrytis* protoplast protocols (9,18,19), but primarily following protocols to obtain rice shoot protoplasts (19). The first step in discussing the materials and methods needed for plant growth are the preparation of the plant material in order to extract protoplasts. Depending on the growth time (days) and conditions (rice plants grown in the dark or light) of the rice (*Oryza sativa*) spp. *Nipponbare*, minor modifications were made based on plant material need for the experiment (described in further detail below). One critical factor for obtaining protoplasts is the osmolarity of the prepared solutions. I will further describe in detail the methods and modifications that were optimized to obtain shoot protoplasts from rice plants.

Plant Growth for Protoplasts Preparation

In order to raise seedlings into rice plants in a controlled environment the seeds were grown in containers (magenta boxes) (figure 1). The magenta boxes are autoclaved for

twenty minutes and filled with 100mL of plant media from Murashige and Skoog medium (MS or MS0 (MS-zero)) (20). In 1962, the MS plant medium was invented by plant scientists Toshio Murashige and Folke K. Skoog (9). The MS plant medium is a well-known plant growth medium (Caisson Labs SKU: MSP09) containing various salts and B5 nutrients needed for plant growth and development (Table 1.0). Preparation of the ½MS media (4.44g in a total of 2 Liters) in 4 (500 mL) bottles. In a big beaker with stirring water (1.5 Liters), pour: 1 packet of Murashige & Skoog salts with Gamborg's Vitamins (referenced above) with the addition of 60 grams sucrose (30% total), pH at 5.8 with 1M KOH, divide the pH media into four (500mL of pH media) 500-mL bottles, and then add 3.5 grams of agar (0.7% total) to each bottle (Table 1.0) to autoclave the ½MS media for 15 minutes. The seed coat of the rice is removed with tweezers, while the media and boxes are being sterilized ~15 minutes. After the appropriate number of seeds are collected for each box, approximately 5-7 seeds per box, the seeds are then washed in 70% ethanol for one minute. They are then washed in <10% bleach for approximately half an hour. The seeds are then washed five times with sterile water to remove any remnants of bleach. After the ½MS media with agar has hardened then seeds are placed gently on top of the media with equal spacing between all of the seeds.

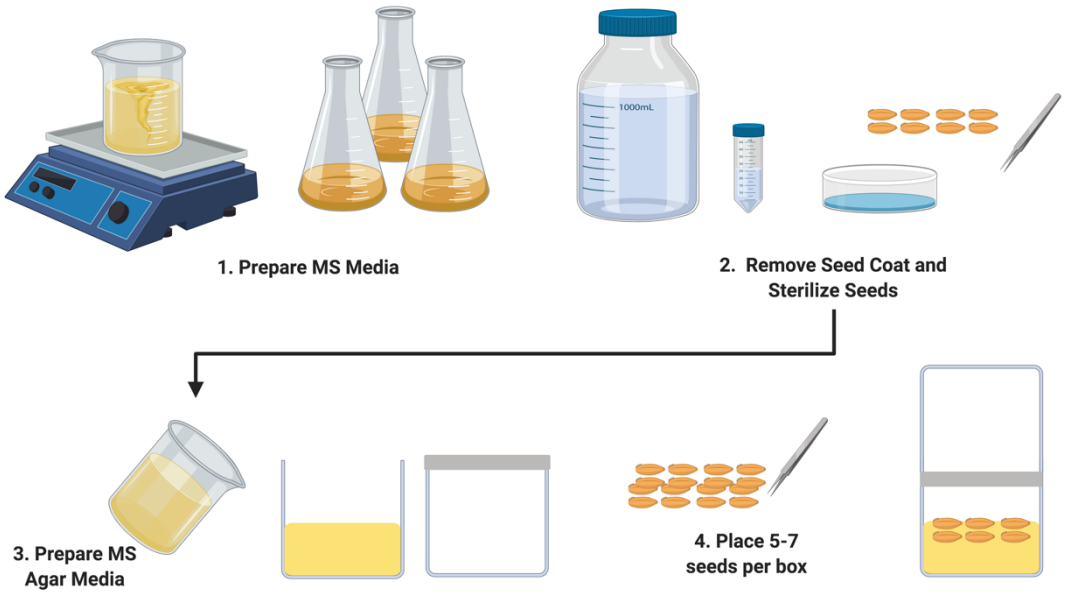

Figure 1. Planting *Oryza sativa cv. Nipponbare* (rice): Planting protocol for rice in order to obtain shoot and root protoplast. (please see text for more details)

Environmental Conditions of Plant Material

The seeds were transferred to a growth chamber with the following environmental settings: the rice plants were grown either in a light environmental chamber at 24°C for 12-16 days (16 hours light/8 hours dark cycle) (21) or placed in the dark around 28-30°C room for approximately 12-14 days in a dark chamber unless otherwise noted to obtain rice shoot protoplasts. In order to obtain rice root protoplasts, rice plants are harvested at approximately 6 days old from a room with temperature of 28–30°C. In order to test the difference between light and dark rice plants, two separate environmental chambers needed to be used. In addition, the rice shoot protoplasts isolated from plants grown in the light were more fragile compared to the rice protoplasts from plants grown in the dark. In order to work around this issue rice was grown in the light and the dark for only one week (19). The plants grown in the light

had more sensitivity to the PEG-transfection and therefore only needed 10 minutes of transient transfection time with the protein of interest. Also, the protoplasts that were obtained from rice plants grown for one week the buffers and reagents, except the Extraction buffer and PEG buffer were stored at -20°C, were made fresh for each protoplast transfection experiment in order to obtain a consistent number of more than $5x10^6$ cells/ml of shoot protoplasts (17,22). Further discussed in chapter 3, rice shoot protoplasts were primarily obtained from plants grown in the dark to avoid acquiring chloroplasts whose red fluorescence could potentially interfere with our red fluorescent protein signal.

Reagents and solutions

In order to begin the protoplast process, reagents need to be obtained to make sterile stock solutions (table 1.1). The buffer solutions made from the stock solutions were re-made fresh every 3 weeks (table 1.2-1.7) in order to sustain optimal osmolarity and were kept at 4 or -20°C (as indicated in the table) to prevent bacterial growth. However, the extraction buffer of shoot protoplasts requires specific enzymatic solutions (Table 1.3) which were kept at -20°C until needed in order to sustain enzymatic activity.

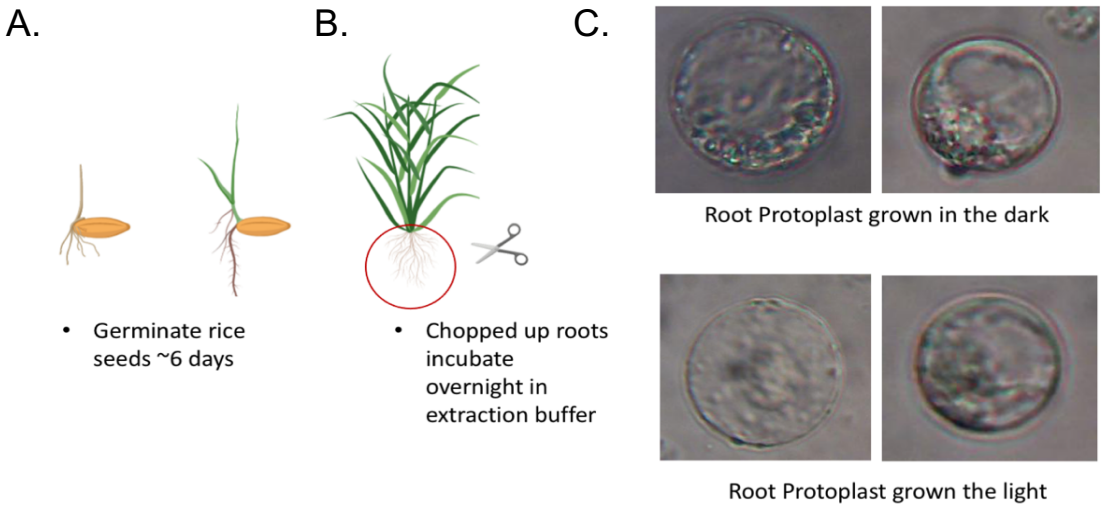

Figure 2. General root protoplast methods: **(A)** *Oryza sativa cv. Nipponbare* seeds were harvested ~6 days. **(B)** Chopped up roots were incubated overnight in extraction buffer (see main text for details). **(C)** Representative Images of root protoplast were obtained through a light microscope (Nikon TMS Inverted microscope).

Protocols for isolation and transfection of rice root protoplasts

The first step is to prepare the stock solutions and root extraction buffer (figure 2, table 1.2), which is made with W5 buffer (125 mM CaC12, 154 mM NaC1, 5 mM KC1, 5 mM glucose, 2 mM MES), 1.5% cellulase, 0.4% Macerozyme, 2mM Sucrose, 5mM MES at pH 5.7 and stored at 4°C . The extraction buffer solution is warmed up at 55°C for 10mins and then cooled slowly to room temperature. The root tissues are cut to around 1mm in 2ml of W5 buffer. The root tissue in W5 buffer is then incubated in 12ml of Extraction buffer solution overnight (12 to 14 hours) in the dark at room temperature (do not shake the solution). Using light microscopy, the root tissue and protoplast solution is then imaged the next day to make sure that the roots have digested

in the solution. The root tissue is gently grabbed by a large pair of tweezers to push protoplasts out by mechanical force, then the protoplasts were separated from plant debris by washing them with W5 solution ~10mL. The protoplasts solution (extraction buffer and W5 solution) was filtered through a 70μm nylon mesh into a 50mL conical tube (total 24ml of protoplast solution). The protoplast extraction solution is then gently centrifuged in a 50mL conical tube at 17g/317.5rpm in a swinging bucket rotor for 5 minutes at room temperature. A small visible pellet will be seen in the 50ml conical tube. The pellet is resuspended in 1 mL of MGG buffer (MGG buffer has 0.4M Mannitol with 15 mM MgCl2 and 4 mM MES (pH 5.7)). As anticipated, application of the above protocol yielded ~10,000 rice root protoplasts from rice plants grown in light and dark conditions at *28–30*°C (Figure 2). For DNA transfection, the root protoplast solution was separated into two 1.5mL centrifugation tubes for transient transfections (no DNA and OsIAA11-mVenus ~10-15 μg total). The DNA volume was raised to 20 μL with MGG Buffer (Table 1.5). The addition of 220 μL of protoplasts (~2, 200 root protoplasts) and 220 μL of 40% PEG buffer (40% PEG 4000, 0.2M Mannitol, 0.1M $CaCl_2$, Table 1.6) incubated at room temperature for 5 minutes and the side of the tube was tapped 3 times to mix the PEG buffer into the solution. Then the addition of 900 μL W5 buffer (Table 1.4) by gradually added by rocking the tube gently to stop the transfection process. Methods of collecting transiently transfected root protoplasts were attempted by modifying two different known root protoplasts methods (2,23). First, in Mathur et al. (1995) *Arabidopsis* root protoplasts methods, PEG-mediated DNA uptake had root protoplasts incubated for 5 minutes at room temperature 20-23°C and then pelleted by centrifugation at 17g/317.5rpm in a swinging bucket rotor. A pellet of root

protoplasts was not visible, but the addition of WI caused the solution to become cloudy indicating no viable protoplasts were obtained. Secondly, in Jia et al. (2018) legume root protoplast methods, we modified the root protoplasts protocol to collect transfected root protoplast by centrifuged using swinging-bucket rotor at 17g/317.5rpm at 4°C discarding the supernatant and re-suspending a visible pellet in 1mL of WI solution. However, many attempts resuspend the transiently transfect rice root protoplasts with our plasmids did not yield viable protoplasts. Further work will be required to determine how to successfully transiently transfect rice root protoplast. Due to the constraints of transfecting rice root protoplasts, this study utilized well established rice green tissue protoplasts protocols to obtain rice shoot protoplasts (21).

Harvesting and isolating rice shoot protoplasts

The first step in obtaining rice shoot protoplasts is to slowly pull the rice out of the MS agar media. The plants are then placed on a glass plate, where X-acto blades are used to isolate shoots from the roots and leaves. The shoots are then cut into approximately 0.5-1.0mm pieces and placed into 10 cm^2 dish. A 0.6M Mannitol solution is then added to wash the plant material. The Mannitol is removed and then replaced with approximately 10mL of extraction buffer. Vacuum infiltration is then performed using a vacuum pump at -15 to -20 mmHg. The dish containing the rice shoot materials and extraction buffer is placed with the lid of the container halfway off for 20 to 30mins, respectively. Next, digestion of the media in enzymatic solution is performed by gently shaking the protoplasts in the extraction buffer on an orbital plate (60-80 rpm) for 4 to 5 hours in the dark. The media is transferred through a 40 μm nylon mesh filter to get rid of any plant debris. The addition of W5 buffer (Table 1.4) to the solution then inhibits further

digestion (2,24). The residual plant material collected in 40 μm nylon mesh filter is compressed by mechanical force in order to release more media containing protoplasts. The media is centrifuged at approximately 1,111 RPM or 210xg for 5 minutes. The fragile pellet is obtained, and removal of the supernatant is done with a pipet. This process of adding W5 buffer and removing the supernatant is repeated 2 more times. Finally, the pellet is resuspended in an appropriate volume of MGG buffer (Table 1.5) to have $1x10^6$ protoplasts/mL (figure 3).

In obtaining viable protoplasts there are several sources of error. One source of error is the addition of solution to the protoplast media. It is important that the solution has the same osmolarity as the cytosol of the protoplasts (3). Another error is the amount of centripetal force (25) that is used to collect the pellet since protoplasts are very fragile. Also, removing the supernatant from the solution too quickly can damage the integrity of the plant cell membrane. Lastly, adding the new media to the exposed pellet should not be done directly over the protoplasts but pipetted along the side of the collection tube.

Transient transfection of rice shoot protoplasts

After protoplasts are obtained and resuspended in the appropriate volume of MGG buffer they are appropriately distributed in 200 μL or 400μL of $1x10^6$ protoplasts/mL, 10-30μg of DNA per sample is calculated (Table 1.8) and added to each protoplast sample. The protoplasts are transiently transfected with 40% Polyethylene glycol buffer (PEG) (Table 1.6). It is important to note that the PEG buffer was made fresh for optimal results. The protoplast sample with the DNA and PEG was incubated at room temperature for approximately 10-12minutes. The W5 Buffer was added to inhibit the

extraction buffer and to stop the DNA being transfection into the protoplasts. It is important to note that by changing the osmolarity of the solution and the protoplast would burst or collapse (17). The protoplasts are resuspended in 1.0mL or 0.5mL of WI buffer (Table 1.7). Protoplasts are then incubated on a poly-lysine dish overnight (~13-14 hours) at room temperature (unless noted in the dark at a 28-30°C room).

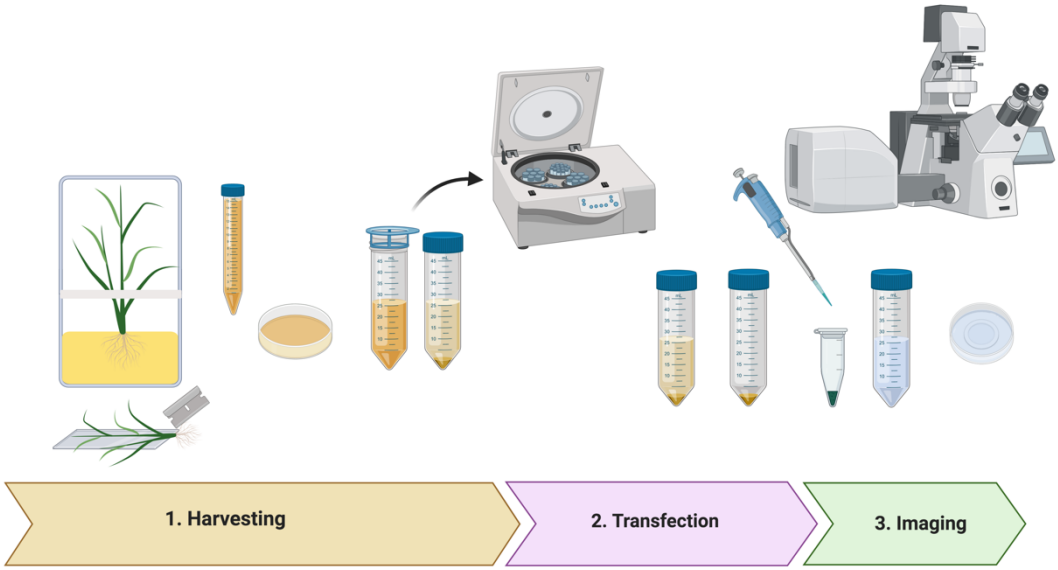

Figure 3. An Overview of rice protoplasts from shoots: **Step 1.** Harvesting rice plants, **Step 2.** Transiently transfecting protoplasts with fluorescent protein, **Step 3.** Imaging protoplasts under a fluorescent microscope (Please see main text for additional details).

Imaging of Rice Shoot Protoplasts

To measure the fluorescence intensity of our protein of interest in shoot protoplasts, confocal microscopy was used to obtain images of these transfected live plant cells over time (26,27). For time-lapse imaging many researchers have utilized bovine serum albumin (BSA), poly-lysine, and gelatin in the past in order to image live human cells (28,29). However, in some protoplast protocols, it is common to image these live plant

cells over a long period of time by coating the slides or dishes with poly-lysine (13,30,31). In order to test which coating would be more suitable for our rice shoot protoplasts we coated 35mm glass dishes with 1mg/mL of gelatin, BSA and Poly-D-lysine. Only the Poly-D-lysine coated dishes were able to keep the rice shoot protoplast stable when performing a cycloheximide chase (discussed in detail in a subsequent section). All the work in this dissertation was carried out coating the 35 mm glass bottom dish which was pre-coated for at least 1 hour with 1 ml of Poly-D-lysine hydrobromide concentration at 100 μg/mL (mol wt. 70,000, 150,000, and >300,000; Sigma P0899 and P1024). Excess poly-lysine was removed by washing the plates five times with sterile water. The plates were then dried overnight at room temperature. The protoplasts were incubated on these poly-lysine dishes (approximately 13-14 hours), which aided in preventing the protoplasts from moving out of focus(2). The Poly-D-lysine coat prevented the movement of protoplasts which otherwise would move around the dish in solution when on the microscope stage.

Using confocal microscopy, I was able to live image transient-transfected protoplasts expressing a modified yellow fluorescent protein Venus or mVenus, which is derived from *Aequorea* green fluorescent proteins, and the red fluorescent protein mCherry, which is derived from *Discosoma sp*. (plasmids prepared were OsIAA11mVenus, OsIAA17-Venus, OsIAA31-Venus, LRT2-mCherry, and OsTIR1-mCherry plasmids (32,33)(Appendix Fig. 2.1)). In Chapter 3, I will be displaying data obtained through the Zeiss Laser Scanning Microscope (LSM) 710 (34) and Perkin-Elmer Spinning Disc Confocal microscopes (SDCM) (35). Imaging using the LSM 710 was done on a 40x water immersion objective. The SDCM imaging was done on a 60x

oil immersion objective. Using both confocal microscopes I was able to capture a z-stack image (range of up to 40μm) of the protoplast, capturing the total fluorescence intensity from the nucleus which occasionally moved within the protoplast (36). Lastly, for temperature sensitive experiments the LSM 710 confocal microscope had a heater stage that could be set at 28°C and the SDCM had a heated chamber set to approximately 28°C.

Another important aspect to visualizing protoplasts using microscopy is the problem of photobleaching. The settings on the microscope have to be set so that the high intensity laser is able to sufficiently excite the chromophore within the fluorescent proteins while not photobleaching. Although minimal photobleaching is inevitable, as long as the settings are properly set then it is possible that a fluorescent protein can be imaged over time (37). First, the appropriate laser power needs to be determined, which is dependent on the signal, which in turn depends on the amount of fluorescent proteins in the sample. In order to control for photobleaching, the range indicator feature of the Zeiss 710 confocal microscope software was used to properly set the laser power and gain before each imaging session. As an additional preventative measure images were taken every 5 or 10 minutes at a laser power setting that gave sufficient fluorescence intensity.

Time Course Imaging

Proper laser intensity is an essential aspect of live-cell imaging with fluorescent proteins. First, the settings on the microscope should be set appropriately. The microscope's laser intensity should induce the most absorption of photons by and emission of photons from the fluorescent protein while not destroying the fluorescent

signal (photobleaching). As mentioned before, minimal amounts of photobleaching are inevitable, especially when live imaging cells over time (36). It is necessary to use the lowest laser intensity (but still capturing fluorescent signals) on the microscope to image a fluorescent protein for a long time (38). It was possible to identify round circular healthy protoplasts using confocal microscopy and look at the mVenus and mCherry fluorescent signal, which is consistent with images in the literature (10,39). In the next section, I explain the instruments used to collect the data. Data were recorded on two confocal microscopes: laser-scanning 710 Zeiss confocal microscope (belonging to BRC imaging facility-Zeiss 710) and a spinning disk Perkin-Elmer confocal microscope (belonging to Dr. Bill Brown).

Cycloheximide Chase

In order to initiate the proteasomal degradation of OsIAA proteins, auxin needs to be present in the cell to cooperatively bind along with the OsIAA substrate to the SCF^{TIR1} E3 ligase (40). For the purpose of obtaining the degradation rate of OsIAA11-mVenus, cycloheximide was also administered to protoplasts, which interferes with the translocation step in protein synthesis blocking translation (41,42). To perform a cycloheximide chase, a new 2.5mM cycloheximide stock solution and 5mM auxin (IAA) solution is made before each time course imaging session. Each cycloheximide chase was performed by simultaneously adding the cycloheximide and auxin (IAA) in 1 mL of WI buffer (final concentration 50μM cycloheximide and 20 μM auxin) to the 1ml of protoplast solution in the dish, which was already sitting on the microscope stage.

For temperature controlled cycloheximide chase of rice shoot protoplasts rice seeds were grown in the dark in an environmental chamber at 28-30°C. Rice shoot

protoplasts that were transiently transfected and incubated overnight at 28-30°C. Importantly, the rice shoot protoplasts were on the microscope in a temperature-controlled environment at 28-30°C.

Imaging analysis

After each of the protoplast time courses were performed, image analysis was done via ImageJ/Fiji software. Selection of each protoplast was made using region of interest (ROI). Two same size ROI's are generated, one for the fluorescent intensity in the nucleus (green channel) and one for the background intensity. This is an important step in order to obtain an accurate fluorescent measurement. Importantly, the same range (z-stack) in microns was measured for each protoplast, which varied with protoplast size. The integrated density was obtained from the ROI, which was calculated using the multi-measure plug-in (43). In Excel, the background was subtracted from the integrated density in order to obtain the fluorescence intensity. The fluorescence intensity was then plotted over time in Excel to analyze the protein of interest (OsIAA11mVenus or LRT2mCherry, further explained in Chapter 3).

Exponential decay calculations

In this dissertation, the degradation rate of OsIAA11mVenus was approximated using the exponential time constant tau (τ) by using the exponential decay equation:

$$\mathbf{y = Aexp(-t/\tau)}$$

In Excel, Solver was used to fit the data to the exponential equation and obtain the parameters A and τ, where y was the estimated fluorescent intensity left in the cell (obtained from last imaging time point), A was estimated as = the total amount of fluorescent intensity arbitrary units (a.u.), and t is the corresponding time point (results

are described in Chapter 3) (44).

Concluding Remarks

Protoplasts are a very useful platform to transfect different proteins into a live plant cell. Cycloheximide chase experiments with the simultaneous addition of auxin allows the degradation rate of transiently transfected OsIAA11-mVenus to be measured. (10,11,39,45) From rice shoots I was able to obtain at least 5 million protoplasts per harvest of 25-30 seeds. However, given the tissue heterogeneity of shoots, it is likely that there is significant heterogeneity among the extracted protoplasts. In theory, the more specific of a region that is collected from plants the less variety of protein machinery the protoplast will contain. Overall, obtaining root protoplast from rice is still a new area of research. Based on previous work from Arabidopsis protoplast protocols (13), we could extract protoplast from rice roots; however, we could not transiently transfect rice root protoplasts with our plasmids. Additionally, rice root protoplasts lack the advantage of obtaining an abundant number of protoplasts. In this dissertation, we utilized rice shoot protoplasts for their great ability to obtain an abundant protoplast(39).

Summary Tables of Protocols and Reagents:

Table 1.0 Rice Germination and Seedling Growth

Step	Detailed Instructions
1	Prepare 2 L of ½ **MS Media:** 4.44g in a total of 2 Liters in 4 (500 mL) bottles. In a big beaker with stirring water (1.5L), pour: 1 packet of Murashige & Skoog salts with Gamborg's Vitamins(20)with the addition of 60 grams sucrose (30% total), pH at 5.8 with 1M KOH, divide the pH media into 4 (500mL of pH media) 500-mL bottles, and then add 3.5 grams (total of 14 gram of agar or 0.7% total to each bottle). Add ~100mL of autoclaved ½ **MS Media** to pre-autoclaved rice growth containers. of Let the MS Media agar solidify overnight.
2	Sterilize and wash rice seeds.

3	Remove the seed coat.
4	Wash seeds in 70% ethanol for 1 minute.
5	Wash seeds in 15% commercial bleach for 30 minutes.
6	Rinse seeds in sterile H_2O five times.
7	Plant about 5-8 seeds in each rice growth container.
8	Place seeds on top of the MS Media agar in rice growth container.
9	Grow seedlings for two weeks (in the dark) at 28°C.

Table 1.1 Sterile Stock Solutions

0.8M Mannitol	72.87 g D(-) Mannitol into 500 mL H_2O	Sigma M1902
0.2M MES, pH 5.7	8.53 g MES into 200 mL H_2O, Adjust pH with 1M KOH	Fisher BP300
2M KCl	74.55 g KCl into 500 mL H_2O	Fisher P217
2M NaCl	58.44 g NaCl into 500 mL H_2O	Fisher S271
1M $CaCl_2$	29.40 g $CaCl_2$•$2H_20$ into 200 mL H_2O	Fisher C69
2M $MgCl_2$	40.66 g $MgCl_2$•$6H_20$ into 100 mL H_2O	Sigma M2670
1M Glucose	9 g Glucose into 50 mL H_2O	Alfa Aesar A16828
10% BSA	1 g BSA into 10 mL H_2O	Sigma A9418

Table 1.2 Root Protoplast Extraction Buffer (100 mL, Aliquot 10 mL, Store at 4°C)

1.5% Cellulase R10	1.5g	Yakult, Japan
0.75% Macerozyme R10	0.75g	Yakult, Japan
0.6 M D(-) Mannitol	75mL	
10 mM $CaCl_2$	1mL	
10 mM MES, pH 5.7	5mL	
0.1% BSA	1mL	

Table 1.3 Rice Shoot Protoplast Extraction Buffer (100 mL, Aliquot 10 mL, Store at -20°C)

1.5% Cellulase R10	1.5g	Yakult, Japan
0.75% Macerozyme R10	0.75g	Yakult, Japan
0.6 M D(-) Mannitol	75mL	
10 mM $CaCl_2$	1mL	
10 mM MES, pH 5.7	5mL	
0.1% BSA	1mL	

Table 1.4 W5 Buffer (1 L, Store at 4°C)

154 mM NaCl	77mL
125 mM $CaCl_2$	125mL
5 mM KCl	2.5mL
5 mM D(+) Glucose	1mL
2 mM MES, pH 5.7	5mL

Table 1.5 MGG Buffer (200 mL, Aliquot 10 mL, Store at 4°C)

0.4 M D(-) Mannitol	100mL
15 mM $MgCl_2$	1.5mL
4 mM MES, pH 5.7	4mL

Table 1.6 PEG Buffer (200 mL, Aliquot 1 mL, Store at -20°C)

40% PEG 4000	80g	Sigma 81240
0.2M D(-) Mannitol	50mL	
0.1M $CaCl_2$	20mL	

Table 1.7 WI Buffer (500 mL, Store at 4°C)

0.5 M D(-) Mannitol	31.25 mL
20 mM KCl	5mL
4 mM MES, pH 5.7	10mL

Table 1.8 Rice Shoot Protoplast Transfection

Step	Summary
1.	Add X μg total of DNA to separate 15 mL centrifuge tubes for each transfection. Raising the volume to 30 μL with MGG Buffer as necessary.
2.	Total DNA needed for OsIAA11, OsIAA17, and OsIAA31 is 10μg
3.	Total DNA needed for LRT2 is 15μg
4.	Add 200 μL of 1x10^6 protoplasts/mL to each Sample
5.	Add 230 μL of 40% PEG Buffer to each 15 mL centrifuge tubes and incubate at room temperature for 10-12min
6.	Add 900 μL W5 Buffer and centrifuge at (~1,111rpm) for 3 min and remove the supernatant *transfer to new centrifuge tube
7.	Resuspend cells in 1 mL WI buffer
8.	Transfer the protoplast into 60 mm dish (or one well of a 6-well plate)
9.	Incubate at room temperature in the dark for appropriate time needed (approximately 12-14 hours).

REFERENCES

1. Yancheva, S., and Kondakova, V. (2017) Plant Tissue Culture Technology: Present and Future Development. in *Bioprocessing of Plant In Vitro Systems* (Pavlov, A., and Bley, T. eds.), Springer International Publishing, Cham. pp 1-26
2. Mathur, J., Koncz, C., and Szabados, L. (1995) A simple method for isolation, liquid culture, transformation and regeneration of Arabidopsis thaliana protoplasts. *Plant cell reports* **14**, 221-226
3. Eriksson, T. (1977) Technical advances in protoplast isolation and cultivation. in *Plant Tissue Culture and its Bio-technological Application*, Springer. pp 313-322
4. Nanjareddy, K., Arthikala, M.-K., Blanco, L., Arellano, E. S., and Lara, M. (2016) Protoplast isolation, transient transformation of leaf mesophyll protoplasts and improved Agrobacterium-mediated leaf disc infiltration of Phaseolus vulgaris: tools for rapid gene expression analysis. *BMC biotechnology* **16**, 53
5. Vasil, I. K. (2008) A short history of plant biotechnology. *Phytochemistry Reviews* **7**, 387-394
6. COCKING, E. C. (2013) The enzymatic isolation of plant protoplasts: historical perspective. *Plant Protoplasts: International Review of Cytology, Vol. 16* **16**, 1
7. Lin, H.-Y., Chen, J.-C., and Fang, S.-C. (2018) A Protoplast Transient Expression System to Enable Molecular, Cellular, and Functional Studies in Phalaenopsis orchids. *Frontiers in Plant Science* **9**
8. Datta, K., and Datta, S. K. (1999) Transformation of rice via PEG-mediated DNA uptake into protoplasts. in *Plant Cell Culture Protocols*, Springer. pp 335-347
9. Zhang, Y., Su, J., Duan, S., Ao, Y., Dai, J., Liu, J., Wang, P., Li, Y., Liu, B., Feng, D., Wang, J., and Wang, H. (2011) A highly efficient rice green tissue protoplast system for transient gene expression and studying light/chloroplast-related processes. *Plant Methods* **7**, 30
10. Kang, B., Zhang, Z., Wang, L., Zheng, L., Mao, W., Li, M., Wu, Y., Wu, P., and Mo, X. (2013) OsCYP2, a chaperone involved in degradation of auxin-responsive proteins, plays crucial roles in rice lateral root initiation. *Plant J* **74**, 86-97
11. Jing, H., Yang, X., Zhang, J., Liu, X., Zheng, H., Dong, G., Nian, J., Feng, J., Xia, B., Qian, Q., Li, J., and Zuo, J. (2015) Peptidyl-prolyl isomerization targets rice Aux/IAAs for proteasomal degradation during auxin signalling. *Nat Commun* **6**, 7395
12. Zheng, H., Li, S., Ren, B., Zhang, J., Ichii, M., Taketa, S., Tao, Y., Zuo, J., and Wang, H. (2013) LATERAL ROOTLESS2, a cyclophilin protein, regulates lateral root initiation and auxin signaling pathway in rice. *Mol Plant* **6**, 1719-1721

13. Lee, M. H., Lee, Y., and Hwang, I. (2013) In vivo localization in Arabidopsis protoplasts and root tissue. *Methods Mol Biol* **1043**, 113-120
14. Jia, N., Zhu, Y., and Xie, F. (2018) An Efficient Protocol for Model Legume Root Protoplast Isolation and Transformation. *Frontiers in Plant Science* **9**
15. Ortiz-Ramírez, C., Arevalo, E. D., Xu, X., Jackson, D. P., and Birnbaum, K. D. (2018) An efficient cell sorting protocol for maize protoplasts. *Current protocols in plant biology* **3**, e20072
16. Roest, S., and Gilissen, L. (1989) Plant regeneration from protoplasts: a literature review. *Acta botanica neerlandica* **38**, 1-23
17. Yoo, S.-D., Cho, Y.-H., and Sheen, J. (2007) Arabidopsis mesophyll protoplasts: a versatile cell system for transient gene expression analysis. *Nature protocols* **2**, 1565
18. Priyadarshani, S. V. G. N., Hu, B., Li, W., Ali, H., Jia, H., Zhao, L., Ojolo, S. P., Azam, S. M., Xiong, J., Yan, M., Ur Rahman, Z., Wu, Q., and Qin, Y. (2018) Simple protoplast isolation system for gene expression and protein interaction studies in pineapple (Ananas comosus L.). *Plant methods* **14**, 95-95
19. Page, M. T., Parry, M. A., and Carmo-Silva, E. (2019) A high-throughput transient expression system for rice. *Plant, cell & environment* **42**, 2057-2064
20. Murashige, T., and Skoog, F. (1962) A revised medium for rapid growth and bio assays with tobacco tissue cultures. *Physiologia plantarum* **15**, 473-497
21. Zhang, Y., Su, J., Duan, S., Ao, Y., Dai, J., Liu, J., Wang, P., Li, Y., Liu, B., and Feng, D. (2011) A highly efficient rice green tissue protoplast system for transient gene expression and studying light/chloroplast-related processes. *Plant methods* **7**, 1-14
22. Li, Z., Burow, M. D., and Murai, N. (1990) High frequency generation of fertile transgenic rice plants after PEG-mediated protoplast transformation. *Plant Molecular Biology Reporter* **8**, 276-291
23. Jia, N., Zhu, Y., and Xie, F. (2018) An efficient protocol for model legume root protoplast isolation and transformation. *Frontiers in plant science* **9**, 670
24. Chen, S., Tao, L., Zeng, L., VEGA-SANCHEZ, M. E., Umemura, K., and WANG, G. L. (2006) A highly efficient transient protoplast system for analyzing defence gene expression and protein–protein interactions in rice. *Molecular plant pathology* **7**, 417-427
25. Pasternak, T. P., Prinsen, E., Ayaydin, F., Miskolczi, P., Potters, G., Asard, H., Van Onckelen, H. A., Dudits, D., and Fehér, A. (2002) The Role of auxin, pH, and stress in the activation of embryogenic cell division in leaf protoplast-derived cells of alfalfa. *Plant physiology* **129**, 1807-1819
26. Birnbaum, K., Jung, J. W., Wang, J. Y., Lambert, G. M., Hirst, J. A., Galbraith, D. W., and Benfey, P. N. (2005) Cell type–specific expression profiling in plants via cell sorting of protoplasts from fluorescent reporter lines. *Nature Methods* **2**, 615-619
27. Guo, J., Morrell-Falvey, J. L., Labbé, J. L., Muchero, W., Kalluri, U. C., Tuskan, G. A., and Chen, J.-G. (2012) Highly Efficient Isolation of Populus Mesophyll Protoplasts and Its Application in Transient Expression Assays. *PLOS ONE* **7**, e44908

28. Sameni, M., Moin, K., and Sloane, B. F. (2000) Imaging proteolysis by living human breast cancer cells. *Neoplasia* **2**, 496-504
29. Sharma, V. P., Entenberg, D., and Condeelis, J. (2013) High-resolution live-cell imaging and time-lapse microscopy of invadopodium dynamics and tracking analysis. *Methods in molecular biology (Clifton, N.J.)* **1046**, 343-357
30. Vaňková, R., and Bornman, C. H. (1987) Immobilization of plant protoplasts on solid supports. *Physiologia Plantarum* **70**, 1-7
31. Isner, J.-C., and Maathuis, F. J. (2013) In Vivo Imaging of cGMP in Plants. in *Cyclic Nucleotide Signaling in Plants*, Springer. pp 57-65
32. Rekas, A., Alattia, J.-R., Nagai, T., Miyawaki, A., and Ikura, M. (2002) Crystal structure of venus, a yellow fluorescent protein with improved maturation and reduced environmental sensitivity. *Journal of biological chemistry* **277**, 50573-50578
33. Nagai, T., Ibata, K., Park, E. S., Kubota, M., Mikoshiba, K., and Miyawaki, A. (2002) A variant of yellow fluorescent protein with fast and efficient maturation for cell-biological applications. *Nature biotechnology* **20**, 87-90
34. Huff, J. (2015) The Airyscan detector from ZEISS: confocal imaging with improved signal-to-noise ratio and super-resolution. *Nature methods* **12**, i-ii
35. Wang, E., Babbey, C., and Dunn, K. W. (2005) Performance comparison between the high-speed Yokogawa spinning disc confocal system and single-point scanning confocal systems. *Journal of microscopy* **218**, 148-159
36. Gräf, R., Rietdorf, J., and Zimmermann, T. (2005) Live cell spinning disk microscopy. in *Microscopy techniques*, Springer. pp 57-75
37. St. Croix, C. M., Shand, S. H., and Watkins, S. C. (2005) Confocal microscopy: comparisons, applications, and problems. *Biotechniques* **39**, S2-S5
38. Wayne, R. O. (2019) Light and video microscopy. Academic Press
39. Zhu, Z.-X., Liu, Y., Liu, S.-J., Mao, C.-Z., Wu, Y.-R., and Wu, P. (2012) A gain-of-function mutation in OsIAA11 affects lateral root development in rice. *Molecular Plant* **5**, 154-161
40. Gray, W. M., Kepinski, S., Rouse, D., Leyser, O., and Estelle, M. (2001) Auxin regulates SCF(TIR1)-dependent degradation of AUX/IAA proteins. *Nature* **414**, 271-276
41. Siegel, M. R., and Sisler, H. D. (1963) Inhibition of protein synthesis in vitro by cycloheximide. *Nature* **200**, 675-676
42. Schneider-Poetsch, T., Ju, J., Eyler, D. E., Dang, Y., Bhat, S., Merrick, W. C., Green, R., Shen, B., and Liu, J. O. (2010) Inhibition of eukaryotic translation elongation by cycloheximide and lactimidomycin. *Nature chemical biology* **6**, 209-217
43. Ferreira, T., and Rasband, W. (2012) ImageJ user guide. *ImageJ/Fiji* **1**, 155-161
44. McGraw-Hill. (1987) *McGraw-Hill Encyclopedia of Science & Technology*, McGraw-Hill Book Company

45. Chen, Y., Yang, Q., Sang, S., Wei, Z., and Wang, P. (2017) Rice inositol polyphosphate kinase (OsIPK2) directly interacts with OsIAA11 to regulate lateral root formation. *Plant and Cell Physiology* **58**, 1891-1900

CHAPTER 3

FACTORS INFLUENCING OSIAA11 DEGRADATION IN RICE SHOOT PROTOPLASTS

Abstract

In *Oryza sativa* (Asian rice), the phytohormone auxin regulates the expression of OsIAA11, an auxin/indoleacetic acid (Aux/IAA) transcription repressor protein involved in lateral root initiation. In the absence of auxin, OsIAA11 inhibits its own expression, as well as that of other genes involved in lateral root initiation. When auxin is present, the cis isomer of a conserved prolyl peptide bond in OsIAA11 binds to an E3 ubiquitin ligase, facilitating proteasomal degradation of OsIAA11. Depletion of OsIAA11 activates the expression of the genes it represses, including its own gene, creating an auxin-responsive negative feedback circuit. This cis-specific degradation pathway involves a peptidyl-prolyl isomerase (PPIase), lateral rootless 2 (LRT2), which catalyzes isomerization of OsIAA11 and is essential for lateral root development. In order to determine the auxin-induced degradation rate of OsIAA11 and investigate its dependence on LRT2 activity, rice protoplasts isolated from shoots were transiently transfected with a fusion protein, OsIAA11-mVenus, containing OsIAA11 fused to the fluorescent reporter mVenus. Cycloheximide, an inhibitor of protein translation, and auxin were added and Venus fluorescence in protoplasts was monitored over time by confocal fluorescence microscopy. Initial experiments performed at room temperature showed inconsistent results. In a small subset of protoplasts, OsIAA11-mVenus exhibited exponential decay with a time constant of approximately 33 to 39 minutes.

However, in a majority of protoplasts the fluorescence signal did not significantly decay. Co-transfection with LRT2-mCherry showed no significant effect on OsIAA11-mVenus degradation. More consistent results were obtained by maintaining protoplasts at 29°C during post-transfection incubation and imaging periods and imaging at 13–14.5 hours post-transfection. These results suggest that factor(s) necessary for OsIAA11 degradation in shoot protoplasts might be regulated by temperature, and that the known role of Hsp90 in stabilizing the TIR1 E3 ligase machinery in *Arabidopsis thaliana* might also be important in *Oryza sativa*.

Introduction

In Asian rice, *Oryza Sativa*, there are 31 Aux/IAA proteins involved in a plant's auxin response (1-4). The indole-3-acetic acid (OsIAA) number eleven (OsIAA11) represses genes involved with lateral root development by binding to and inhibiting a transcription activator of the auxin responsive factor (ARF) family(5,6). In the presence of auxin, OsIAA11 is released from the ARF, binds to auxin and the TIR component of the SCR TIR1 E3 ubiquitin ligase complex (7-11). Binding of OsIAA11 to TIR1 and auxin is mediated by a sequence motif in OsIAA11, referred to as the degron motif. The interaction requires the cis-conformation of a Trp-Pro peptide bond within the degron motif. OsIAA11 is then ubiquitinated and irreversibly degraded via the proteasome (8). In the rice, there is an equilibrium of cis-trans isomers of OsIAA11, which is maintained by lateral rootless2 (LRT2)(1,4). In the Auxin Circuit, rapid maintenance of equilibrium is needed as OsIAA11 is being depleted by proteasomal degradation upon the addition of auxin (see chapter 1, figure 1). Without maintenance of this equilibrium, only the cis form of the protein would be depleted, and the rest of OsIAA11 would repress gene

transcription, therefore no lateral roots would be present The negative feedback loop is quantifiable by the expression of a given protein of interest, such as OsIAA11, fused with a fluorescent reporter protein.

The auxin negative feedback circuit points to the key role of an Aux/IAA protein degradation rate in a dynamic circuit. Molecular circuits can be mathematically modeled, similar to a simple predator-prey relationship, using differential equations to gain insight and predictive power by identifying factors that influence circuit dynamics. For example, recent work has modeled a negative feedback loop in regulatory circuits of gene transcription (8,12,13). The negative feedback loop is the expression of a given gene that is then repressed by its own protein product. Previous research has established that the sensitivity of the circuit dynamics to parameters in the negative feedback loop include the repressor proteins degradation rate (14). As previously described above, the auxin circuit is the ideal model for this type of negative feedback loop. Recent mathematical modeling of the auxin circuit has provided information regarding the sensitivities to the specific auxin circuit components as well as the theoretical framework aiding in the understanding of experimental data(12,14). This dissertation investigates the degradation rate of a specific Aux/IAA protein, OsIAA11, which is essential for lateral root development in rice (6).

The Aux/IAA protein degradation rate plays a critical role in the auxin circuit dynamics. Experimental research using *Arabidopsis thaliana* genes in yeast that creates a partial auxin signaling circuit supports the inference that the Aux/IAA degradation rate plays central role on the circuit dynamics, which extends to the phenotype level (15-19). In that work, yeast was used as a tool for quantifying individual components

response to auxin by using a "forward" auxin response circuit, meaning there is no negative feedback loop (19). In this system, researchers identified "rate motifs" flanking the degron motif. However, these "rate motifs" cause broad variability in the degradation rates of Aux/IAA proteins across different organisms. In particular, *Arabidopsis* has been used as a model organism to study Aux/IAA family members (19). In previous studies on *Arabidopsis,* the Aux/IAA protein IAA14 was shown to determine the timing of lateral root development. Taken together, these studies illustrate that Aux/IAA proteins serve as an auxin-regulated timer. Understanding the direct link between the rate of proteasomal degradation of Aux/IAA proteins and the organism level phenotype, such as lateral roots, will help provide information to coordinate developmental stages within the framework of the whole plant (20). However, missing from these groundbreaking studies was the potential role of *cis-trans* isomerization of the conserved Trp-Pro sequence in the Aux/IAA protein degron motif, which could serve as a fundamental timing device in the proteasomal degradation of Aux/IAA proteins.

In rice, the Aux/IAA protein OsIAA11 and LRT2 are associated with an equivalent step in lateral root development. This has been previously observed by mutagenizing seedlings and screening for the lateral rootless phenotype (i.e., nonappearance of lateral roots). Using such screens, LRT2 (lrt2, cyp2-1, and cyp2-2) and OsIAA11 (Osiaa11) mutants were identified as displaying a lateral rootless phenotype in rice. The corresponding LRT2 mutations were identified as a 50-base pair deletion in the LRT2 gene (lrt2), a premature stop codon that truncates LRT2 by 21 residues (cyp2-1), and a single amino acid substitution G72A (cyp2-2)(4). The lrt2

mutant indicated that LRT2 plays a regulatory role in lateral root initiation and redial cell management by exhibiting no patterned cell division for lateral root initiation. The cyp2-1 displayed a role in lateral root development by having the process blocked prior to the first asymmetric anticlinal division, leading to the conclusion that LRT2's catalytic activity controls lateral root development in initiation and patterning stages. Importantly, the OsIAA11 mutant strain, which has the P106L mutation, (in the degron sequence adjacent to the W_{104}-P_{105} peptide bond (fig.1A)) displays no induction or development of lateral roots. Drawing upon the research above, this study attempts to explore the degradation rate of OsIAA11, which is dependent on the direct and specific LRT2-catalyzed isomerization of the OsIAA11 degron sequence in rice.

The stability of Aux/IAA protein OsIAA11 is directly regulated by the cyclophilin LRT2 in rice. The prolyl *cis-trans* isomerase enzymes, cyclophilins, are

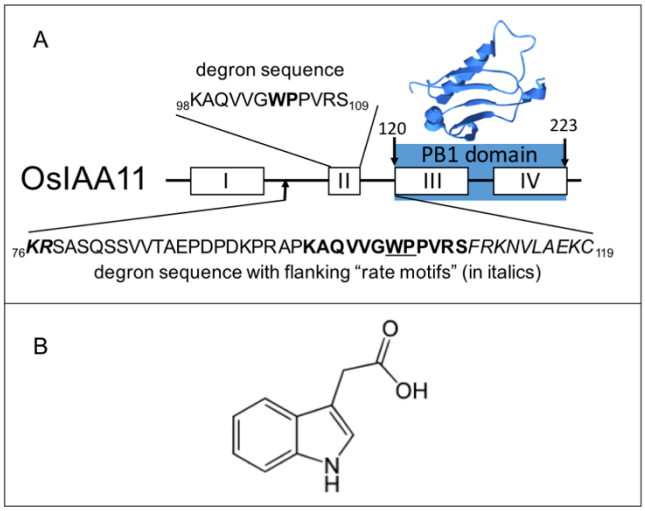

Figure 1. Central components of this study. **(A)** Diagram of OsIAA11 domains I-IV, with the domain III-IV structure (the PB1 domain) and degron sequence displayed above (W_{104}-P_{105} highlighted in bold), and flanking rate motifs shown below (in italics). **(B)** The most common naturally-occurring auxin, indole-3 acetic acid (IAA).

present in biological systems from bacteria to humans. Originally, cyclophilins were thought to only be involved in protein folding. However, cyclophilins have emerged as being involved in many biological processes, such as signal transduction, intracellular trafficking, gene transcription, and cell cycle regulation (21-23). Research to date has not yet determined the mechanisms by which the rate of peptide bond isomerization regulates a given biological process. Understanding the mechanism requires the ability to alter the isomerization rate and observe its effect on a biological process. As described above, cyclophilin LRT2 and the Aux/IAA protein OsIAA11 have been independently linked to the lateral rootless phenotype in *Oryza sativa*(5). LRT2 and OsIAA11 have been shown to be an enzyme/substrate pair that regulates lateral root development through LRT2-mediated regulation of OsIAA11 (4,24). Investigators used *lrt2* (50-bp deletion) and cyp2-2 (G72A) mutant strains providing "off" or "nearly off" states, respectively, of LRT2 compared to wild-type. However, the determination of the quantitative relationship between the isomerization rate of LRT2 and the auxin circuit dynamics of OsIAA11 have not been addressed.

This chapter will describe the results we obtained utilizing rice shoot protoplasts to investigate the degradation rate of OsIAA11-mVenus with and without co-transfection with LRT2-mCherry. We also examined the effects of growing plants in light versus dark conditions, which does not influence the nuclear localization of OsIAA11 or LRT2 or the degradation rate of OsIAA11. Non-native nuclear localization signal (NLS) is not needed for the nuclear localization of OsIAA11 or LRT2. Importantly, the mutation of Venus to generate a monomeric form is necessary for eliminating the observation of nuclear protein bodies (NPBs). The degradation rate of

OsIAA11 is not altered by the co-transfection with LRT2. Interestingly, investigation of the effect of temperature an OsIAA11 degradation rate revealed that at 28–30 °C many more protoplasts displayed OsIAA11 degradation. This result is consistent with Hsp90 being involved with Aux/IAA protein degradation in rice, as was found in Arabidopsis (25). The amount of time elapsed post-transfection is also found to be a variable that influences the detection of OsIAA11 degradation during cycloheximide chase experiments. This possibly reflects a balance between having sufficient fluorescence signal as the constitutively expressed OsIAA11 builds up, and potentially overloading the proteasomal machinery if cycloheximide chase experiments are started at later times.

Results

Initial characterization of transfected OsIAA11-mVenus and LRT2-mCherry confirmed nuclear localization in rice shoot protoplasts.

The cell wall is a fundamental feature of a plant cell critical for overall cell and vascular tissue structure. When the plant cell wall is removed, the plasma membrane serves as the sole boundary between the inside and outside of a cell, resulting in a spherical protoplast and enabling the use of standard transfection techniques to deliver DNA plasmids to the cell interior. For the work described in this chapter, in which transfection of rice cells is essential, it was necessary to obtain significant numbers of viable protoplasts. As described in chapter 2, we developed protocols for a robust extraction of protoplasts from rice shoots and for subsequent transfection. Significant effort was also devoted to optimizing protoplast extraction from roots, and although protoplasts were obtained, they did not withstand transfection. Therefore, rice shoot protoplasts

were used for all studies presented here.

In order to detect the levels of OsIAA11 and LRT2 proteins in rice shoot protoplasts, vectors were constructed for OsIAA11 fused to the rapidly folding fluorescent protein Venus (26,27) and for LRT2 fused to mCherry (28). Expression from both vectors is driven by the p35s constitutive promoter, and both vectors were made with and without an additional nuclear localization signal (NLS) (fig. 2). A non-native NLS was initially included in each vector to ensure proper localization of both proteins to the nucleus where the auxin gene regulation circuit operates (fig.2). However, since it is possible that a non-native NLS could introduce unintended effects, both vectors were also constructed without the additional NLS (Appendix Figure 2.1).

Although it is standard to perform studies on Aux/IAA proteins in protoplasts obtained from etiolated shoots (i.e., from the shoots of plants grown in the dark) (29-32), it is possible that factors necessary for a given process might only be produced under light conditions (33). To investigate the potential influence of light on the expression and intracellular localization of OsIAA11, protoplasts extracted from plants grown in the light and from plants grown in the dark (etiolated) were imaged on a Zeiss 710 confocal microscope (figs. 2 and 3). Protoplasts without transfection that were grown in the light show the chlorophyll present (red) whereas protoplasts grown in the dark are missing this feature (fig. 3A). Protoplasts transfected with the OsIAA11-Venus-NLS that were grown in the light show the chlorophyll present (red) and the nucleus (green) confirming the nuclear location of OsIAA11-Venus-NLS plasmid. Similarly, the fusion protein OsIAA11-Venus-NLS localized to the nucleus in transfected protoplasts extracted from plants grown in dark conditions (fig. 3B).

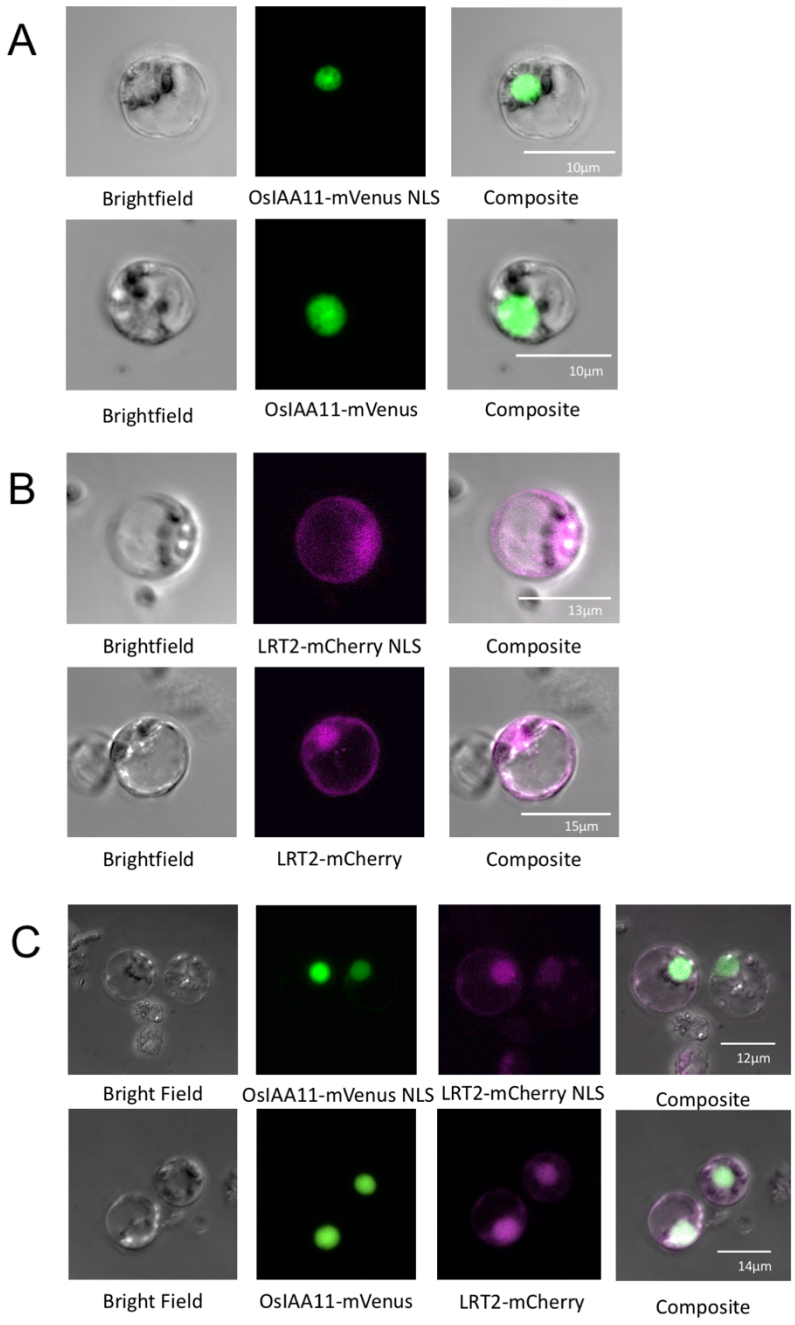

Figure 2: **Rice Shoot protoplasts expressing fusion proteins with and without the nuclear localization signal (NLS).** (**A)** OsIAA11-mVenus (green) was excited at 488nm and emission was detected at 520nm. **(B)** LRT2-mCherry (magenta) was excited at 561nm and emission was detected at 597 nm. **(C)** OsIAA11-mVenus and LRT2-mCherry were co-transfected in rice shoots. The resolution of images shown in A – C was 0.264µm.

These results show that OsIAA11-Venus-NLS localized to the nucleus of rice shoot protoplasts extracted from plants grown in both light and dark conditions and serve as an initial characterization of our fusion protein (fig 2).

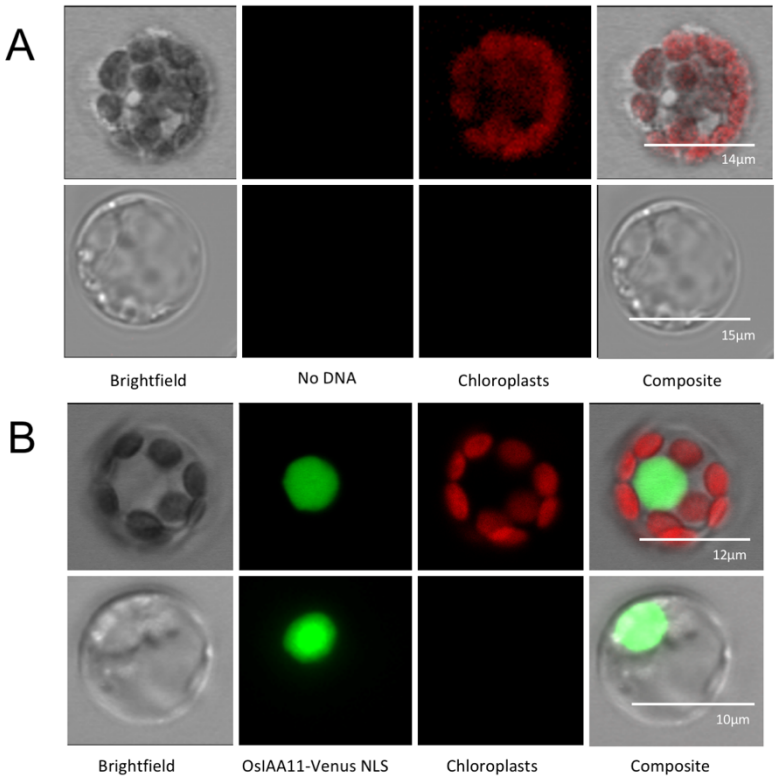

Figure 3: **Rice shoot protoplast transiently transfected with OsIAA11-Venus in plants grown in the light and etiolated (dark-grown) plants. (A)** Rice shoot protoplasts grown in the light (top row) and the dark (bottom row) transiently transfected with 0.2mM MES buffer (control-no DNA present). **(B)** Rice shoot protoplast grown in the light (top row) and the dark (bottom row) with transiently transfected OsIAA11-Venus (DNA plasmid in 0.2mM MES buffer). Green channels were excited and emitted at 488nm and 520nm, respectively. Chloroplasts (Chlorophyll A) were excited and emitted at 684nm and 633nm. The resolution of images shown in A – B was 0.264µm.

Existing studies of Aux/IAA proteins in protoplasts commonly employ plant plasmids containing a nuclear localization signal added onto the native protein sequence (34). However, Aux/IAA proteins contain a native nuclear localization signal (20,35).

To ensure that the NLS tag was not interfering with OsIAA11-Venus expression or degradation by the proteasome, the NLS tag was removed. Nuclear localization of OsIAA11-Venus is observed in protoplasts transfected with either OsIAA11-Venus-NLS or OsIAA11-Venus plasmids, demonstrating that the additional NLS is not needed for this fusion protein to properly localize (fig. 2A). Similarly, the fusion protein LRT2-mCherry is mainly localized to the nucleus and located in some areas of the plasma membrane and cytosol independent of the added NLS (fig. 2B). When rice shoot protoplasts were co-transfected with OsIAA11-mVenus and LRT2-mCherry, again the nuclear localization of both fusion proteins shows no dependence on the added NLS (fig. 2C). Notably, the nuclear localization of LRT2-mCherry is enhanced when protoplasts are co-transfected with OsIAA11-mVenus, which is consistent with *in vivo* interaction of OsIAA11 and LRT2 (comparison of figs.2B and 2C). Overall, the removal of the NLS did not change the nuclear localization of OsIAA11-Venus and LRT2-mCherry, and a larger fraction of the whole cell LRT2-mCherry signal is in the nucleus when OsIAA11 is abundant (fig. 2). In conclusion, OsIAA11-mVenus localized to the nucleus in dark shoot protoplasts (Appendix figure 3.1).

Initial characterization of rice shoot protoplasts transfected with OsIAA17 and OsIAA31.

In order to perform initial characterizations of other OsIAA proteins that might display different degradation rates, the fusion proteins OsIAA17-Venus and OsIAA31-Venus were also imaged in protoplasts with and without co-transfection of LRT2-mCherry. Both OsIAA17-Venus and OsIAA31-Venus contain the additional NLS. Indeed, both

OsIAA17-Venus-NLS and OsIAA31-Venus-NLS localized to the nucleus of shoot

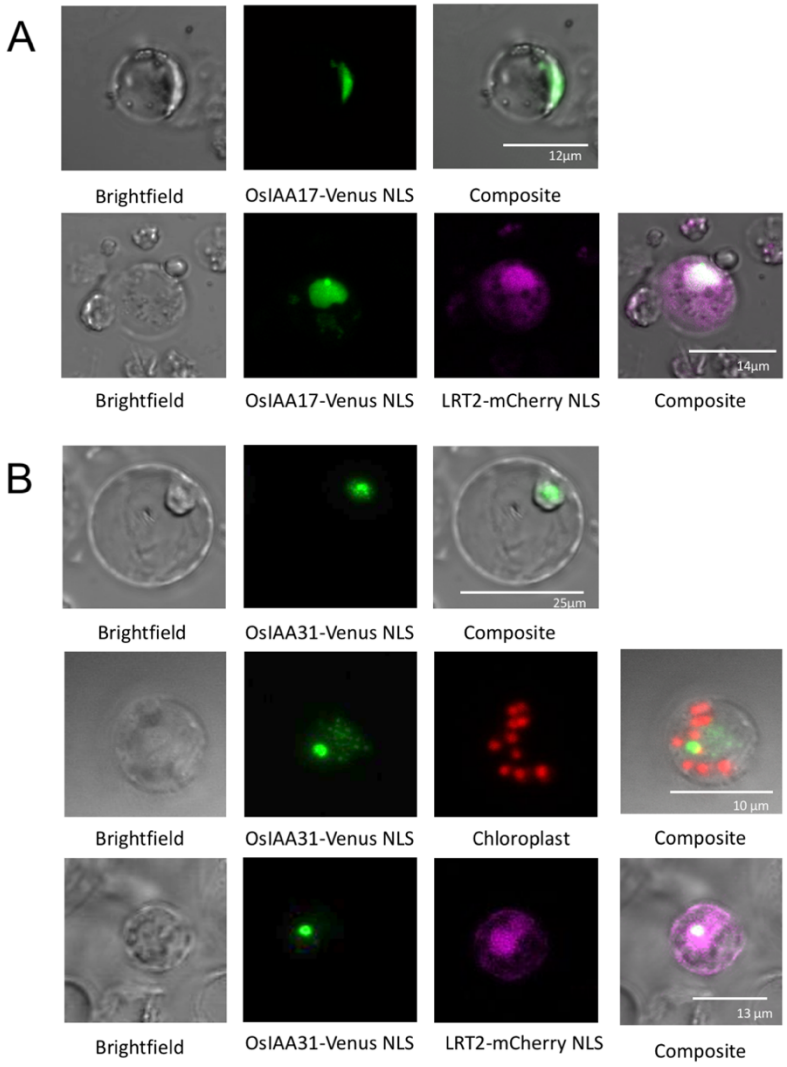

Figure 4: Rice shoot protoplast transfected with OsIAA proteins. (A) OsIAA17-Venus (green) channels were excited at 488nm and 520nm, respectively (top row). OsIAA17-Venus and LRT2-mCherry were co-transfected in rice shoot protoplasts. LRT2-mCherry (magenta) channels were excited at 561nm and 597 nm (bottom row). **(B)** OsIAA31-Venus (green) channels were excited and emitted at 488nm and 520nm, respectively (top row). Chlorophyll A (red) channels excited and emitted at 633 and 685, respectively (middle row). OsIAA31-Venus and LRT2-mCherry were co-transfected in rice shoot protoplasts.LRT2-mCherry (magenta) channels were excited at 561nm and 597 nm, respectively (bottom row). The resolution of images shown in A – B was 0.264µm. Protoplasts were imaged using a Zeiss 710 confocal fluorescence microscope with a 40x objective.

protoplasts that were grown in the dark for approximately 12–14 days (fig. 4A, B). As described above, LRT2-mCherry was confirmed to be localized to the nucleus, cytosol, and plasma membrane of rice shoot protoplasts grown in the dark for approximately 14

days (fig. 2). However, rice shoot protoplasts grown in the dark and co-transfected with either OsIAA17-Venus-NLS or OsIAA31-Venus-NLS and LRT2-mCherry showed significantly less colocalization of LRT2 with these OsIAA proteins, as compared with the corresponding OsIAA11 colocalization with LRT2 (fig. 2C).

Time course imaging of endogenous OsIAA11 with Auxin.

The OsIAA11 endogenous promoter contains an auxin responsive element (ARE) that regulates the expression of OsIAA11 in response to auxin (36). In order to mathematically model the auxin circuit, we needed to obtain the degradation rate of OsIAA11 *in vivo*. To investigate the auxin-circuit negative feedback loop we obtained confocal fluorescence microscopy images over time of protoplasts transiently expressing the protein OsIAA11-Venus whose expression was driven from an endogenous promoter. However, only one protoplast was observed expressing OsIAA11-Venus at a post-transfection time of 24hours. Upon the addition of auxin (20μM), one protoplast expression OsIAA11-Venus was observed with a gradual decrease in OsIAA11mVenus fluorescent intensity.

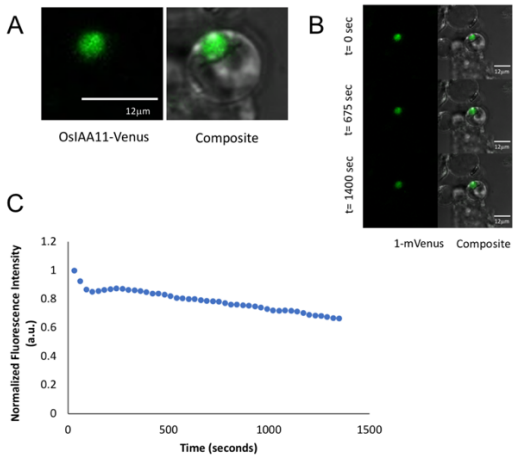

Figure 5: Time course imaging of transiently expressed OsIAA11-mVenus with the endogenous promoter in shoot derived protoplasts. (A) Confocal fluorescence microscopy image of protoplast at t=0 (the time at which 20µM auxin was added). **(B)** Confocal fluorescence microscopy images at three representative time points. **(C)** Time dependence of the observed fluorescence signal of monomeric OsIAA11-mVENUS in rice green tissue protoplasts after addition of auxin at t=0. OsIAA11-Venus (green) channels were excited at 488nm and 520nm, respectively. Temperature was not controlled, and auxin was added, and imaging began at post-transfection time of 24 hours.

Observation of nuclear protein bodies (NPB) is dependent on dimerization of Venus.

Interestingly, "nuclear protein bodies" (NPB) were observed in the nucleus of some protoplasts transfected with OsIAA11-Venus, OsIAA17-Venus, and OsIAA31-Venus (fig. 6). This feature was previously observed for AtIAA17-green fluorescent protein (GFP) expressed in Tobacco and Arabidopsis protoplasts, where the "nuclear protein bodies" (NPB) concept was introduced (36-38).

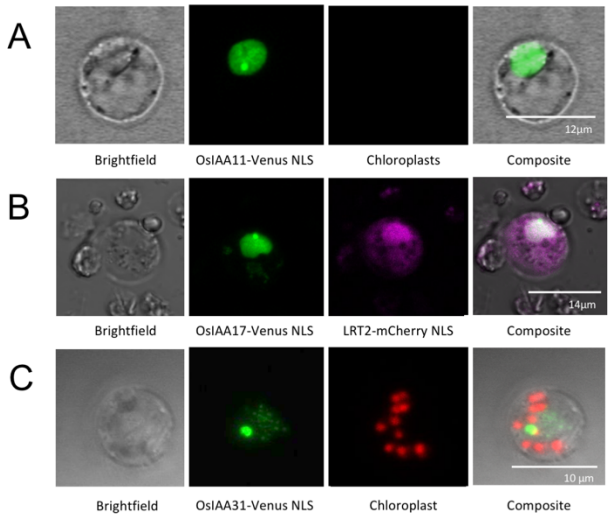

Figure 6: Rice shoot protoplast transfected with OsIAA-Venus fusion proteins display nuclear protein bodies (NPBs). Rice shoot protoplast transfected with **(A)** OsIAA11-Venus (green) channels were excited at 488nm and 520nm, respectively. **(B)** OsIAA17-Venus and LRT2-mCherry were co-transfected in rice shoot protoplasts. OsIAA17-Venus (green) channels were excited at 488nm and 520nm, respectively. LRT2-mCherry (magenta) channels were excited at 561nm and 597 nm, respectively. **(C)** OsIAA31-Venus (green) channels were excited and emitted at 488nm and 520nm, respectively. Chlorophyll A (red) channels excited and emitted at 633 and 685, respectively. A-C images were acquired at a resolution of 0.264µm. Protoplasts were imaged using a Zeiss 710 confocal fluorescence microscope with a 40x objective.

Previous studies have shown that a subset of Rac GTPases are activated by auxin, and stimulate the auxin-responsive gene expression. It is important to note that the studies have used GFP and not VENUS as their fluorescent tag (37). At high concentrations, GFP is known to dimerize in live cells (38). In the literature, Venus is a rapidly folding fluorescent protein known to weakly dimerize in cells (27,28,39). To determine whether our observation of NPBs might be induced by the dimerization of Venus, we added the (A206K) mutation to convert Venus into the monomeric Venus fluorescent protein (mVenus) (26,39). Notably, protoplasts transfected with OsIAA11-mVenus showed no NPBs, indicating that the monomerizing mutation of Venus was sufficient to eliminate this feature in the nucleus (fig. 2). Therefore, mVenus was employed for all time course studies of the constitutively expressed OsIAA11 (Appendix, figure 2.1).

Time Course Imaging: Laser-Scanning vs. Spinning Disk Confocal Microscopes

The first set of data (fig. 1-10) was recorded on a laser-scanning confocal microscope (Zeiss 710, .czi files converted to .tiff and analyzed in Fiji) with a stage to control the

temperature. The second set of data (fig. 11-13) was recorded on a spinning disk confocal microscope (Perkin-Elmer, .tiff files were obtained and analyzed in Fiji), which had a temperature-controlled chamber. Many researchers have utilized microscopes to measure the fluorescence of structures of interest from thick biological specimens (40-45). However, there are different confocal systems often used. The two different confocal systems allow microscopists to control the balance between rejecting unwanted light and capturing a detectable signal. The laser scanning confocal microscope utilizes small pinholes, which reject a great deal of unwanted light. Therefore, thin optical sections of specimens can be captured to display intracellular features and structures. This system is typically used with specimens that do not move during imaging, but it is the most widely used confocal microscope. Notably, the spinning disk microscope uses a rotating disk with a pattern of slits or holes that block out-of-focus light from excitation and emission light paths, which reduces the laser's toxicity during time-lapse imaging of living cells (45). One advantage of the spinning disk confocal microscope is that it allows for faster imaging times but has decreased intracellular specimen details. In this dissertation, we used both confocal microscopes to image our fluorescent proteins of interest in rice shoot protoplasts.

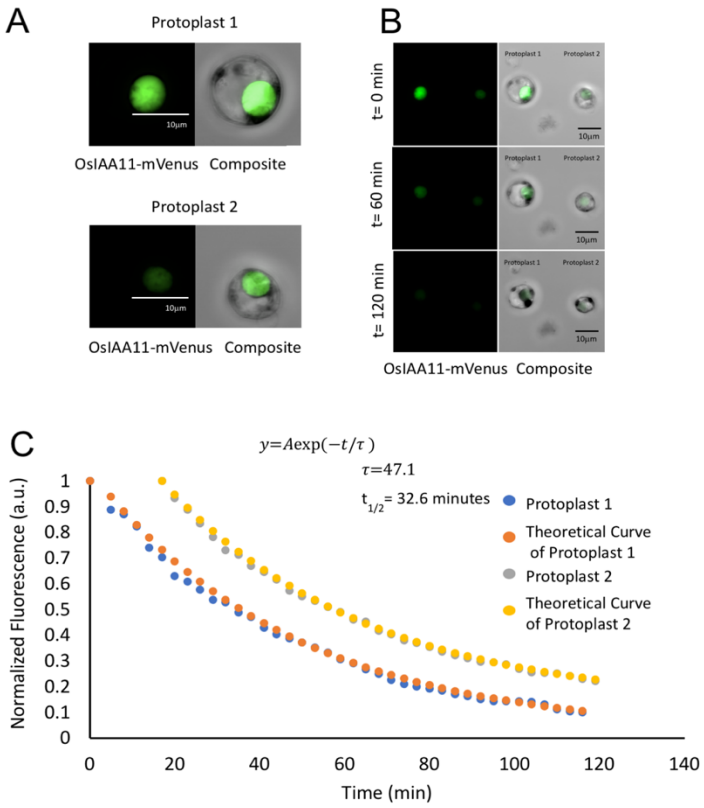

Figure 7: Exponential decay data of the fluorescent monomeric OsIAA11-mVENUS in rice green tissue protoplasts. (A) Images of two protoplasts having OsIAA11-mVenus localized to the nucleus. **(B)** Images displaying the decrease of fluorescence in OsIAA11-mVenus over time. **(C)** Exponential decay data of the degradation rate of constitutive promoter OsIAA11-mVenus in green tissue protoplasts upon the addition of 20µM Auxin and 50µM CHX. Protoplast 1 has a rate constant $(\tau) = 47.1$. Protoplast 2 has a rate constant $(\tau) = 47.7$. OsIAA11-mVenus (green) channels were excited at 488nm and 520nm, respectively. Temperature was not controlled. Imaged

Cycloheximide Chase experiments using Constitutive (p35s) promoter.

In order to image a fluorescent protein in the cell, the p35s promoter is commonly used in protoplast to visualize the protein of interest. The purpose of using the constitutive (p35s) promoter is to constantly express the fusion protein OsIAA11-mVenus, which is localized to the nucleus of rice shoot protoplasts that were imaged on a Zeiss 710 laser

scanning confocal microscope (Figure 7).

For control sample, we added auxin to a protoplast dish, resulting in no exponential decrease of OsIAA11-mVenus fluorescence (Appendix figure 3.2). This observation is expected since we are using a constitutive promoter. In live cell imaging, the degradation rate of a protein of interest can be measured by utilizing a cycloheximide chase. Cycloheximide is a known protein inhibitor that stops the translation of any new protein in the cell (37,46,47). For an additional control sample, we added cycloheximide to a protoplast dish. We observed no exponential decay of OsIAA11-mVenus. This observation is expected since no additional auxin was added to the protoplasts to initiate the proteasomal degradation of OsIAA11 (Appendix figure 3.3). In this dissertation, we utilized a cycloheximide chase, which is simultaneously adding auxin and cycloheximide. To investigate the degradation rate of OsIAA11-mVenus in vivo, a cycloheximide chase, was performed observing two protoplasts (fig. 7).

To observe OsIAA11-mVenus in the nucleus, Protoplast 1 and Protoplast 2 were imaged at high magnification (100x). Results show both protoplasts displayed a similar

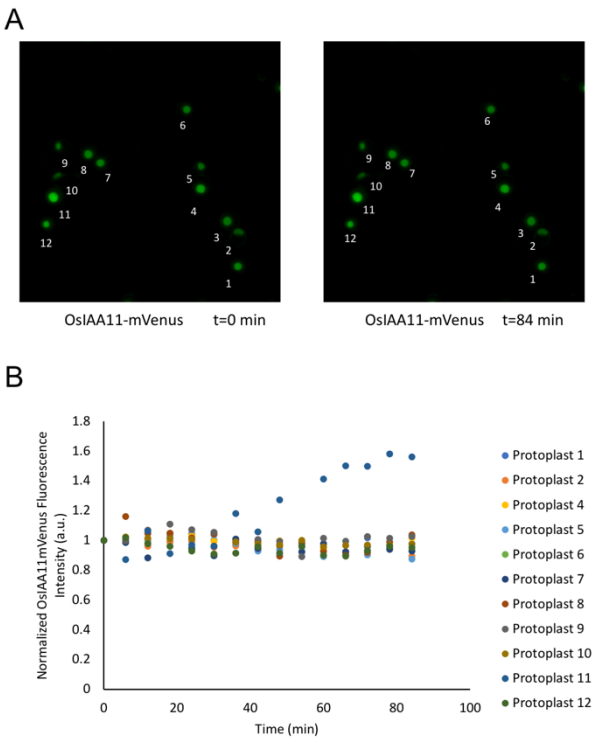

Figure 8: Exponential decay data of the fluorescent monomeric OsIAA11-mVENUS in rice green tissue protoplasts. (A) No degradation rate of constitutive promoter OsIAA11-mVenus in green tissue protoplasts upon the addition of 20µM Auxin and 50µM CHX in numerous protoplasts. **(B)** A total of 13 Protoplast did not decrease in fluorescence intensity, (green) channels were excited at 488nm and 520nm, respectively. The temperature was not controlled. Protoplasts were imaged at a post-transfection time of 18 hours.

exponential decay rate constant of τ =47, $t_{1/2}$ = 32.6 minutes (fig. 7). However, in an independent time course at a lower magnification (40x wider field of view), thirteen protoplasts transfected with OsIAA11-mVenus did not show an exponential decay after 84 minutes (fig. 8). Surprisingly, none of the thirteen protoplasts showed decay of fluorescence intensity after the addition of auxin 20μM and cycloheximide (CHX) 50μM.

The rate of OsIAA11 degradation is not altered by co-transfection with LRT2.

To investigate whether expression of LRT2 alters the degradation rate of OsIAA11, protoplasts can be transiently transfected with multiple proteins (2,5,24,48,49). The rice shoot protoplasts grown in the dark were co-transfected with OsIAA11-mVenus and LRT2-mCherry (fig. 9A) and magnified at a higher level (100x) showed an exponential decay of τ=56, $t_{1/2}$ = 38.8 minutes (fig. 9B). However, in a wide field of view (40x), numerous rice shoot protoplasts co-transfected with OsIAA11-mVenus and LRT2-

mCherry showed constant fluorescence signals for over 120 minutes (fig. 8B). Following the addition of cycloheximide, the amount of OsIAA11-mVenus expression in 23 protoplasts did not significantly decrease (fig. 10).

We hypothesize from these findings that the heterogenous population of protoplasts extracted from rice shoots might lead to the observed variability in the degradation of OsIAA11. It should be noted that additional protoplasts were imaged at high magnification and did not display an exponential decay as in figure 7. Additionally, the data collected on the Zeiss 710 laser confocal microscope was first analyzed with a range indicator in order to not saturate pixels and obtain optimal image quality. The results need to be interpreted with caution. In the next section, we investigate other possible factors that could influence the degradation of OsIAA11-mVenus, such as dependence on heat and time on post-transfection using a spinning disk confocal microscope (further details referenced in Chapter 2).

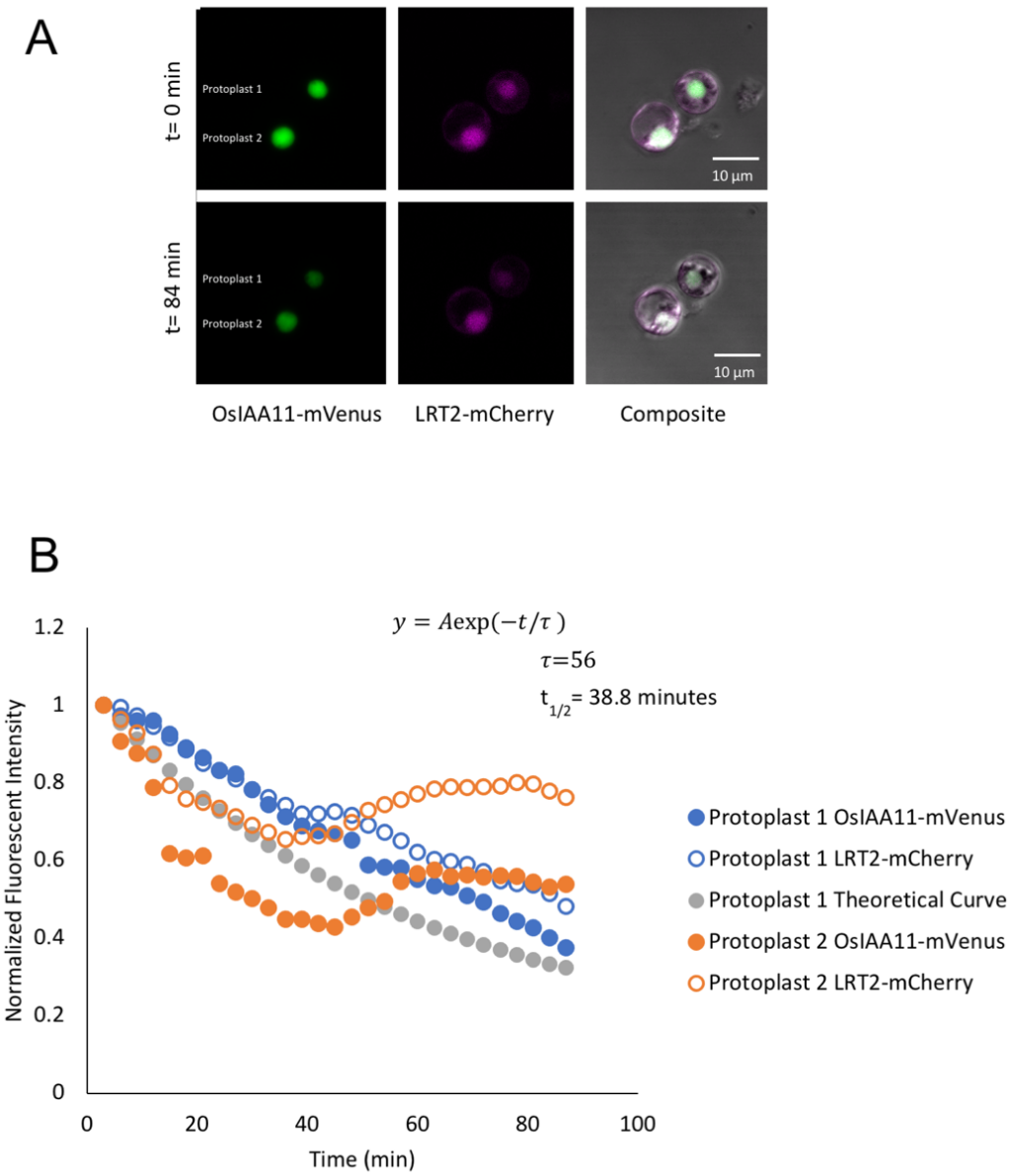

Figure 9: Degradation of OsIAA11-mVenus with LRT2 co-transfected in rice shoot protoplasts. (A) OsIAA11-mVenus fusion protein (green) channels were excited and emitted at 488nm and 520 nm, respectively. LRT2-mCherry (magenta) channels were excited and emitted at 561nm and 597nm, respectively. **(B)**The degradation rate of constitutive promoter OsIAA11-mVenus in shoot protoplasts upon the addition of 20µM Auxin and 50µM CHX with a rate constant (τ) = 56. Images were obtained overtime at a resolution of 0.264µm. Protoplasts were imaged using the Zeiss 710 confocal fluorescence microscope with 40X objective. The microscope stage was heated at ~28 °C . The protoplasts were imaged at a post-transfection time of 14-15 hours.

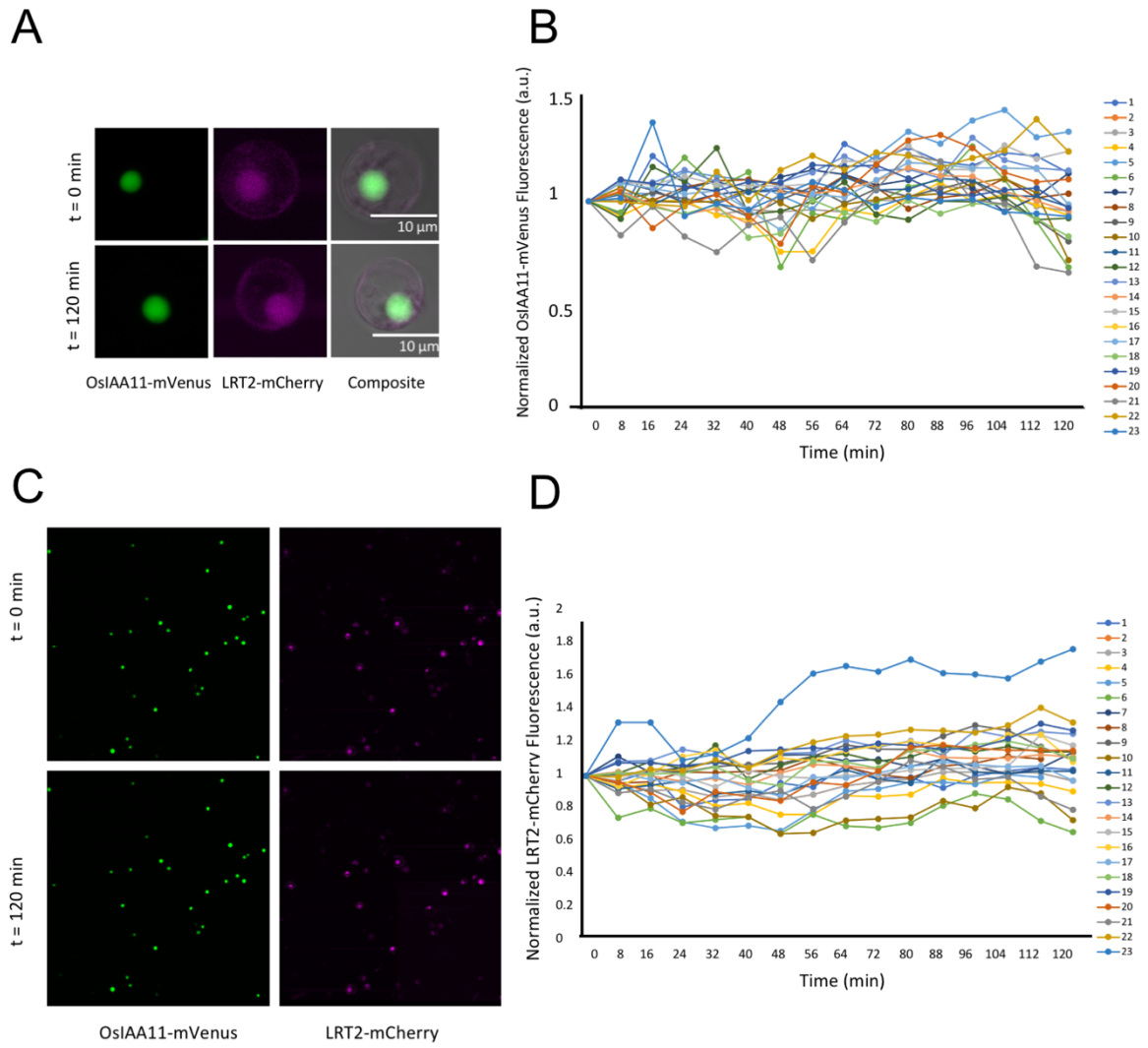

Figure 10: Expression of co-transfected protoplasts show OsIAA11-mVenus does not show degradation after the addition of auxin and cycloheximide. (A) One protoplast (from panel C) showing the localization of OsIAA11mVenus and LRT20mCherry in the nucleus. **(B)** No exponential decay of the constitutive promoter OsIAA11-mVenus in green tissues protoplasts was visible upon the addition of 20 µM auxin and 50 µM cycloheximide. **(C)** Numerous rice shoot protoplasts were transfected with OsIAA11-mVenus (green) channels were excited and emitted at 488nm and 520nm, respectively. LRT2-mCherry channels (magenta) were excited and emitted at 561nm and 597nm, respectively. Protoplasts were imaged over time using a Zeiss 710 confocal fluorescence microscope with 40X objective. (large view) **(D)** Normalized fluorescence intensity of LRT2-mCherry fluorescence overtime upon the addition of 20 µM auxin and 50 µM cycloheximide. Note: Temperature was not controlled. The protoplasts were imaged at a post-transfection time of 14-15 hours.

Temperature influences the OsIAA11 degradation at 28-30°C

While examining the degradation rate of OsIAA11(5,6), it is possible that other factors exist for a given protoplast that might only be produced under warmer conditions. To investigate the potential influence of heat on the expression and degradation of OsIAA11-mVenus or co-transfected with OsIAA11-mVenus and LRT2-mCherry, after transfection the rice shoot protoplasts were incubated overnight in a controlled temperature room at *28–30*°C. The protoplasts were then imaged in a controlled temperature chamber ~*28–30*°C on a spinning disk confocal microscope (fig. 11 and 12).

Upon the addition of buffer (control-WI buffer), which was the buffer that the protoplasts were incubated in post-transfection, there was no significant decay in OsIAA11-mVenus fluorescence over time (figs. 11A and 11B). However, the addition of auxin 20μM and cycloheximide (CHX) 50μM to four protoplasts in a dish displayed a distinctly different decrease in the OsIAA11-mVenus fluorescence with τ= 55, $t_{1/2}$ = 38.1 (figs. 11C and 11D). These results suggest that the degradation rate of OsIAA11-mVenus is dependent on temperature (25). Then, we turned to protoplasts co-transfected with OsIAA11-mVenus and LRT2-mCherry to investigate if LRT2 effects the degradation rate of OsIAA11.

It is possible that the degradation rate of OsIAA11 is influenced by the presence of LRT2-mCherry based on the auxin circuit. To investigate the effect of LRT2 on the degradation rate of OsIAA11, protoplasts extracted from plants grown in the dark were co-transfected with OsIAA11-mVenus and LRT2-mCherry. The majority of the protoplasts were successfully co-transfected with both plasmids (fig. 12) and imaged

for a total of 95 minutes. In the control experiment where only WI buffer was added, there was no significant decay of OsIAA11-mVenus or LRT2-mCherry fluorescence over time (fig. 12A and 12B). Upon the addition of auxin 20μM and cycloheximide (CHX) 50μM to four protoplasts, the two were co-transfected with OsIAA11-mVenus or LRT2-mCherry (fig. 12C and 12D). Results show a dramatic decrease in the OsIAA11-mVenus fluorescence with half-life in the range of 30–40 mins (fig. 12D). Importantly, the LRT2-mCherry fluorescence signal, which serves as an internal control, does not degrade over time (Fig.12D). These results suggest that LRT2-mCherry does not accelerate the degradation rate of OsIAA11. Additionally, the results show that temperature is an important factor in the degradation rate of OsIAA11 in rice shoot protoplasts (Fig. 12).

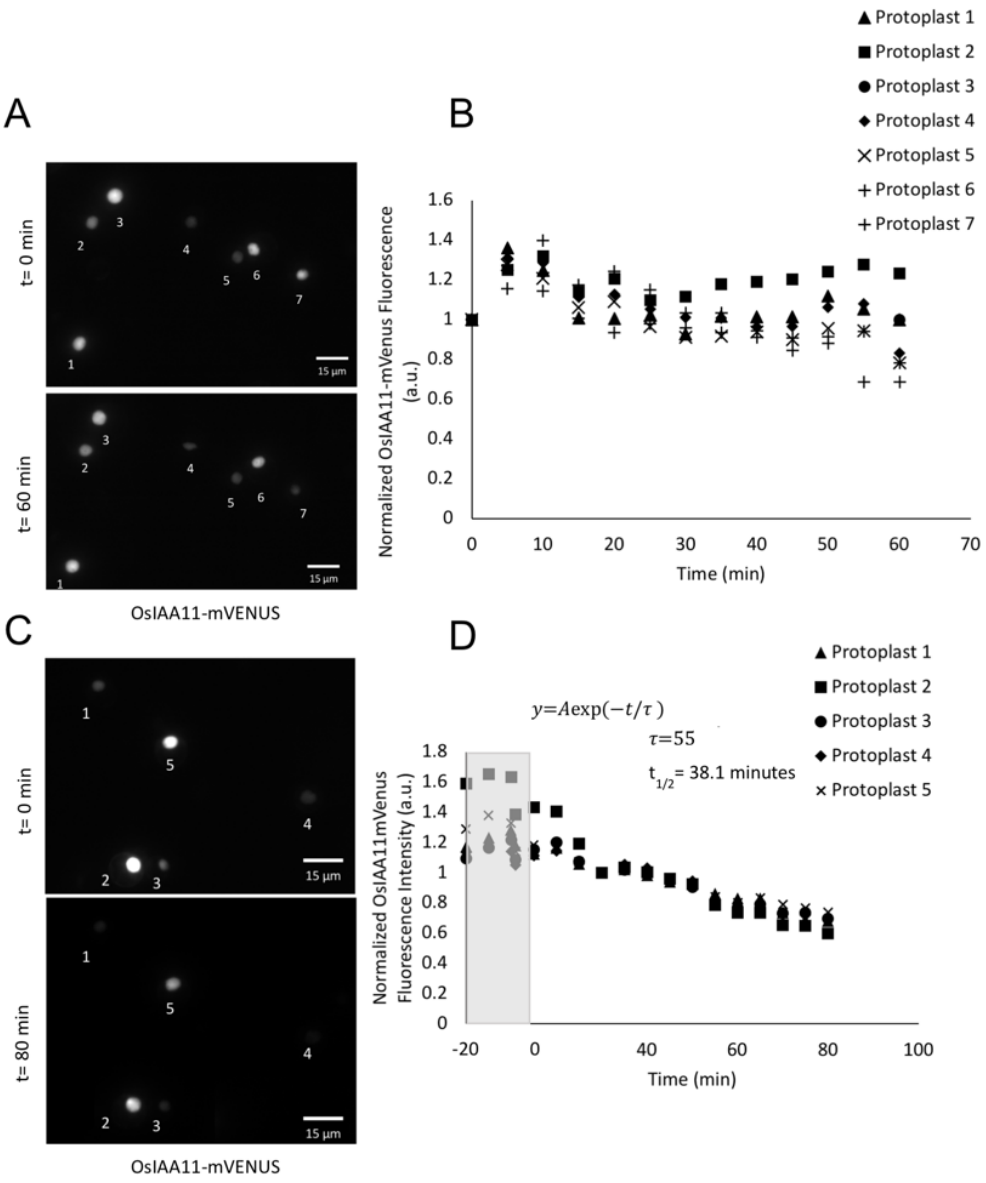

Figure 11: Degradation of OsIAA11mVenus in rice shoot protoplasts at controlled temperature of 28-30°C. (A,B) Time course of shoot protoplasts expressing OsIAA11-mVenus with of Wi buffer (control time). **(C)** Images displaying the exponential decay of the constitutive promoter OsIAA11-mVenus in shoot protoplasts upon the addition of 20µM Auxin and 50µM CHX. **(D)**The average protoplast has a rate constant (τ) = 55, half-life of 38.1 minutes. OsIAA11-mVenus (green) channels were excited at 488nm and 520nm, respectively. Protoplasts were imaged using the spinning disk confocal fluorescence microscope with 60X Temperature controlled at 28–30°C and protoplasts were imaged at a post-transfection time of 13-14 hours.

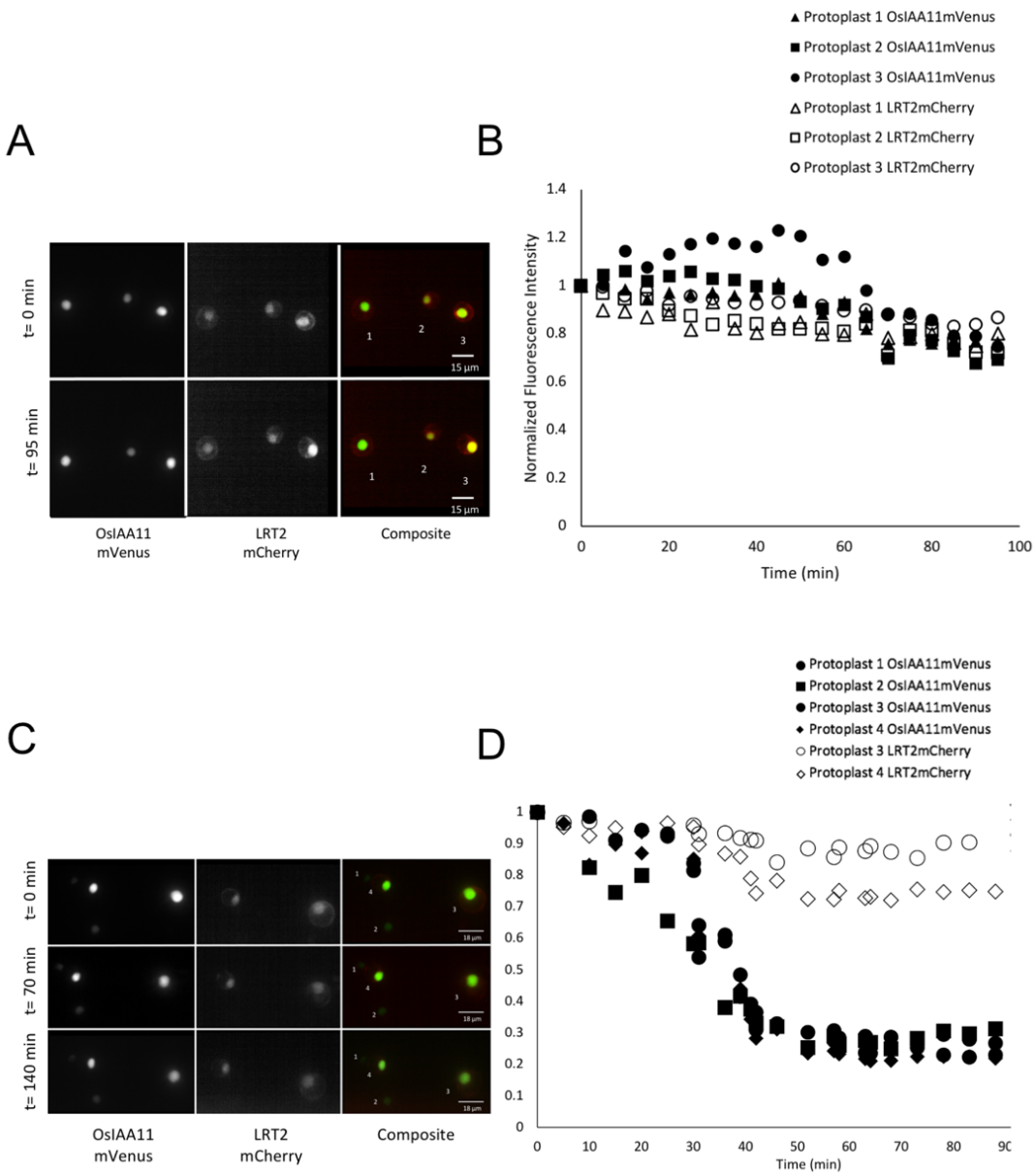

Figure 12: **Degradation of co-transfected OsIAA11-mVenus and LRT2-mCherry rice shoot protoplasts at controlled temperature of 28-30°C. (A, B)** Time course of shoot protoplasts expressing OsIAA11-mVenus and LRT2mCherry with the addition of WI buffer (control time). **(C,D)** The Exponential decay of the constitutive promoter OsIAA11-mVenus in shoot protoplasts upon the addition of 20µM Auxin and 50µM CHX. The fluorescent intensity of OsIAA11mVenus decreases ~30mins. OsIAA11-mVenus (green) channels were excited at 488nm and 520nm, respectively. LRT2-mCherry channels (red) were excited and emitted at 561nm and 597nm, respectively. Protoplasts were imaged using the spinning disk confocal fluorescence microscope with 60X objective. Temperature controlled at 28–30°C and protoplasts were imaged at a post-transfection time of 13-14 hours.

Post-transfection time influences OsIAA11 degradation in rice shoot protoplasts.

It is standard to transiently transfect protoplasts obtained from etiolated shoots (30), however it is possible that the amount of post-transfection time influences the degradation rate of OsIAA11. The standard post-transfection time to image rice shoot protoplast is 13–14 hours (fig. 11, 12). To investigate the potential influence of post-transfection time of OsIAA11-mVenus and LRT2-mCherry in rice shoot protoplast, three cycloheximide chases were performed after the cycloheximide chase described above (fig. 12). The first cycloheximide chase was performed at a post-transfection of 15–16 hours (fig. 13A), the second at a post-transfection time of 17–18 hours (fig 13B), and the third at a post-transfection time of 19–20 hours (fig. 13C). As shown in fig. 13, the addition of auxin (20μM) and CHX (50μM) showed a slow decrease in fluorescence intensity over time. This indicates that there is a slower degradation of OsIAA11-mVenus at later post-transfection times compared to the standard post-transfection time (fig. 12,13). Overall, these results indicate that the degradation rate of OsIAA11 is dependent on time elapsed post-transfection.

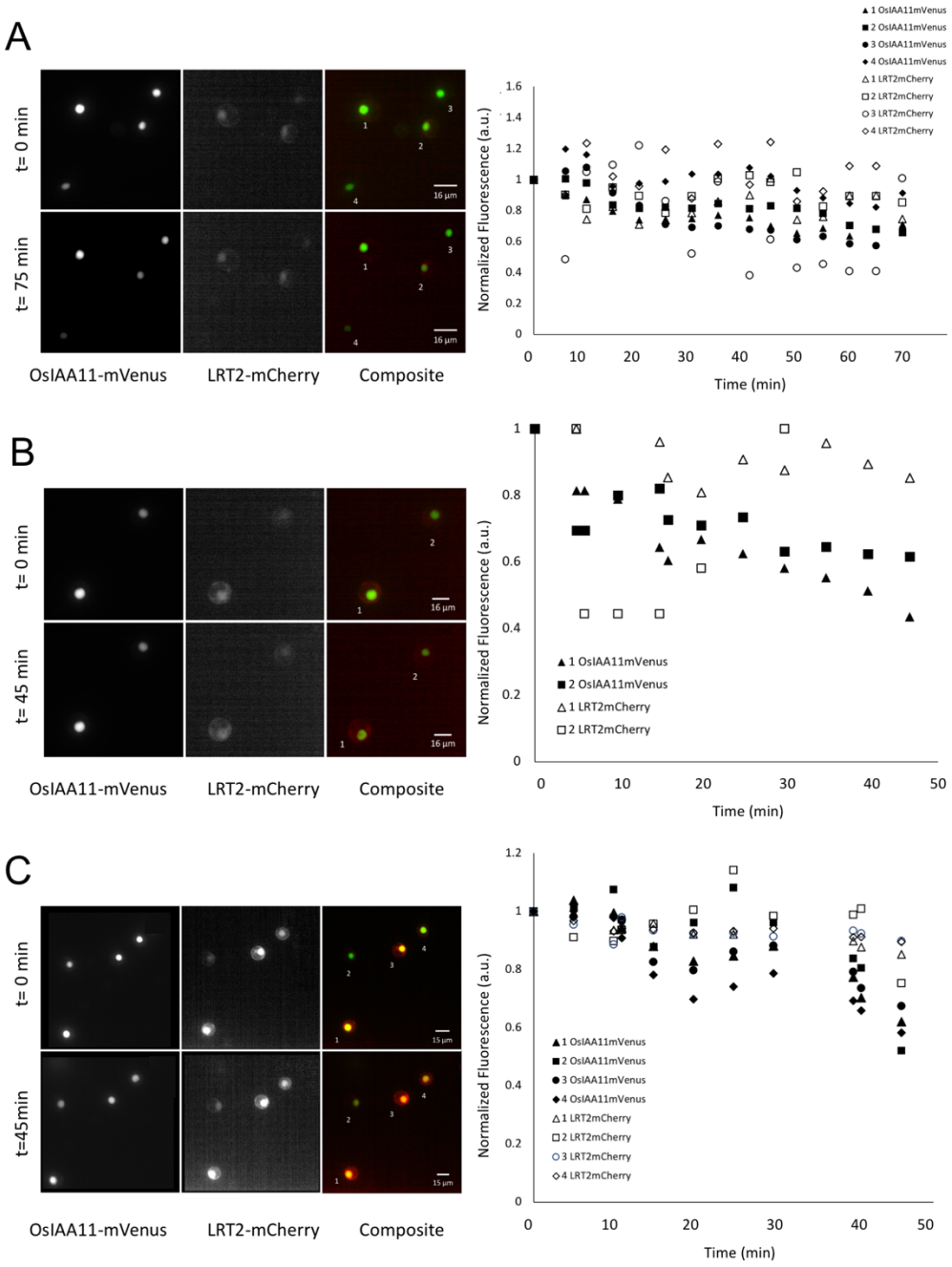

Figure 13: Post-transfection time affects the degradation of OsIAA11mVenus in shoot protoplast. No exponential decay of the constitutive promoter OsIAA11-mVenus in shoot protoplasts upon the addition of 20µM Auxin and 50µM CHX. **(A)** Co-transfected OsIAA11-mVenus and LRT2-mCherry rice shoot protoplasts at 15-16hrs (top panel). **(B)** Co-transfected OsIAA11-mVenus and LRT2-mCherry rice shoot protoplasts at 17-18hrs (middle panel). **(C)** Co-transfected OsIAA11-mVenus and LRT2-mCherry rice shoot protoplasts at 19-20hrs. OsIAA11-mVenus (green) channels were excited at 488nm and 520nm, respectively. LRT2-mCherry channels (red) were excited and emitted at 561nm and 597nm, respectively (bottom panel). Protoplasts were imaged using the spinning disk confocal fluorescence microscope with 60X objective. All cycloheximide chase was temperature controlled at 28–30°C.

Discussion

This study's initial objective was to determine the auxin-induced degradation rate of OsIAA11 and investigate its dependence on LRT2 activity to model the auxin-responsive negative feedback circuit mathematically (5,24,48,49). Investigations of the degradation rate of OsIAA11 were carried out with and without co-transfection of LRT2 in rice shoot protoplasts. Here we have determined that the degradation rate of OsIAA11 is not accelerated when co-expressed with LRT2 (fig. 7, 9, 11). We have performed cycloheximide chase experiments with auxin in rice shoot protoplasts and imaged fluorescence by confocal microscopy over time (52). Importantly, the decrease in fluorescence of OsIAA11mVenus is readily detected in protoplasts at a post-transfection time of 13-14 hours (fig. 12) compared to later time points (fig. 13). Additionally, the effects of temperature on OsIAA11 degradation rate were significant, with higher numbers of protoplasts displaying a decay of fluorescence intensity at 28–30 °C. Using this approach, we have demonstrated that many protoplasts are strongly influenced by temperature and the amount of time elapsed after transfection (fig. 12, 13). Moreover, our results are consistent with Arabidopsis experiments showing HSP90 associated with degradation of Aux/IAA proteins (25,50,51). Further research should be undertaken to investigate the role of HSP90 by co-transfection with OsIAA11 in rice shoot protoplasts.

The first set of questions are aimed at visualizing the OsIAA11-mVenus fusion protein in rice shoot protoplasts. As mentioned before, protoplasts are commonly obtained from etiolated shoot. In order to eliminate fluorescence from chloroplasts, we grew rice in the dark to obtain etiolated shoot protoplasts. Growing plants in the light

versus the dark do not influence the nuclear localization of OsIAA11mVenus or LRT2 (Fig. 3). Interestingly, nuclear "protein bodies" (NPB) were observed for OsIAA11-Venus, OsIAA17-Venus and OsIAA31-Venus (37) (figs. 2 and 6). However, a cycloheximide chase displayed no decrease in fluorescence in the protoplasts containing NPB of OsIAA11-Venus, where VENUS is a rapidly folding yellow fluorescent protein (27,39). To rule out the possibility that our NPB was Venus dimerizing in the cell, we added the (A206K) mutation to convert Venus to mVenus (monomeric Venus). In the observation of OsIAA11-mVenus in the nucleus of protoplasts, we saw no NPB (Fig. 2). Additionally, we demonstrated that the intrinsic OsIAA11 nuclear localization signal (NLS) was sufficient for localization of OsIAA11mVenus to the nucleus (Fig. 2).

An additional objective of this project was to utilize the endogenous promoter of OsIAA11mVenus to determine changes in OsIAA11 protein level as a function of time after auxin addition, time course data that would be used to model the auxin circuit. In this study, auxin was added to protoplasts transiently expressing OsIAA11mVenus driven by the OsIAA11 endogenous promoter. One protoplast was observed to be transiently transfected with OsIAA11-mVenus and displayed a damped oscillation of fluorescence over time (fig. 5). Despite these promising results, further research should be undertaken to obtain the native levels of OsIAA11 in multiple protoplasts in order to quantitatively evaluate a mathematical model the auxin circuit.

This study was designed to use a fluorescent protein's signal to determine the degradation rate of OsIAA11-mVenus. Our laser-scanning confocal microscopy results observed two protoplasts displaying the degradation of OsIAA11-mVenus. In figure 7, two protoplasts show at a τ=47, $t_{1/2}$ = 32.6 minutes. In figure 9, the degradation rate of

protoplasts co-transfected with OsIAA11-mVenus and LRT2-mCherry a tau of a τ=56, $t_{1/2}$ = 38.8 minutes The co-transfection of OsIAA11 and LRT2 does not accelerate the degradation rate of OsIAA11. These results further support the prior finding that LRT2 is optimized for its role in supplying cis-OsIAA11 to the proteasomal degradation pathway (5,24,49). This study confirms that wild type LRT2 reaction is much faster than the downstream degradation process of OsIAA11 to the proteasome (24,49). However, the degradation rate of these findings (n=4) must be interpreted with caution since many rice shoot protoplasts did not display a similar exponential decay (fig. 8, 10). According to these data, we can infer that in many protoplasts extracted from rice shoots additional intrinsic or extrinsic factors are required to carry out the degradation rate of OsIAA11 in rice shoot protoplasts.

An important consideration to address is what other environmental factors influence the degradation of OsIAA11 in protoplasts from rice shoots. Our spinning disk confocal microscopy results with a temperature-controlled environment showed reliable degradation of OsIAA11mVenus with and without LRT2. The results showed OsIAA11mVenus signal decaying while the LRT2mCHerry signal displayed constant expression. In figure 11, the degradation rate of OsIAA11mVenus has a τ=55, $t_{1/2}$ = 38.1 minutes. This result is consistent with our previous findings. In reviewing the literature, the increased temperature possibly promoted the TIR1 auxin co-receptor's rapid accumulation, dependent on the chaperone Hsp90, in many more of the shoot protoplasts (25,50,51). Surprisingly, at ±29°C many protoplasts were seen to display OsIAA11 degradation. This finding is consistent with that of Wang (2016), who found

in *Arabidopsis* that Hsp90 and SGT1 integrate temperature and auxin signaling to regulate plant growth in a modifying environment(25).

It is essential to consider the amount of time that has elapsed post-transfection when performing a cycloheximide chase. One unanticipated finding was that the amount of time that has elapsed since the transfection of OsIAA11 influences the detection of OsIAA11 degradation in rice shoot protoplasts (fig. 13). In figure 9, cycloheximide chase of OsIAA11mVenus started to degrade approximately 30minutes with a post-transfection time of 13-14hours(52). As the elapsed time of post-transfection increased the degradation of OsIAA11mVenus was harder to obtain. Because the lifetime of protoplasts under these conditions is known to be limited these results could reflect a general loss of cellular function at longer post-transfection times (31, 32, 51). Alternatively, these results might reflect a balance between having enough versus too much protein, with sufficient fluorescence signal from OsIAA11-mVenus built up at 13 – 14 hours, and potentially overloading the proteasomal machinery with too much OsIAA11-mVenus at later post-transfection times (Appendix table 3.1).

In conclusion, these studies suggest that the degradation rate of OsIAA11 *in vivo* is dependent on both temperature and elapsed time post-transfection. Our findings that increasing the level of LRT2 in vivo had no impact on OsIAA11 degradation rate are consistent with our prior work showing that LRT2 is optimized for supplying maximal OsIAA11 in the cis conformation for binding to the SCF-TIR1 E3 ligase. Finally, these results support the idea of Hsp90 having a potential role in the rice auxin circuit. Further research should be undertaken *in vivo* to obtain all the necessary factors to model the rice's auxin circuit mathematically.

Acknowledgements

We thank Dr. Brown for letting us use his Spinning Disk microscope during COVID times. We thank Johanna Dela Cruz and the Biotechnology Resource Center of Cornell Institute of Biotechnology for their help with time-course imaging. Imaging data was acquired through the Cornell Institute of Biotechnology's Imaging Facility, with NIH 1S10RR025502 funding for the shared Zeiss LSM 710 Confocal Microscope.

Supplemental Information

Plasmids: The genes for the OsIAA11-Auxin-responsive gene family member (LOC_Os03g43400, Rice Genome Annotation Project, Michigan State University) was purchased from Genscript (Piscataway, NJ). The OsIAA17-Auxin-responsive gene family member (LOC_Os05g14180, Rice Genome Annotation Project, Michigan State University) and the OsIAA31-Auxin-responsive gene family member (LOC_Os12g40900, Rice Genome Annotation Project, Michigan State University) were from IDT (Coralville, Iowa). The gene for LRT2 (hCypA: to be consistent find similar info from Rice genome project above) was gift from C. Kalodimos (Rutgers University, Piscataway, NJ) and the pEXSG-eYFP and pEXSG-mCherry plant expression vectors utilizing the p35SS promoter were gifts from Dr. Maureen Hanson (Cornell University, Ithaca,NY). A pSLIK-Venus vector was obtained from Addgene (donated by Iain Fraser at California Institute of Technology, Pasedena CA). The QuikChange II Site-Directed Mutagenesis Kit was from Agilent Technologies (Santa Clara, CA). Please see Appendix for further vector information.

Generation of OsIAA11 and LRT2 expression vectors:

The OsIAA11 gene was inserted into the pEXSG-eYFP plasmid by Gateway recombination strategy (LR reaction) to generate the pEXSG-OsIAA11-eYFP construct. The pSLIK-Venus vector was used as a template for PCR to generate the Venus gene containing the terminal ClaI and XbaI restriction sites and the resulting fragment was used to replace eYFP to generate the pEXSG-OsIAA11-Venus plasmid. Site-directed mutagenesis was used to insert the C-terminal nuclear localization signal (NLS; KKKRKVPKKKRKV) and introduce the A206K point mutation into Venus to generate mVenus (the monomeric version) and create the pEXSG-OsIAA11-mVenus and pEXSG-OsIAA11-mVenus-NLS expression vectors.

The OsIAA17 and OsIAA31 genes were subjected to PCR to produce DNA fragments containing the terminal XhoI and ClaI restriction sites which were used to individually substitute for OsIAA11 to generate the pEXSG-OsIAA17-mVenus-NLS and pEXSG-OsIAA31-mVenus-NLS expression vectors respectively.

The genes for LRT2 and the mCherry were individually subjected to PCR to generate fragments containing the terminal XhoI/HindIII and HindIII/XbaI restriction sites respectively and used to sequentially replace OsIAA11 and mVenus to create the pEXSG-LRT2-mCherry-NLS expression vector.

All vectors contained a GAGAGAGAGAGP spacer between the Rice gene and the fluorescent tag and a GAGAGAGP spacer between the fluorescent tag and the NLS where applicable, please see Appendix for further information.

REFERENCES:

1. Kang, B., Zhang, Z., Wang, L., Zheng, L., Mao, W., Li, M., Wu, Y., Wu, P., and Mo, X. (2013) OsCYP2, a chaperone involved in degradation of auxin-responsive proteins, plays crucial roles in rice lateral root initiation. *Plant J* **74**, 86-97
2. Zheng, H., Li, S., Ren, B., Zhang, J., Ichii, M., Taketa, S., Tao, Y., Zuo, J., and Wang, H. (2013) LATERAL ROOTLESS2, a cyclophilin protein, regulates lateral root initiation and auxin signaling pathway in rice. *Mol Plant* **6**, 1719-1721
3. Zhu, Z. X., Liu, Y., Liu, S. J., Mao, C. Z., Wu, Y. R., and Wu, P. (2012) A gain-of-function mutation in OsIAA11 affects lateral root development in rice. *Mol Plant* **5**, 154-161
4. Jing, H., Yang, X., Zhang, J., Liu, X., Zheng, H., Dong, G., Nian, J., Feng, J., Xia, B., Qian, Q., Li, J., and Zuo, J. (2015) Peptidyl-prolyl isomerization targets rice Aux/IAAs for proteasomal degradation during auxin signalling. *Nat Commun* **6**, 7395
5. Chen, Y., Yang, Q., Sang, S., Wei, Z., and Wang, P. (2017) Rice inositol polyphosphate kinase (OsIPK2) directly interacts with OsIAA11 to regulate lateral root formation. *Plant and Cell Physiology* **58**, 1891-1900
6. Zhu, Z.-X., Liu, Y., Liu, S.-J., Mao, C.-Z., Wu, Y.-R., and Wu, P. (2012) A gain-of-function mutation in OsIAA11 affects lateral root development in rice. *Molecular Plant* **5**, 154-161
7. Fendrych, M., Akhmanova, M., Merrin, J., Glanc, M., Hagihara, S., Takahashi, K., Uchida, N., Torii, K. U., and Friml, J. (2018) Rapid and reversible root growth inhibition by TIR1 auxin signalling. *Nature plants* **4**, 453-459
8. Del Pozo, J. C., and Manzano, C. (2014) Auxin and the ubiquitin pathway. Two players-one target: the cell cycle in action. *J Exp Bot* **65**, 2617-2632
9. Gray, W. M., Kepinski, S., Rouse, D., Leyser, O., and Estelle, M. (2001) Auxin regulates SCF(TIR1)-dependent degradation of AUX/IAA proteins. *Nature* **414**, 271-276
10. Kepinski, S., and Leyser, O. (2005) The Arabidopsis F-box protein TIR1 is an auxin receptor. *Nature* **435**, 446-451
11. Tan, X., Calderon-Villalobos, L. I., Sharon, M., Zheng, C., Robinson, C. V., Estelle, M., and Zheng, N. (2007) Mechanism of auxin perception by the TIR1 ubiquitin ligase. *Nature* **446**, 640-645
12. Middleton, A. M., King, J. R., Bennett, M. J., and Owen, M. R. (2010) Mathematical modelling of the Aux/IAA negative feedback loop. *Bull Math Biol* **72**, 1383-1407
13. Moss, B. L., Mao, H., Guseman, J. M., Hinds, T. R., Hellmuth, A., Kovenock, M., Noorassa, A., Lanctot, A., Villalobos, L. I., Zheng, N., and Nemhauser, J. L. (2015) Rate Motifs Tune Auxin/Indole-3-Acetic Acid Degradation Dynamics. *Plant Physiol* **169**, 803-813

14. Havens, K. A., Guseman, J. M., Jang, S. S., Pierre-Jerome, E., Bolten, N., Klavins, E., and Nemhauser, J. L. (2012) A Synthetic Approach Reveals Extensive Tunability of Auxin Signaling. *Plant Physiology* **160**, 135-142
15. Nemhauser, J. L., and Torii, K. U. (2016) Plant synthetic biology for molecular engineering of signalling and development. *Nature plants* **2**, 1-7
16. Nemhauser, J. L., Zambryski, P. C., and Roe, J. L. (1998) Auxin signaling in Arabidopsis flower development?: Commentary. *Current Opinion in Plant Biology* **1**, 531-535
17. Leydon, A. R., Gala, H. P., Guiziou, S., and Nemhauser, J. L. (2020) Engineering Synthetic Signaling in Plants. *Annual Review of Plant Biology* **71**, 767-788
18. de Lange, O., Klavins, E., and Nemhauser, J. (2018) Synthetic genetic circuits in crop plants. *Current opinion in biotechnology* **49**, 16-22
19. Vert, G., Nemhauser, J. L., Geldner, N., Hong, F., and Chory, J. (2005) Molecular mechanisms of steroid hormone signaling in plants. *Annu. Rev. Cell Dev. Biol.* **21**, 177-201
20. Reed, J. W. (2001) Roles and activities of Aux/IAA proteins in Arabidopsis. *Trends Plant Sci* **6**, 420-425
21. Ivanchenko, M. G., Zhu, J., Wang, B., Medvecká, E., Du, Y., Azzarello, E., Mancuso, S., Megraw, M., Filichkin, S., Dubrovsky, J. G., Friml, J., and Geisler, M. (2015) The cyclophilin A DIAGEOTROPICA gene affects auxin transport in both root and shoot to control lateral root formation. *Development* **142**, 712-721
22. Lu, K. P., Finn, G., Lee, T. H., and Nicholson, L. K. (2007) Prolyl cis-trans isomerization as a molecular timer. *Nat Chem Biol* **3**, 619-629
23. Wang, P., and Heitman, J. (2005) The cyclophilins. *Genome Biol* **6**, 226-226
24. Acevedo, L. A., Korson, N. E., Williams, J. M., and Nicholson, L. K. (2019) Tuning a timing device that regulates lateral root development in rice. *Journal of biomolecular NMR* **73**, 493-507
25. Wang, R., Zhang, Y., Kieffer, M., Yu, H., Kepinski, S., and Estelle, M. (2016) HSP90 regulates temperature-dependent seedling growth in Arabidopsis by stabilizing the auxin co-receptor F-box protein TIR1. *Nature Communications* **7**, 10269
26. Rekas, A., Alattia, J.-R., Nagai, T., Miyawaki, A., and Ikura, M. (2002) Crystal structure of venus, a yellow fluorescent protein with improved maturation and reduced environmental sensitivity. *Journal of biological chemistry* **277**, 50573-50578
27. Nagai, T., Ibata, K., Park, E. S., Kubota, M., Mikoshiba, K., and Miyawaki, A. (2002) A variant of yellow fluorescent protein with fast and efficient maturation for cell-biological applications. *Nature biotechnology* **20**, 87-90
28. Shaner, N. C., Steinbach, P. A., and Tsien, R. Y. (2005) A guide to choosing fluorescent proteins. *Nature methods* **2**, 905-909
29. Page, M. T., Parry, M. A., and Carmo-Silva, E. (2019) A high-throughput transient expression system for rice. *Plant, cell & environment* **42**, 2057-2064

30. Komatsu, S., Muhammad, A., and Rakwal, R. (1999) Separation and characterization of proteins from green and etiolated shoots of rice (Oryza sativaL.): Towards a rice proteome. *ELECTROPHORESIS: An International Journal* **20**, 630-636
31. Au - Wu, F., and Au - Hanzawa, Y. (2018) A Simple Method for Isolation of Soybean Protoplasts and Application to Transient Gene Expression Analyses. *JoVE*, e57258
32. Davey, M., Kothari, S., Zhang, H., Rech, E., Cocking, E., and Lynch, P. (1991) Transgenic rice: Characterization of protoplastderived plants and their seed progeny. *Journal of experimental botany* **42**, 1159-1169
33. Ahn, J. C., Kim, D.-W., You, Y. N., Seok, M. S., Park, J. M., Hwang, H., Kim, B.-G., Luan, S., Park, H.-S., and Cho, H. S. (2010) Classification of rice (Oryza satival. japonica nipponbare) immunophilins (FKBPs, CYPs) and expression patterns under water stress. *BMC Plant Biology* **10**, 253
34. Giraud, G., Stadhouders, R., Conidi, A., Dekkers, D. H. W., Huylebroeck, D., Demmers, J. A. A., Soler, E., and Grosveld, F. G. (2014) NLS-tagging: an alternative strategy to tag nuclear proteins. *Nucleic acids research* **42**, e163-e163
35. Zenser, N., Ellsmore, A., Leasure, C., and Callis, J. (2001) Auxin modulates the degradation rate of Aux/IAA proteins. *Proceedings of the National Academy of Sciences* **98**, 11795-11800
36. Lavenus, J., Goh, T., Roberts, I., Guyomarc'h, S., Lucas, M., De Smet, I., Fukaki, H., Beeckman, T., Bennett, M., and Laplaze, L. (2013) Lateral root development in Arabidopsis: fifty shades of auxin. *Trends Plant Sci* **18**, 450-458
37. Tao, L.-z., Cheung, A. Y., Nibau, C., and Wu, H.-m. (2005) RAC GTPases in tobacco and Arabidopsis mediate auxin-induced formation of proteolytically active nuclear protein bodies that contain AUX/IAA proteins. *The Plant Cell* **17**, 2369-2383
38. Zacharias, D. A., Violin, J. D., Newton, A. C., and Tsien, R. Y. (2002) Partitioning of Lipid-Modified Monomeric GFPs into Membrane Microdomains of Live Cells. *Science* **296**, 913-916
39. Ilagan, R. P., Rhoades, E., Gruber, D. F., Kao, H. T., Pieribone, V. A., and Regan, L. (2010) A new bright green-emitting fluorescent protein–engineered monomeric and dimeric forms. *The FEBS journal* **277**, 1967-1978
40. Jonkman, J., and Brown, C. M. (2015) Any way you slice it—a comparison of confocal microscopy techniques. *Journal of biomolecular techniques: JBT* **26**, 54
41. Erie, E. A., McLaren, J. W., Kittleson, K. M., Patel, S. V., Erie, J. C., and Bourne, W. M. (2008) Corneal subbasal nerve density: a comparison of two confocal microscopes. *Eye & contact lens* **34**, 322
42. St. Croix, C. M., Shand, S. H., and Watkins, S. C. (2005) Confocal microscopy: comparisons, applications, and problems. *Biotechniques* **39**, S2-S5

43. Wang, E., Babbey, C., and Dunn, K. W. (2005) Performance comparison between the high-speed Yokogawa spinning disc confocal system and single-point scanning confocal systems. *Journal of microscopy* **218**, 148-159
44. Stoeva, D., Göschl, C., Corliss, B., and Busch, W. (2017) Long-Term Confocal Imaging of Arabidopsis thaliana Roots for Simultaneous Quantification of Root Growth and Fluorescent Signals. in *Plant Genomics: Methods and Protocols* (Busch, W. ed.), Springer New York, New York, NY. pp 169-183
45. Gräf, R., Rietdorf, J., and Zimmermann, T. (2005) Live cell spinning disk microscopy. in *Microscopy techniques*, Springer. pp 57-75
46. Siegel, M. R., and Sisler, H. D. (1963) Inhibition of protein synthesis in vitro by cycloheximide. *Nature* **200**, 675-676
47. Schneider-Poetsch, T., Ju, J., Eyler, D. E., Dang, Y., Bhat, S., Merrick, W. C., Green, R., Shen, B., and Liu, J. O. (2010) Inhibition of eukaryotic translation elongation by cycloheximide and lactimidomycin. *Nature chemical biology* **6**, 209-217
48. Acevedo, L. A., and Nicholson, L. K. (2018) 1 H, 13 C and 15 N NMR assignments of cyclophilin LRT2 (OsCYP2) from rice. *Biomolecular NMR assignments* **12**, 171-174
49. Acevedo, L. A., Kwon, J., and Nicholson, L. K. (2019) Quantification of reaction cycle parameters for an essential molecular switch in an auxin-responsive transcription circuit in rice. *Proceedings of the National Academy of Sciences* **116**, 2589-2594
50. Kadota, Y., Amigues, B., Ducassou, L., Madaoui, H., Ochsenbein, F., Guerois, R., and Shirasu, K. (2008) Structural and functional analysis of SGT1-HSP90 core complex required for innate immunity in plants. *EMBO Rep* **9**, 1209-1215
51. Zhang, X.-C., Millet, Y. A., Cheng, Z., Bush, J., and Ausubel, F. M. (2015) Jasmonate signalling in Arabidopsis involves SGT1b–HSP70–HSP90 chaperone complexes. *Nature Plants* **1**, 15049
52. Zhang, Y., Su, J., Duan, S., Ao, Y., Dai, J., Liu, J., Wang, P., Li, Y., Liu, B., and Feng, D. (2011) A highly efficient rice green tissue protoplast system for transient gene expression and studying light/chloroplast-related processes. *Plant methods* **7**, 1-14

CHAPTER 4

PHOSPHO-CYCLIC DIPEPTIDE INHIBITS Aβ PRODUCTION BUT NOT ENDOCYTOSIS OF APP

Abstract

In the United States, Alzheimer's disease care is estimated to cost $277 billion per year (2). Alzheimer's disease (AD) is a major health crisis with no prevention and/or treatment. One of the key pathological features of AD are senile plaques, which are aggregates of the amyloid-β peptide (Aβ). The Aβ peptide is derived from the sequential proteolytic cleavage of the amyloid precursor protein (APP). However, current methods of treatment targeting Aβ producing enzymes have proven unsuccessful. Previously, we developed a cis-locked cyclic dipeptide to mimic the cis isomer of prolyl peptide bonds, referred to as pCDP-DB (phospho-Cyclic Dipeptide, Di-Benzyl), which inhibits the generation of Aβ and secretion of new APP fragments. We found pCDP-DB inhibits generation of Aβ and sAPPβ in human AD cell models and mouse primary astrocytes without blocking APP endocytosis. An unbiased proteomics study revealed that pCDP-DB interactome included several endocytic pathway proteins that are implicated in AD pathogenesis, which are by mechanisms that are not yet fully understood. In order to investigate the importance of the cis-conformation in the cytosolic tail of APP (APPc) we found that a single point mutation, P685A, greatly reduced sAPPβ secretion while, P669A, increased this secreted fragment. Further colocalization analysis showed the internalization of the P685A mutant, located in the APPc, showed that the decrease in sAPPβ was not due to the inhibition of endocytosis. These results suggest that pCDP-

DB decreases Aβ production, does not inhibit endocytosis, and interacts with factors that are involved in endosomal maturation, while providing important insights for the relationship between Aβ production and the pathogenesis of AD.

Introduction

In the United States, AD is one of the most common causes of dementia and is a growing public health concern (1). In 2020, a total of 5.8 million people age 65 and older made health care payments totaling $305 billion dollars for AD health care, long-term care, and hospice services (2). There is an urgent need to address the AD crisis by studying the molecular mechanisms that promote AD pathogenesis. A key issue is that there is currently no prevention and/or treatment for AD. It is now well established that senile plaques are one of the hallmark indicators for AD (3-5). Senile plaques are known as aggregates of the 42 amino acid Aβ peptide, which is a neurotoxic fragment (4). It has been previously observed that Aβ peptide found in the senile plaques are derived from the proteolytic cleavage of the amyloid precursor protein (APP) (3,6-8). Despite the evidence of Aβ peptide found in the senile plaques, there remains a paucity of evidence on understanding why humans produce Aβ and whether scientists can target this peptide as a treatment of AD.

The proteolytic processing of APP has been found to occur through two pathways, the non-amyloidogenic pathway or the amyloidogenic (AD pathway) (9-16). First, in the non-amyloidogenic pathway an enzyme called α-secretase (ADAM10)

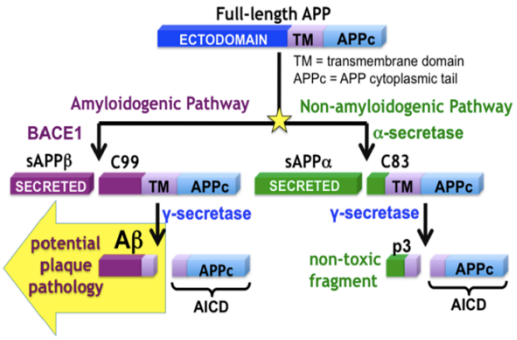

Figure 1: Proteolytic processing of APP. *Amyloidogenic*: β-secretase (BACE1) cleaves APP generating sAPPβ and C99, then γ-secretase cleaves C99 generating Aβ and AICD. *Non-amyloidogenic*: α -secretase cleaves APP generating sAPPα and C83, then γ-secretase cleaves C83 into p3 and AICD.

extracellularly cleaves APP, resulting in sAPPα and a c-terminal 82 amino acid fragment bound to the new membrane-bound stub known as C83(17). Alternatively, in the amyloidogenic pathway the transmembrane APP is extracellularly cleaved by the β-secretase (BACE1) enzyme, resulting in sAPPβ and a c-terminal 99 amino acid fragment bound to the membrane known C99(18). The next step in the non-amyloidogenic pathway involves the γ-secretase enzyme recognizing and cleaving C83, which generates the APP intracellular domain (AICD) and a non-toxic fragment p3. Eventually, AICD is relocated to the nucleus in order to effect transcriptional regulation and neuroprotection pathways in the cell(16,19-24) The existing body of research concludes that sAPPα gets secreted from the neurons and leads to normal synaptic signaling and plasticity, learning and memory functions, as well as emotional behaviors(25). In the amyloidogenic pathway, the γ-secretase enzyme recognizes and cleaves C99 fragment, generating AICD and the Aβ peptide. Again, the AICD effects transcriptional regulation and neuroprotection pathways in the nucleus. However, the Aβ 42 amino acid neurotoxic peptide is involved in many downstream signaling pathways resulting in AD. It has been previously observed that the Aβ peptide interacts with ApoE, which results in an aggregation of Aβ oligomers that generate amyloid plaques (18). Overall, in the brain Amyloid plaques result in blocked ion channels, disrupt Ca+ homeostasis, dysregulated energy and glucose

metabolism, mitochondrial oxidative stress, neuronal apoptosis resulting in memory loss and dementia. To date, several studies have concluded the amyloidogenic pathway is the only pathway to produce Aβ (26). In the next section, I will further explain the Aβ precursor protein's (APP) dependence on APP intracellular trafficking, which is central to our understanding of how Aβ production will be inhibited in future AD treatments.

Previous research has been done to investigate the connection between APP intracellular trafficking and Aβ in the cell. The APP protein has been identified as a type 1 transmembrane protein (15,19) meaning that its single helix spans across the membrane with the N-terminal region towards the extracellular space and the C-terminus in the cytosol. The enzyme α-secretase is a plasma membrane protein, therefore if APP is delivered and retained at the plasma membrane it will be cleaved by α-secretase to produce sAPPα. The sorting of cargo in acidic endosomes would allow for BACE 1, activity requires a low pH, to interact with APP and for endosomes to release sAPPβ into the extracellular space (27). However, late endosomes, which sort cargo to exosomes for release of sAPPβ, contain γ-secretase activity, providing a route for releasing sAPPβ and Aβ into the extracellular space. The sAPPβ has been shown to be proteolytically cleaved *in vivo* (28,29) meaning the cargo from early and late endosomes trafficked from the trans Golgi network could provide another route for sAPPβ and Aβ into the extracellular space. We do not yet understand the overall regulatory mechanisms that govern the trafficking, processing, and degradation of APP within the cell. In the next section, I will describe how our lab has developed a novel a small molecule designed to mimic the cis isomer of prolyl peptide bonds, referred to as pCDP-DB.

Existing research recognizes the critical role played by the transient structure of the 47-residue APP cytoplasmic domain (APPc) (residues 649-695), which has been studied in depth by the Nicholson Lab using protein NMR spectroscopy (30). The APP cytoplasmic tail (APPc) contains two Pro-containing motifs (T**P669**EER and GYEN**P685**TY) that each have known *trans*-specific binding interactions (15,31,32). Previous research has established that within the cytoplasmic tail of APP (AβPPc) the level of phosphorylation of the Thr668-Pro669 (TP) motif (33) is increased in an AD brain (33), and may be an important signaling motif that could be dysregulated in the development of AD (33), and is correlated with an increase in amyloidogenic processing of sAPPβ and the production of amyloid beta (Aβ). Before the phosphorylation of the trans-isomer of the TP peptide bond, which is stabilized by the formation of the helix-capping box structure, there is no cis-TP isomer detected (34,35). After phosphorylation, the helix-capping box is destabilized and a cis-phosphorylated-TP (pTP) population emerges, which gives a total abundance of ~10% cis-pTP isomer and ~90% trans-pTP isomer. The exchange between the cis and trans isomers are normally very slow, but may be accelerated ~2000 fold by the enzyme Pin1 (36,37). Previous research analyzed brain tissue from Pin1 knockout mice, which showed an increase in amyloidogenic APP processing by the phosphorylation of T668 in APP. In order to test the importance of the cis-pTP conformation as a signal for APP processing our lab previously designed a small molecule, phosphor-Thr-Pro cyclic dipeptide (pCDP) that is a 100% “cis-locked” small molecule, which was made to mimic the cis-pTP motif in the APP cytoplasmic tail (30,35,38). In Fisher et al. (2017), results suggested that the cyclic cis-locked phospho-dipeptide DB was able to inhibit the entry of APP into the

amyloidogenic Aβ processing pathway, which provides novel insights for the development of AD therapeutic treatments.

The mechanism of Cyclic dipeptides (CDPs, 2,5-diketopiperazine): CDP's are not well understood, but they are small and have been shown to diffuse through the blood brain barrier (39,40). Using a small molecule (phosho-cyclic-dipeptide-dibenzyl, pCDP-DB) Fischer 2017, showed the importance of cis-phosphorylated-Thr668-Pro669 (TP) motif (cis-pTP) conformation as a signal for sAPPβ processing (30). Our lab's novel cis-locked probe (pCDP-DB) mimics the cis conformation and reduces amyloidogenic processing (fig. 2). Although the mechanism is still not determined, our novel pCDP-DB does not directly inhibit BACE1 cleavage of APP but was designed to inhibit entry of APP entry into amyloidogenic processing. Our novel small molecule provides an avenue to understand the mechanisms and interactors that govern Aβ production in relation to AD.

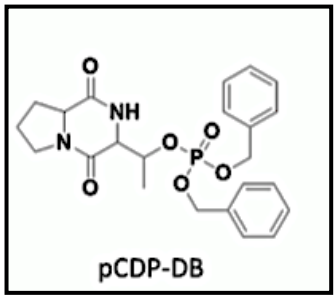

Figure 2: Structure of small molecule, phoso-cyclic-dibenzel-peptide (pCDP-DB) from Fisher 2017.

Overall, APP processing is strongly dependent on intracellular trafficking (16,19-22,24,41). The α secretase activity is primarily located in the plasma membrane. APP is delivered to and retained in the plasma membrane in order to be cleaved by α secretase. The amyloidogenic pathway leads to BACE1 catalytic activity that is highest at a low pH, which is found in endosomal compartments. This pathway enables APP traveling from the plasma membrane in order to encounter cleavage by BACE1 through acidic endosomes. In the endocytic pathway, APP enters via clathrin-coated vesicles which are then taken up as vesicles into the lumen of early endosomes. During sorting of cargo within early endosomes, APP is able to encounter

BACE1 in this acidic compartment and can be cleaved to generate sAPPβ. Subsequently APP can be trafficked to recycling endosomes facilitating the release of sAPPβ into the extracellular space. Endosomal maturation is the process of transferring cargo from early to late endosomes, and late endosomes can subsequently fuse with lysosomes (27). Fusion of late endosomes with lysosomes induces hydrolytic degradation of cargo proteins. Thus, acceleration of endosomal maturation could be a potential therapeutic strategy for eliminating Aβ and sAPPβ. The development of such treatment strategies for AD will require an in-depth understanding of factors that facilitate the rapid trafficking of APP and/or BACE1 into endosomal/lysosomal compartments.

RESULTS

Treatment with pCDP-DB causes a reduction of sAPPβ production in H4 cell lines.

The purpose of using H4 cell lines (of astrocyte origin) is to enable detection of pCDP-DB targets, specifically Aβ production and clearance. The H4 neuroglioma cell line is derived from a malignant tumor of astrocyte origin. H4 cells are easily propagated and adapted to cell culture and are used broadly in biochemical studies of AD (42-44). We have previously used two H4 AD cell models overexpressing either human APP (H4-APP695) or human BACE1 (H4-BACE1) (45,46). In figure 1, each model cell line produced detectable sAPPβ. Upon treatment with pCDP-DB a significant reduction of sAPPβ production was observed. In H4 cells the same result was observed with 2.5 times higher sample loading and 30 times longer exposure (Figure 3A). As shown in Figure 3B, treatment of mouse primary astrocytes with pCDP-DB displayed the same change of suppression of sAPPβ. Importantly, using purified recombinant human BACE1 and a fluorogenic substrate, previous work from our lab showed that pCDP-DB

does not directly inhibit BACE1 catalytic activity *in vitro* (30). Our goal is to use both cell models H4-APP695 (WT7) or BACE1 H4-BACE1 (B18) to generate two distinct causative mechanisms in order to evaluate the effects of pCDP-DB treatment on amyloidogenic processing.

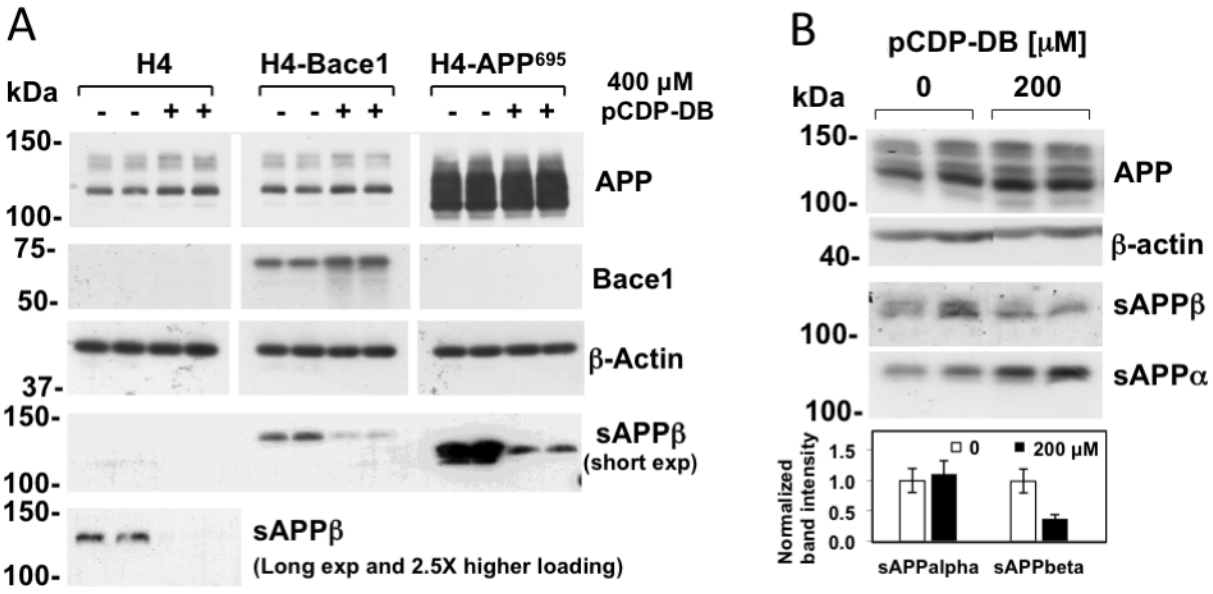

Figure 3: Treatment with pCDP0DB causes specific reduction of sAPPβ production.(A) pCDP-DB inhibits sAPPβ production in human H4, H4 BACE1 and H4-APP695 cells. (B) pCDP-DB inhibits sAPPβ production in mouse primary astrocytes.

Treatment of B18 cells with pCDP-DB does not change the colocalization of APP and BACE1.

In order to assess whether inhibition of sAPPβ production was due to APP and BACE1 being trafficked to different places in the cell, we analyzed the colocalization of APP/BACE1 in cells with and without treatment of pCDP-DB. In cells over expressing BACE1 ("B18"), we analyzed the colocalization of APP using the APP C-terminal antibodies CT C1.6.1 and Y188 and a BACE1 antibody (please see Materials and Methods). Results showed that there was no significant difference in colocalization of APP and BACE1 in cells treated/untreated with pCDP-DB (fig. 4). Next, we turn to investigation of the effects of pCDP-DB on APP and BACE1 trafficking to early endosomes.

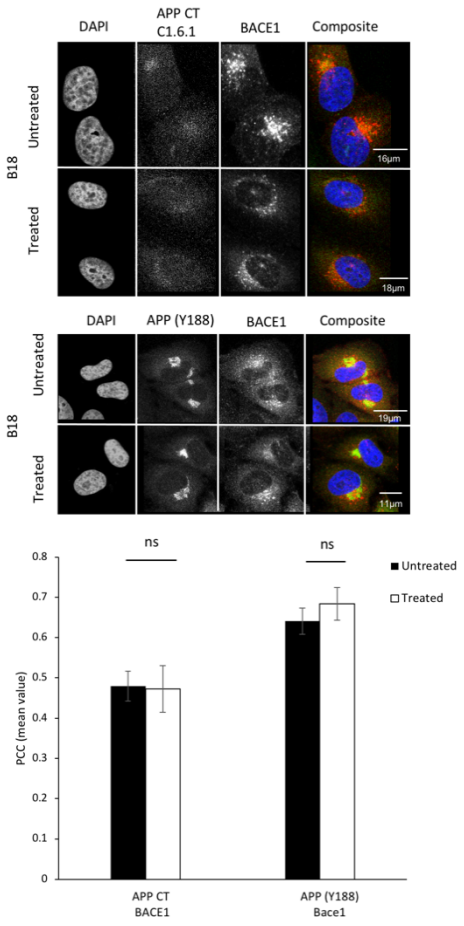

Figure 4: pCDP-DB does not inhibit colocalization of AAP and BACE1. There is no significant difference (ns) between treated and untreated cells (B18 cells overexpressing BACE1). The nucleus was stained with DAPI ext/em: 405/446, BACE1 (Cy3) 561/634, APP CT C1/6.1 and APP (Y188) AlexaFluor 488/524.

Treatment of pCDP-DB decreases the colocalization of APP and BACE1 with Early Endosome antigen (EEA1).

As mentioned earlier, cleavage of APP by BACE1 occurs in acidic endosomes. In order to assess the location of APP and BACE1 in the cell we used an early endosome marker to investigate sAPPβ and Aβ being released through exocytosis. The EEA1 antibody is a

membrane bound effector protein that is specific to a C-terminal FYVE domain that binds to phosphatidylinositol-3-phosphate, which targets early endosomes that are involved in membrane trafficking (47). Interestingly, in cells overexpressing BACE1, treatment with pCDP-DB decreases the colocalization of BACE1 with EEA1 (fig. 6). Additionally, in cells overexpressing APP, treatment with pCDP-DB decreases the colocalization of full-length APP and EEA1 (fig. 6). These results indicate that treatment of cells with pCDP-DB reduces the amount of APP and BACE1 found in early endosomes. While there are many possible explanations for these observations, these results are consistent with pCDP-DB inducing the accelerated maturation of endosomes containing APP and BACE1.

Treatment of cells with pCDP-DB does not block internalization of APP-WT.

To investigate whether treatment with pCDP-DB might inhibit the endocytosis of APP, we performed an endocytosis assay using immunolabeling of the APP ectodomain and confocal fluorescence microscopy. H4-APP695 cells were treated with and without pCDP-DB for 24hours. Labeling of APP at the cell surface was performed by adding the APP mouse monoclonal N-terminal antibody 22C11 (the epitope is the sequence corresponding to amino acid residues 66-81) to live cells, which labels the extracellular N-terminus of APP, at time t=0 mins. After 10 minutes, cells were fixed and labeled with the rabbit monoclonal antibody Y188, which labels the C-terminus of APP (will bind to full length APP, AICD, C83, and C99). Overlap of signal from the 22C11 (N-terminal antibody) and Y188 (C-terminal antibody) showed internalization of full-length APP in the cells (fig. 5). These results show that APP has been predominately endocytosed, meaning that it has been brought from the cell surface and into the cell

within 10 minutes, and that endocytosis has not been affected by treatment of pCDP-DB (figure 5).

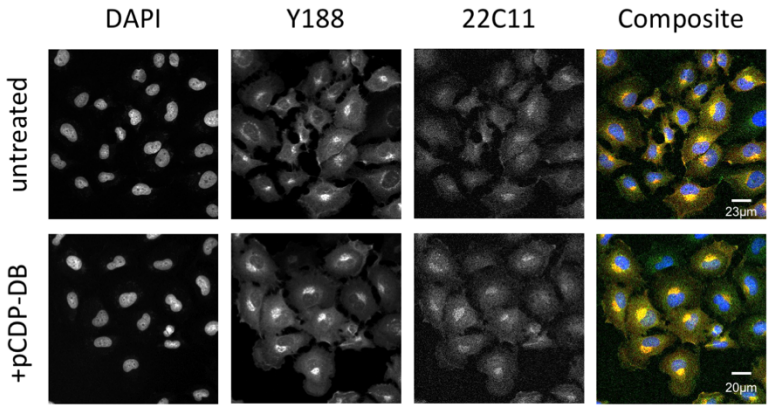

Figure 5: Internalization of APP is not inhibited by pCDP-DB treatment. The H4-APP696 cells were cultured on glass cover slips and treated with 400nM pCDP-DB or with the same volume of DMSO for 24hrs. The 22C11 ectodomain antibody (mouse) was briefly added at t=0 minutes and then washed. At t=10 min the cells were fixed and Alexa 488-tagged secondary (mouse IgG) antibody (green channel), and the N-terminal Y188 (rabbit) APP antibody and its secondary rabbit IgG antibody Cy3 (red channel) were added. The nucleus is visualized by DAPI staining (blue channel). Images were obtained using a Zeiss 710 confocal microscope. DAPI ext/em: 405/446 nm, AlexaFluor (Green) 488/524 nm, and Cy3 (Red) 561/634 nm.

To further investigate the effects of pCDP-DB on early endocytic trafficking of APP and BACE1, we used an early endosome associated (EEA1) marker in B18 cells to visualize BACE1 (Rabbit anti-BACE1 monoclonal antibody D10E5 (5606) was from Cell Signaling Technology (Danvers MA) and in WT7 cells to visualize APP (Y188) in fixed cells (Rabbit anti-APP monoclonal antibody Y188 (ab32136) from Abcam (Cambridge, MA)) (fig. 6). A statistical analysis of the colocalizations of BACE1 with EEA1 and of APP with EEA1 was performed using the EzColocalization plugin in ImageJ (48). For all cases positive PCC values were obtained, consistent with known localization of APP and BACE1 to early endosomes. Notably, pCDP-DB treatment induced a significant reduction in colocalization of both BACE1 and APP with EEA1

(fig. 6). These results indicate that treatment of cells with pCDP-DB reduces the amount of BACE1 and APP in early endosomes and is consistent with a pCDP-DB-induced acceleration of endosomal maturation for endocytic compartments containing BACE1 and/or APP (fig. 6).

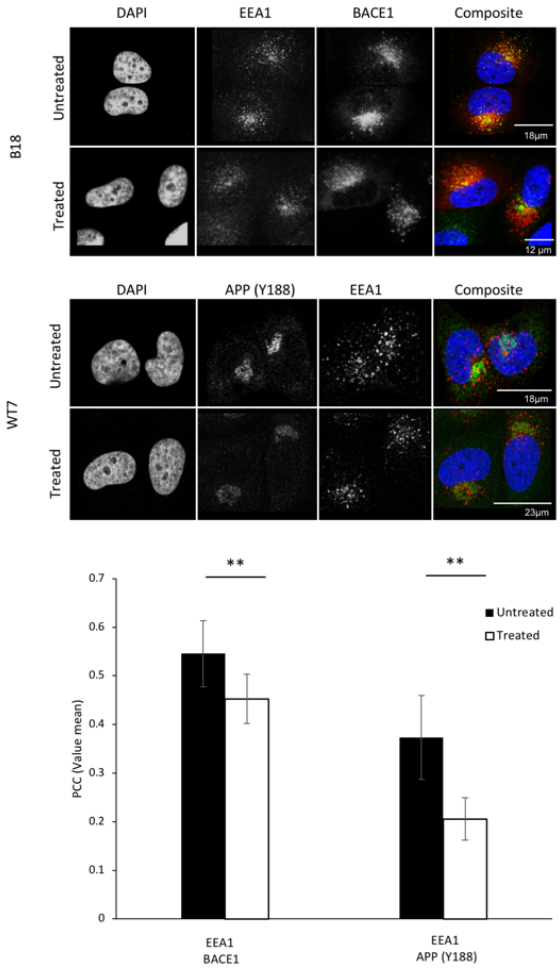

Figure 6: pCDP-DB decreases colocalization of APP and BACE1 with early endosome marker (EEA1). There is a statistically significant reduction of BACE1/EEA1 and APP/EEA1 PCC values between untreated and treated cells (B18 and WT7 cells, respectively). The nucleus was stained with DAPI ext/em: 405/446, in B18 cells BACE1 (Cy3) 561/634 and EEA1 AlexaFluor 488/524. P=0.004 In WT7 cells APP (Y188) AlexaFluor 488/524 and EEA1(Cy3) 561/634. P=0.002.

Proline point mutations within the cytoplasmic C-terminal tail of APP mimicking the cis-conformation do not inhibit endocytosis.

To investigate whether the cis-conformation connects APP to BACE1 cleavage, our lab generated novel Pro to Ala mutants in the cytoplasmic tail of APP (APPc)(30). APPc contains two Pro-containing motifs (T**P669**EER and GYEN**P685**TY). For example, each of the prolines are known to have *trans*-specific binding partners like Pin1-WW domain, Fe65, and X11 (15,31,32). To test the hypothesis that the *cis* conformation of one or both of the proline residues in the cytoplasmic tail of APPc was responsible for promoting BACE1 cleavage, each proline was substituted to alanine in order to further understand the function, trafficking and degradation of APP. To additionally investigate how treatment with pCDP-DB, which contains two benzyl groups, could mimic the two consecutive Phe residues near the Pro685 in the -GYEN**P**TY**FF**- motif these Phe residues were also mutated to Ala. Stable H4 neuroglioma cell lines were generated to stably express an N-terminal FLAG-tag followed by APP-695 wild type (WT) or mutants of APP (P669A, P685A, P669A/P685A or F689A/F690A) in order to measure their effects on the amount secreted sAPPβ and sAPPα. Robust expression of each FLAG-tagged protein was confirmed by Western blot (WB) (Figure 7A and 7B, data acquired and analyzed by Ross J. Resnick). Also assayed by WB were the relative amounts of sAPPβ and sAPPα secreted to the conditioned media, and of intact APP and the Thr668- phosphorylated form of APP, with GAPDH used as a loading control for whole cell lysate samples. Secreted sAPPβ and sAPPα represent the first steps in amyloidogenic and non-amyloidogenic pathways, respectively. In figure 7A, the P669A mutants displayed an increased sAPPβ secretion, whereas the P685A and P685A/P685A

mutations showed no sAPPβ secretion. Interestingly, the F689A/F690A mutant also showed a significant decrease sAPPβ secretion. However, the mutations in the -GYEN**P**TY**FF**- motif display no noticeable change in pT668 levels relative to the loading control (Fig. 7A). Importantly, pCDP-DB treatment of cells expressing the P669A mutant greatly diminished the secretion of sAPPβ, showing that the mechanism by which the P669A mutation promotes amyloidogenic processing of APP can be blocked by pCDP-DB (Fig. 7B). The relative protein ratios of sAPPβ/sAPPα show that our mutations in the -GYEN**P**TY**FF**- motif suppress the relative activity of the pathway that creates Aβ secretion showing that the cis-conformation plays a role in APP processing. The phospho-Thr668-specific antibody shows no interaction with mutants bearing the P669A substitution within this antibody's epitope. The next set of experiments were to determine if the Proline mutants alter internalization relative to WT APP.

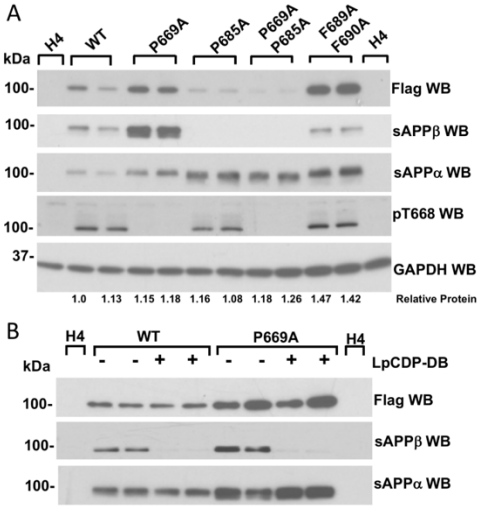

Figure 7: Proline point mutations within the cytoplasmic C-terminal tail of APP effect sAPPβ and sAPPα secretion. A) H4 cells stably expressing the indicated FLAG-APP construct (WT and mutants) were plated at 200K/cells per well in DMEM/FBS/PS/G418 and grown for 48h. Cells were washed twice with DMEM only, re-fed with 1ml DMEM/FBS/PS without G418 and incubated for an additional 24hrs. Conditioned media was harvested and WCL was prepared and both were combined with 4xSB. Aliquots were separated by SDS-PAGE and analyzed by immunoblotting for the proteins indicated. D) As in A, except FLAG-APP proteins were immunoprecipitated with anti-FLAG, captured proteins were separated by SDS-PAGE and analyzed by immunoblotting for the proteins indicated. (Figure legend from Nicholson 2020 NIH Grant)

Endocytosis assay to evaluate proline-to-alanine mutations within the cytoplasmic C-terminal tail of APP.

In figure 8, endocytosis time course assays were performed using H4 mass cultures containing cells stably transfected (all cell lines generated by Ross J. Resnick) with versions of N-terminal FLAG-tagged APP (P669A, P685A,

P669A/P685A, or F689A/F690A). At time, t=0 minutes anti-FLAG is briefly added to the media and quickly washed in order to label APP molecules via the N-terminal FLAG tag on the ectodomain, and cells continue in culture for a given period of time (0, 5, 10 min) (Fig 8). At a given time point the cells are fixed and then stained with the desired primary and secondary antibodies. In figure 8, time t=0 shows APP molecules at the plasma membrane at time t=0 minutes. In all four cases (WT, P669A, P685A and FFAA), the APP is primarily at the cell surface at t = 0 (Fig. 8, panel 1). Both wild type and the P669A mutant showed a significant decrease in production of sAPPβ upon treatment with pCDP-DB. As expected, the internalization of these APP mutants colocalized into early endosomes (Fig. 8, panel 2).

The colocalizations of WT and mutant APP proteins with the early endosome marker EEA1 were quantified in replicate confocal images using the Pearson's Correlation Coefficient (PCC) (where PCC values range from -1 to +1; no association between proteins is 0, and negative or positive correlations are indicated by sign). The PCC values for WT at 0min, 5mins and 10mins (PCC=0.2, 0.5, 0.5, respectively) displayed the expected positive colocalization as APP proteins are internalized to early endosomes during this timeframe.

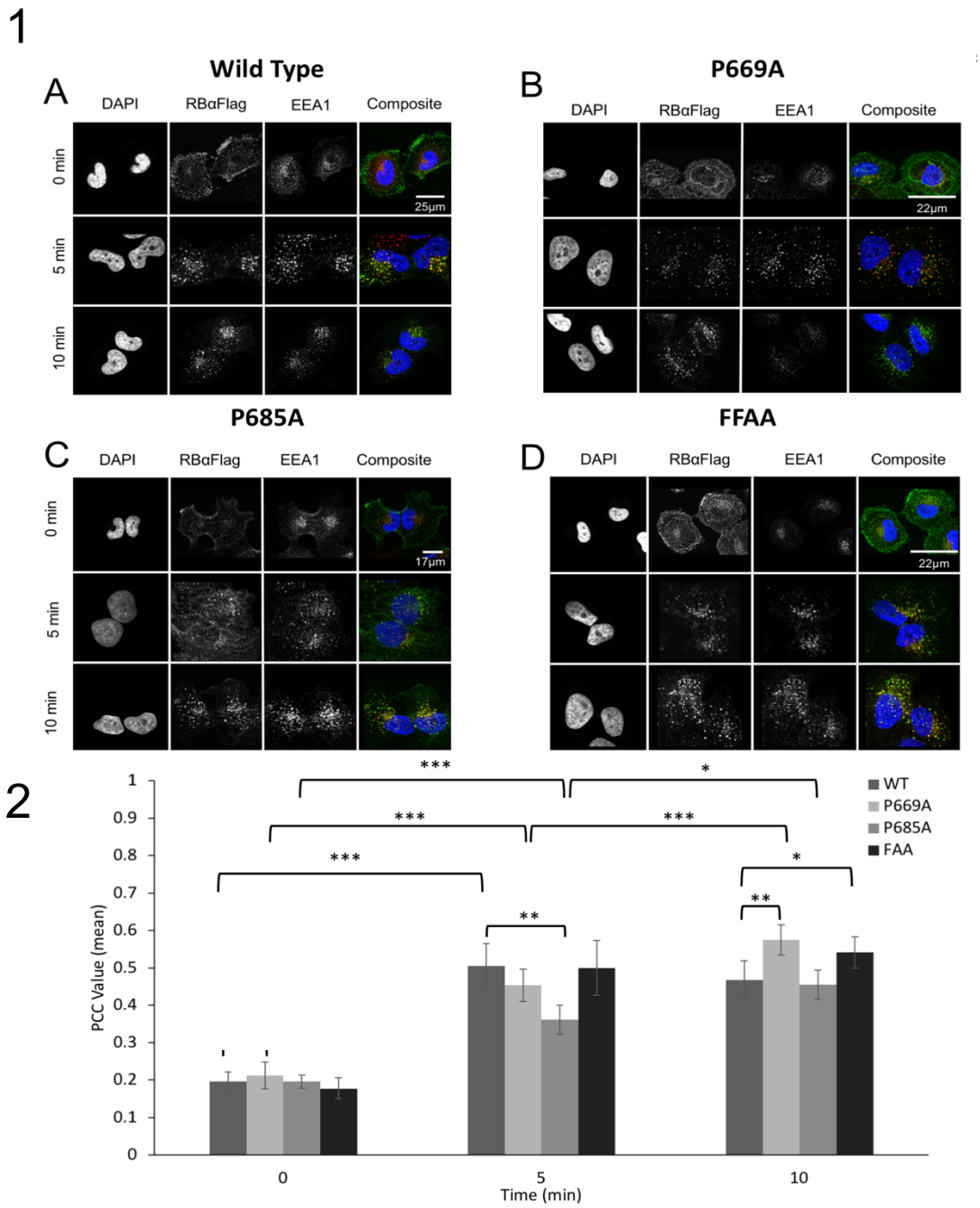

Figure 8. Internalization of APP harboring proline-to-alanine mutations does not alter endocytosis. (1) Mass cultures of H4 cells stably transformed with N-terminally FLAG-tagged APP-WT, APP-P669A, or APP-P685A were cultured on glass cover slips, anti-FLAG was briefly added at time t=0 and quickly washed, and cells were fixed at t=0, 5 and 10 minutes. FLAG-APP proteins were visualized in fixed cells by addition of secondary antibody anti-IgG (green), early endosomes (rabbit IgG) and washed, then secondary anti-rabbit (red). The nucleus is visualized by DAPI staining (blue). Cells were imaged using a Zeiss 710 confocal fluorescence microscope. **2)** Summarized data shows the Pearson Correlation Coefficient (PCC) of APP and EEA1with pCDP treatment over time (please see Appendix table 4.1 or text for significant p-values). DAPI ext/em: 405/446, AlexaFluor (Green) 488/524 and Cy3 (Red) 561/634.

three mutant groups compared to WT at each time point (0, 5, and 10 minutes) and within each group across different time points (fig. 8 panel 2). As expected, there was no obvious difference between WT and the mutants at t=0 minutes since antibody-labeling of FLAG-APP proteins occurs at the cell surface. The PCC values for P669A at 0min, 5mins, and 10mins were PCC= 0.2, 0.5, and 0.6, respectively. These differences across the time points for the P669A mutant were statistically significant ($p \leq 0.001$) between 0mins to 5mins, and 5mins to 10mins. Similarly, the PCC values for P685A at 0min, 5mins, and 10mins were PCC=0.2, 0.4, 0.5, respectively. However, the PCC value difference between time points for the P685A mutant was only statistically significant between 0mins to 5 mins (Fig. 8D), consistent with the hypothesis that this mutant might be trafficked away from early endosomes more rapidly. In support of this idea, the PCC values at 0min, 5mins, and 10mins for the other imaged mutant that displays greatly reduced sAPPβ secretion, F689A/F690A (FFAA), were PCC=0.2, 0.5, and 0.5, respectively, and the PCC value difference between time points for this mutant was statistically significant (P-value= 0.001) only between 0mins to 5mins. Overall, at t=10minutes APP is internalized in all three cases, but mutants that display reduced sAPPβ secretion are present at lower relative amounts in early endosomes at this time point (Fig. 4C). Notably, the internalization of the P685A and FFAA mutants (Fig. 8C) demonstrate that the lower sAPPβ secretion for these mutants (figure 7A) is not due to endocytosis inhibition. These results indicate that our mutations in the -GYEN**P**TY**FF**-motif alter APP trafficking downstream of endocytosis and are consistent with the idea that acceleration of endosomal maturation might be involved.

Investigating pCDP-DB interaction proteins

In order to investigate what cellular proteins might bind to pCDP-DB our lab has collaborated with the Hening Lin lab (Department of Chemistry and Chemical Biology, Cornell University) to perform SILAC quantitative proteomics studies using bead-tethered pCDP-DB (49). This approach identified 118 potential pCDP-DB binding proteins (Appendix Table 4.2). To explore possible roles of these proteins in the intracellular trafficking of APP and BACE1, we selected seven candidates with known roles in endosomal maturation or autophagy.

These putative pCDP-DP interactor proteins, identified by proteomics and selected for further study in both H4 cell models based on their known functions, were Hsp90AA1, Hsp90AB1, Eno1, Moesin, PDIA4, PDIA3, and Annexin A1 (only in B18 cells, fig. 9). In both cell models the colocalization of Hsp90 AA1 with APP and BACE1 displayed a significant increase upon treatment with pCDP-DB (B18 cells P-value=0.0001, and WT7 cells P-value=0.027). In WT7 cells, Hsp90 AB1 with APPc (C1.6.1) displayed a significant change in colocalization upon treatment (P-value =0.0023). Lastly, in WT7 cells PDIA3 has a significant change in colocalization upon treatment with pCDP-DB (P-value= 0.001) (fig. 10). Taken together, these results display the proteins from the proteomics studies have a modest change in colocalization in cells treated with pCDP-DB.

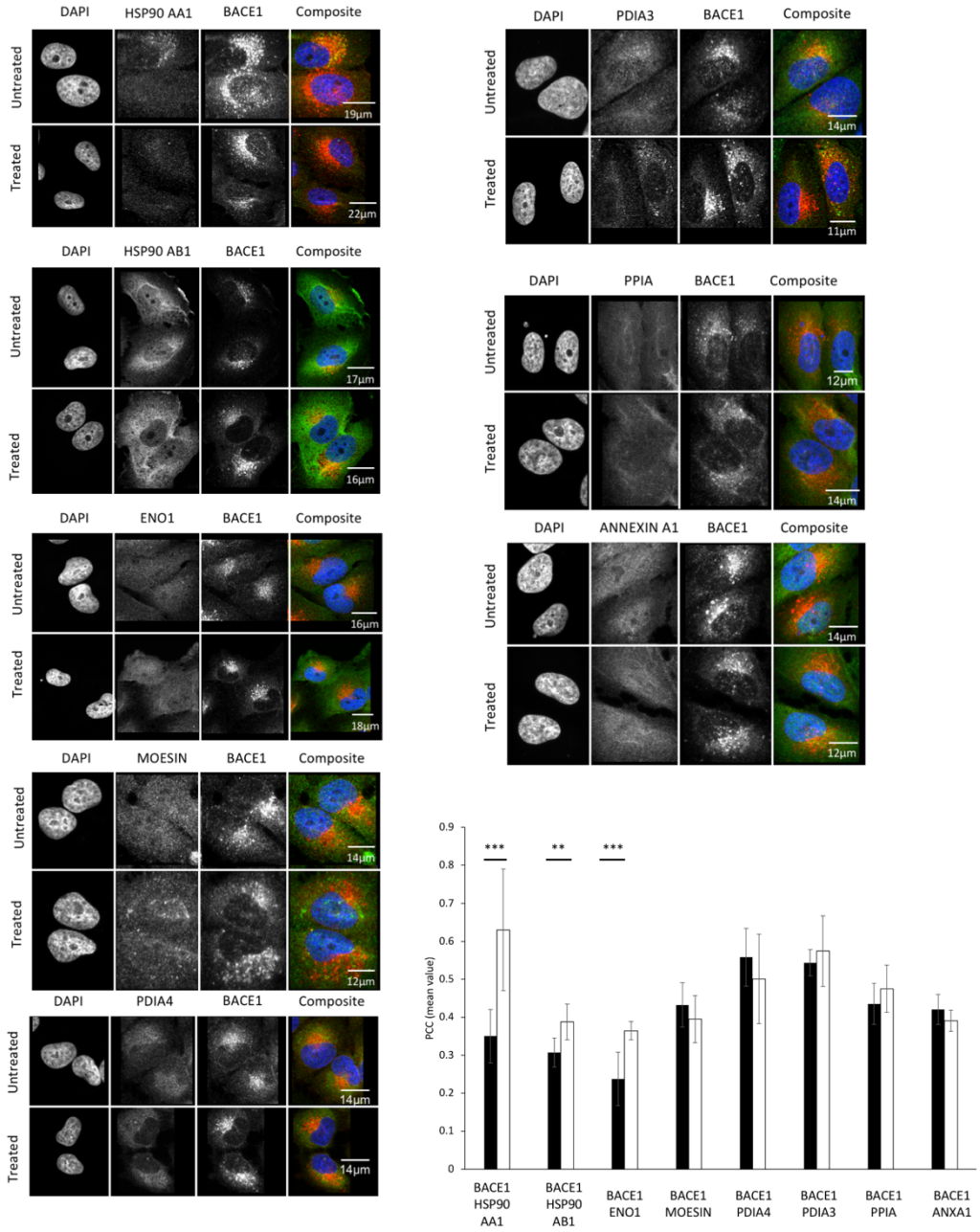

Figure 9: pCDP-DB increases colocalization of HSP90AA1, HSP90 AB1, and ENO1 in B18 cells overexpressing BACE1. There is a statistically significant difference between untreated and treated cells: HSP90AA1 and BACE1 P=0.0001, ENO1 and BACE1 P= 0.0007. The nucleus was stained with DAPI ext/em: 405/446, in B18 cells TIP60 AlexaFluor 488/524 and APP-CT (Cy3) 561/634. Summarized data shows the Pearson Correlation Coefficient (PCC), please see Appendix table 4.3 or text for significant p-values.

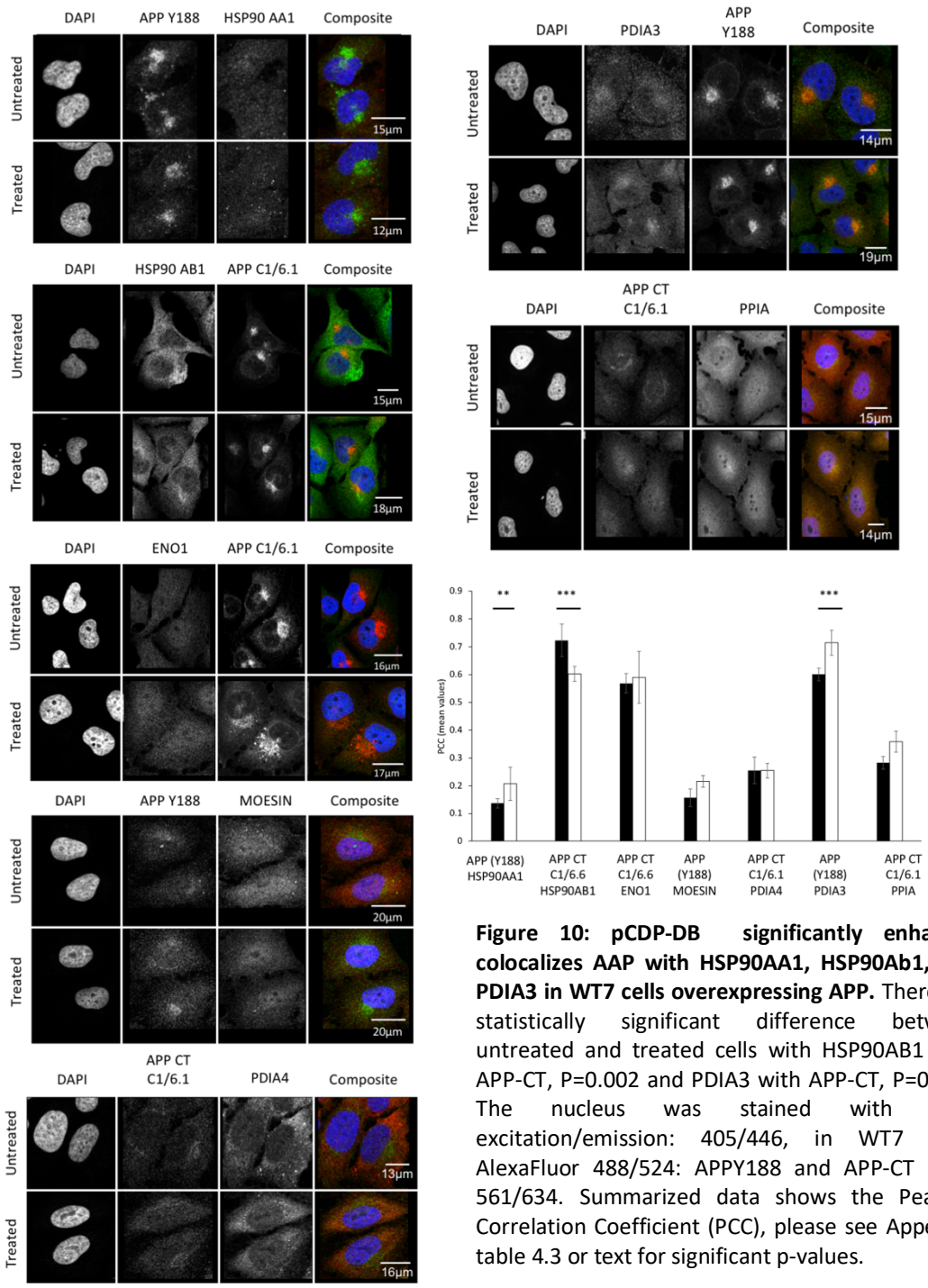

Figure 10: pCDP-DB significantly enhances colocalizes AAP with HSP90AA1, HSP90Ab1, and PDIA3 in WT7 cells overexpressing APP. There is a statistically significant difference between untreated and treated cells with HSP90AB1 with APP-CT, P=0.002 and PDIA3 with APP-CT, P=0.002. The nucleus was stained with DAPI excitation/emission: 405/446, in WT7 cells. AlexaFluor 488/524: APPY188 and APP-CT (Cy3) 561/634. Summarized data shows the Pearson Correlation Coefficient (PCC), please see Appendix table 4.3 or text for significant p-values.

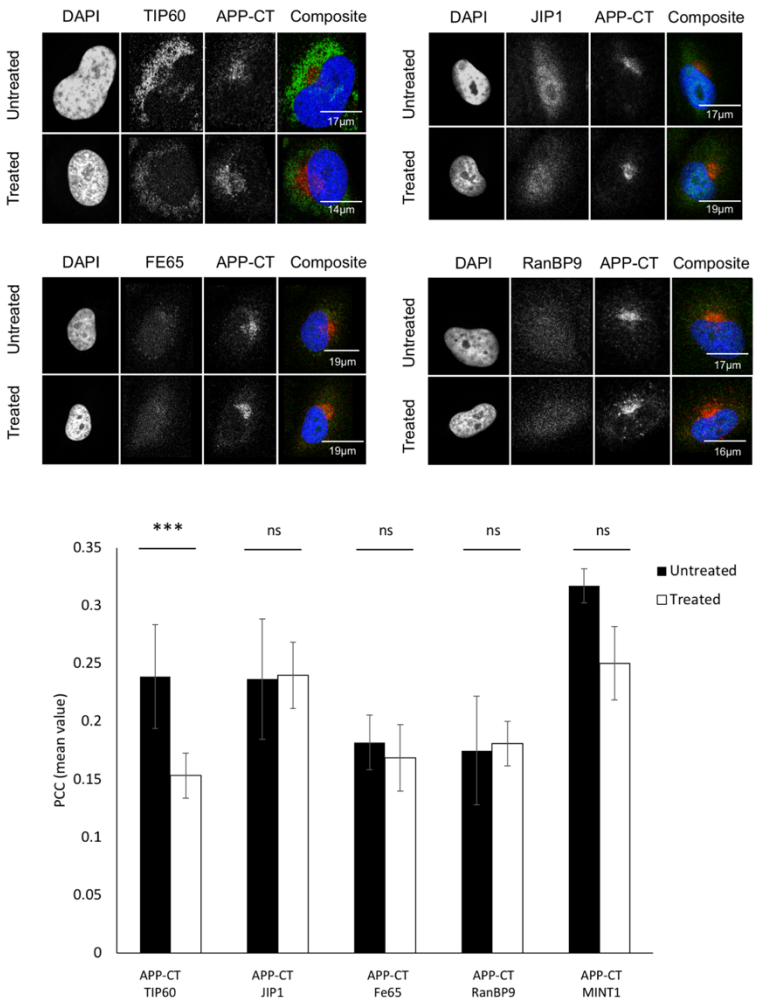

Figure 11: pCDP-DB decreases colocalization of AAP-CT and TIP60 in WT7 cells overexpressing APP. There is a statistically significant difference between untreated and treated cells (WT7) P=0.0003. The nucleus was stained with DAPI ext/em: 405/446, in B18 cells TIP60 AlexaFluor 488/524 and APP-CT (Cy3) 561/634. Summarized data shows the Pearson Correlation Coefficient (PCC), please see appendix table 4.4 or text for significant p-values.

We also investigated the colocalization of APPc tail with known interactor proteins (TIP60, JIP1, FeBP9, and RanBP9) in B18 cells with and without treatment (fig. 11). TIP60 had a significant decrease in colocalization upon treatment (Appendix, Table 4.4) (P-value of 0.0003). In B18 and WT7 cells, there was no significant change in the colocalization with APPc and Mint1 (P-value=0.05 in B18 cells) (fig. 12).

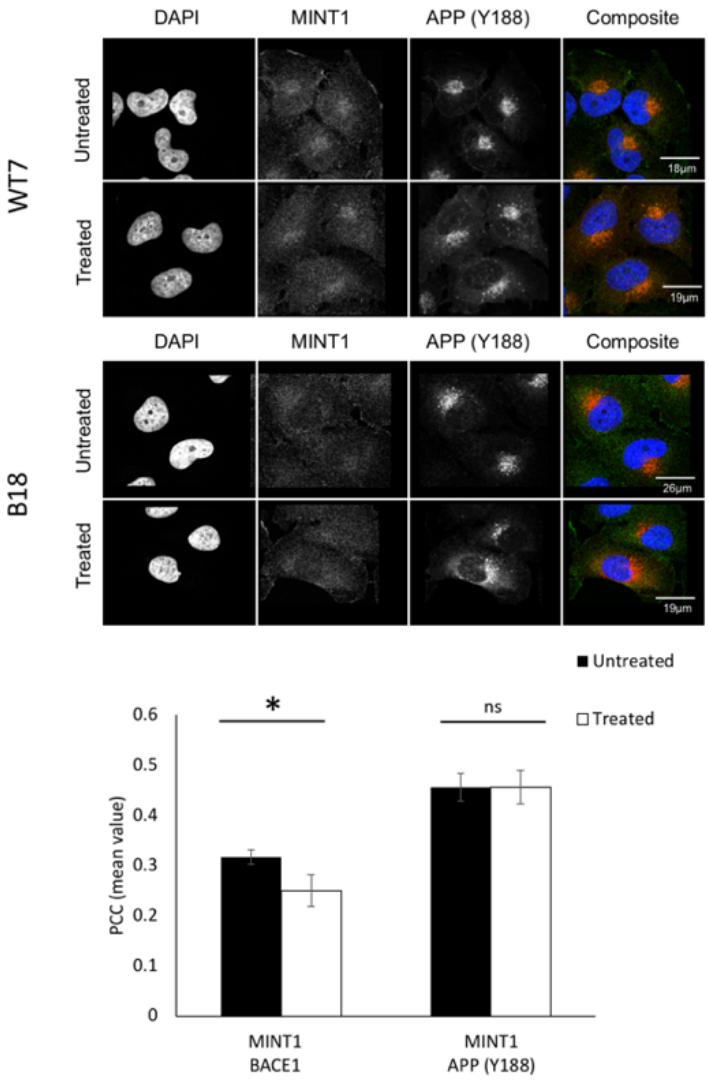

Figure 12: pCDP-DB decreases colocalization of MINT1 and BACE1 in B18 cells overexpressing BACE1. There is a significant difference between untreated and treated cells (B18 cells) P=0.049. The nucleus was stained with DAPI ext/em: 405/446, in B18 cells MINT AlexaFluor 488/524 and APP-Y188 (Cy3) 561/634.

DISCUSSION

Applicable treatment for AD will require a vital understanding of APP processing and APP/BACE1 trafficking in the cell. Although many treatment strategies have targeted Aβ producing enzymes, none have succeeded. The proteolytic processing of APP can occur through two distinct pathways, but only one produces Aβ (11,16). Therefore, decreasing Aβ production and new APP fragments without blocking APP endocytosis is a highly desirable tool to study in the amyloidogenic pathway. This study utilized a "cis-locked" pCDP-DB small molecule that inhibits Aβ generation and sAPPβ in human AD cell models(30).

APP is primarily cleaved by BACE1 in endosomal compartments that provide a route for sAPPβ and Aβ to release through exocytosis (27). Therefore, it was important to take into account the location of APP and BACE1 in the cells. One possibility for the decrease in sAPPβ would be that treatment is causing BACE1 and APP to be trafficked to different places in the cell. However, we performed a whole-cell colocalization analysis to assess the change in location of APP and BACE1 (fig. 4). Surprisingly, no differences were found in the colocalization of APP and BACE1 in treated cells compared to untreated cells. This study set out with the aim of investigating the decrease of sAPPβ with treatment. These findings suggest that our small molecule is not inhibiting APP to be cleaved by BACE1.

An important consideration to be addressed is whether treatment with pCDP-DB inhibits the internalization of APP. Prior studies that have noted the importance of BACE1 have discovered that APP cleavage occurs predominately in acidic endosomes (27). Inhibiting the association of BACE1 with APP in acidic endosomes would reduce

the secretion of sAPPβ. However, the acceleration of APP and BACE1 out of the acidic endosomes and into lysosomes would also reduce the secretion of Aβ and sAPPβ. The immunolabeling of the APP ectodomain in treated cells shows that APP is predominately endocytosed. This result demonstrates that pCDP-DB does not block the endocytosis of APP (fig. 5). Thus, the impact of treatment on the sAPPβ secretion is not due to inhibition of APP endocytosis. One hypothesis is that pCDP-DB may be enhancing endosomal maturation and trafficking of APP to lysosomes for degradation.

As mentioned earlier, cleavage of APP by BACE1 occurs in acidic endosomes. In order to assess the location of APP and BACE1 in cells treated with pCDP-DB we utilized an early endosome antigen (EEA1) antibody (fig. 6). Notably, we discovered that the colocalization of APP/BACE1 with the early endosome marker (EEA1) was decreased by treatment of cells with pCDP-DB. This result suggests that pCDP-DB affects APP and BACE1 trafficking. However, we have observed that pCDP-DB does not block APP endocytosis. It is possible, therefore, that pCDP-DB might be impacting the endocytic pathway by enhancing endosomal maturation and trafficking of APP to lysosomes for degradation.

Previous studies evaluating pT668 accumulating in AD brains have hypothesized that the cis isomer could serve as a molecular signal for the Aβ-producing pathway (30,34). We have mutated two Pro and the two consecutive Phe residues within the APP cytoplasmic tail (P669 and P685, 661-VEVDAAVT**P**EERHLSKMQQNGYEN**P**TYK**FF**-690) to investigate the role of the *cis* conformation in linking APP to BACE1 cleavage. Of the mutations, P685A and F689A/F690A significantly reduced sAPPβ production, consistent with the *cis*

conformation acting as a pathogenic signal to promote APP entry into the Aβ-producing pathway. Surprisingly, the P669A increased sAPPβ production (fig. 7). This result may be explained by the sAPPβ/sAPPα ratio, reflecting the relative amyloidogenic vs. the non-amyloidogenic pathways. Thus, the sAPPβ/sAPPα ratio obtained from -GYEN**P**TY**FF**- motif portrays a suppression of the relative activity Aβ-producing pathway. We used the endosomal marker (EEA1) to evaluate the endocytosis of APP in the proline mutant cells. In the proline mutant cells, treatment did not block the endocytosis of APP. This experiment confirms that the P685A mutant had lower sAPPβ internalization, not due to endocytosis inhibition. Therefore, it is likely that such a *cis* conformation connection occurs, leading APP to the amyloidogenic pathway. Moreover, we discovered that the colocalization of APP/BACE1 with the early endosome marker (EEA1) was decreased due to treatment.

AD is a complex disease, and the treatment of pCDP-DB may potentially influence other factors involved in APP/BACE1 trafficking. Utilizing our previous published two distinct cell models, H4-AβPP695 (WT7, overexpressing APP) and H4-BACE1 (B18, overexpressing BACE1) (30), we were able to investigate how treatment with pCDP-DB affects APP and BACE1 colocalization with known proteins that interact with APP such as, TIP60, JIP1, Fe65, and RanBP9(50,51). Of our known APP interactors treated, TIP60 and MINT1 showed a decrease in colocalization with APP in B18 cells. A part of the histone acetyltransferases (HATs), TIP60, is located in the nucleus playing an essential role in regulating chromatin remodeling, transcription, and other nuclear processes (46). Surprisingly, TIP60 was situated in untreated cells in a cluster to one side of the nucleus. Upon treatment TIP60's colocalization with APP

significantly decreased and was shown to not be in the nucleus but to be dispersed around the nucleus. These results suggest that treatment of TIP60 and APP, while both in clusters near the nucleus may be relocated to the ER or Golgi apparatus, possibly involved in the secretory pathway(52-54).

In the cell, APP can enter the endocytic pathway via clathrin-coated vesicles taken up as vacuoles into the lumen of early endosomes, which eventually leads to the generation of sAPPβ trafficked to the recycling endosomes to release sAPPβ to the extracellular space(16,17). In the literature, MINT1 is known to be localized at the plasma membrane and stabilize APP and is involved in signal transduction (55). In our untreated WT7 cells, MINT1 is mostly localized at internal compartments. However, MINT1 in the untreated WT7 cells, with APP being overexpressed the plasma membrane, has a visually defined structure. Notably, upon the treatment, the plasma membrane structure no longer has a defined plasma membrane. We performed a whole-cell colocalization analysis to assess the amount of protein in the cell. Therefore, our PCC values would not indicate a change in that protein's location in a particular area of the cell. This observation would suggest that MINT1 is no longer heavily located at the plasma membrane, suggesting that pCDP may inhibit APP interacting with MINT1 at the plasma membrane. In B18 cells, MINT1 showed a slight decrease in colocalization with APP upon treatment. In these cells, APP is not overexpressed; therefore, it is plausible that other factors can bring and stabilize APP at the plasma membrane. Although this study focuses on investigating the treatment of pCDP-DB, the findings may well have a bearing on understanding the regulatory mechanisms that govern the trafficking, processing, and degradation of APP within the cell(19,56).

We performed proteomics experiments to identify a total of 44 proteins (Appendix Table 4.2) as potential pCDP-DB binding proteins. Moreover, we have identified subsets of pCDP-DB interactors that are involved in endosomal maturation and lysosomes for degradation from our proteomics study. To investigate additional potential impacts of pCDP-DB in the cell, we looked at a subset of eight interactor proteins (HSP90 AA1, HSP90 AB1, ENO1, MOESIN, PDIA4, PDIA3, PPIA) suggested by the pCDP-DB interactome (fig. 11). These findings will help understand how treatment might regulate APP trafficking, proteolytic processing, and degradation mechanisms.

This paper examines how pCDP-DB affects APP trafficking to provide insights into Aβ production. However, an alternative hypothesis is that pCDP-DB might affect BACE1 trafficking (54,57). B18 cells were overexpressing BACE1 to address this alternative hypothesis. In B18 cells, treatment increased the colocalization of HSP90 AA1, HSP90 AB1, and ENO1 (Alpha-enolase) with BACE1. In the literature, HSP90 AA1 and its paralog gene HSP90 AB1 aid in the proper folding of proteins. First, HSP90 AA1, in untreated B18 cells, is localized to punctate dots. However, treatment displays no visible punctate dots near the nucleus. HSP90 AA1 is known to localize in the lysosome, extracellular matrix, and cytosol. As mentioned above, cleavage of APP by BACE1 occurs in acidic endosomes (27,53). Previous studies have shown HSP90 AB1 is known found in the plasma membrane and lysosomes (58,59). It is possible that when there are low amounts of APP present in the cell that the soluble cleavage product of sAPPβ may be enhanced by pCDP-DB to endosomal maturation and trafficking of APP to the lysosomes for degradation.

Lastly, ENO1 is a glycolytic enzyme expressed in most tissues that may function as a tumor suppressor (60). Previous studies have suggested that enolase is involved in more processes than glucose metabolism in an AD brain but may function to preserve the brain function (60). These results suggest that when low APP levels are present in the cell, pCDP-DB might promote APP/BACE1 trafficking from the plasma membrane to the lysosomes, which degrades Aβ and sAPPβ.

Although trafficking of APP to lysosomes would lead to its degradation, alternative routes for APP degradation are possible, most notably ubiquitin-dependent proteasomal degradation and autophagy (27,61,62). In the WT7 cell model, overexpressing APP, we saw an increase in colocalization of HSP90 AA1 and PDIA3 with APP. Research has located HSP90 AA1 in the extracellular matrix, cytosol, and lysosome(58,62), which suggests that pCDP-DB treatment might promote the trafficking of APP to the lysosome via enhancing the association of Hsp90 with APP. Moreover, PDIA3 in untreated WT7 is minimally colocalized with APP, and upon treatment colocalization is increased. PDIA3 is known to be in the extracellular matrix, endoplasmic reticulum, and endosomes. In the literature, PDIA3 functions as a molecular chaperone to prevent the formation of protein aggregates (63). For example, PDIA3 and Calreticulin have been found in the extracellular fluid as carrier proteins to

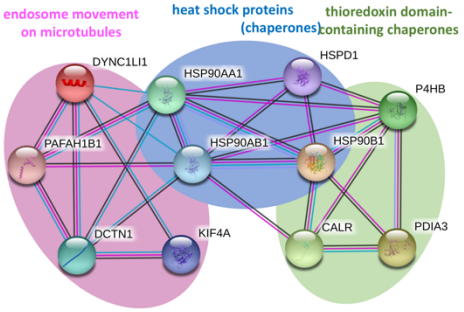

Figure 11: A sub-set of pCDP-DB interactors have key rols in endosomal maturation. The STRING protein-protein interaction network for selected proteins identified as potential pCDP-DB interactors by SLIC/MS was constructed using only experimental database information, at a medium confidence level (0.4). Heat shock proteins connect a network of chaperones to endocytic pathways proteins and motor proteins that facilitate endosome movement along microtubules PDIA3with demonstrated roles in Aβ production and clearance.

prevent Aβ protein aggregation and promote Aβ clearance (63-65). Previous studies evaluating endoplasmic reticulum (ER) stress and autophagy in AD have reported the upregulation of ER chaperons HSPA5, PDIA3 and HSP90B1 in neuroblastoma cells infected with scrapie in vitro and scrapie rodent models in vivo(66). Thus, treatment of pCDP-DB might increase HSP90 AA1 and PDIA3 to an alternative route enhancing endosomal maturation for degrading APP via ubiquitin-dependent proteasomal degradation, or lysosomes leading to autophagy. Further research should be undertaken to examine the colocalization of APP/BACE1 with Lamp1 or another lysosomal protein with pCDP-DB treatment.

One interesting finding is that treatment with pCDP-DB led to a decrease in colocalization of HSP90 AB1 and the c-terminal fragment antibody of APP in WT7 cells. Previous research has demonstrated that HSP90 AB1 is primarily found in the extracellular matrix, nucleus, cytosol, plasma membrane, mitochondrion. However, HSP90AB1 has been found to be minimally located in lysosomes, cytoskeleton and endoplasmic reticulum (27,58,61). In the literature, HSP90AB1 proteins are involved in signal transduction, protein folding, protein degradation, and inflammation. Thus, when over-expression of APP is present, HSP90 AB1 may be promoting APP to a trafficking pathway that degrades Aβ and sAPPβ. Together these results further support the hypothesis of pCDP-DB is interacting in APP trafficking to prevent Aβ aggregation and promote Aβ clearance in the cell through the lysosome or autophagy.

In conclusion, AD is a highly complicated disease heavily impacted by the proteolytic cleavage of the amyloid precursor protein (APP). To understand the regulation of APP trafficking, cleavage, degradation in the cell, small molecules like

pCDP-DB will provide critical insights into understanding how to inhibit Aβ in production leading to the discovery of useful therapeutic strategies. These experiments have confirmed that pCDP-DB inhibition of Aβ and secreted APP fragments produced by BACE1 are not due to APP endocytosis blockage. Here we have used the novel APP P685A, P669A, and FFAA mutants as a tool to identify proteins that alter the trafficking, proteolytic processing, and degradation of APP. Based on these results, we can conclude that pCDP-DB does not block APP endocytosis. Our proteomics experiments yielded 44 interactor proteins with pCDP-DB involved in endosomal maturation and ubiquitin-mediated proteasomal degradation. Previously established H4 neuroglioma cell lines overexpressing AβPP659, and H4-BACE1 investigated the colocalization of pCDP-DB with a subset of the SILAC interactor proteins (fig. 11). Overall, our studies suggest that pCDP-DB disrupts APP intercellular trafficking to inhibit Aβ and sAPPβ. Further work needs to be done to establish treatment of pCDP-DB in APP/BACE1 trafficking to different organelles like early endosomes, late endosomes, recycling endosomes, and lysosomes. This treatment on H4 neuroglioma cells provides a framework for using small molecules like pCDP to promote endosomal maturation of APP trafficking to the lysosomes for degradation. Overall, our studies support the idea that *cis* isomer is a pathogenic indicator that influences APP/BACE1 trafficking. These findings may help us to understand how small molecules can modulate APP trafficking and degradation as a novel way of treating AD.

MATERIALS AND METHODS

Materials. The human H4 neuroglioma cell line was purchased from American Type Culture Collection (ATCC) (Manassas, VA). Dulbecco's Modified Eagle Medium (DMEM; 4500 mg/L Glucose, 4.0 mM L-Glutamine and 3.7g/L sodium bicarbonate) was purchased from either Corning Life Sciences (#10-017-CV; Tewksbury MA) or Hyclone (#SH30022.LS; Cytiva, Marlborough, MA). Penicillin -Streptomycin (10,000 IU- 10,000 µg/ml; 100X), Trypsin (10X) and cell culture dishes were from Corning Life Sciences (Tewksbury MA). Fetal bovine serum was purchased from either R&D Systems (S11550)) (Minneapolis, MN) or ThermoFisher (26140079 and 26400044) (Waltham, MA). DC Protein Assay Kit and Prestained Dual Color Protein Standards were obtained from BioRad (Hercules, CA). PolyScreen PVDF transfer membrane (0.45mM) was from Perkin Elmer (Waltham, MA). Lipofectamine 2000, Pierce ECL Western Blotting substrate, Pierce SuperSignal West Pico Plus Chemiluminescent Substrate, High Capacity Streptavidin Agarose (#20357) and DMEM for SILAC (A33822) were all from ThermoFisher Scientific (Waltham, MA). G418 sulfate (G-418-1) was from Gold Bio (St. Louis, MO). [$^{13}C_6$, $^{15}N_2$]-L-lysine, [$^{13}C_6$, $^{15}N_4$]-L-arginine, L-lysine, protease inhibitor cocktail (P8340), phosphatase inhibitor cocktail 3 (P0044) were purchased from MilliporeSigma (St. Louis, MO). PEG-Biotin was from Santa Cruz Biotechnology (Dallas, TX). EDC and DMAP were from Chem-Impex (Wood Dale, IL).

Plasmids. All numbering for APP plasmids and cell lines reflect the 695 amino acid isoform (APP695) predominantly found in brain and used in these studies. pCAX-APP695 (plasmid #30137)expressing the full-length human non-tagged WT-APP695

protein and pCAX-Flag-APP695 (plasmid #30154) expressing the full-length human N-terminal Flag-tagged WT-APP695 protein were gifts from Dennis Selkoe & Tracy Young-Pearse (Addgene, Watertown, MA). pCMV6-XL5-BACE1 expressing the full length human BACE1 protein, transcript variant a, NM_012104.3 (plasmid #SC115547) was purchased from Origene, (Rockville, MD). pSV2neo which codes for the G418 antibiotic resistance gene was a gift from David Shalloway, Cornell University.

Generation of Flag-APP695 mutant plasmids. pCAX-Flag-APP695 plasmids containing the P669A, P685A, P669A/P685A and F689A/F690A mutations were created by site-directed mutagenisis of the parental WT pCAX-Flag-APP695 plasmid by Genscript (Piscataway, NJ).

Antibodies. Rabbit anti-sAPPβ polyclonal antibody poly8134 (813401), mouse anti-APP monoclonal antibody 6E10 (803001) and mouse anti-APP monoclonal antibody C1/6.1 (802801) were from BioLegend (San Diego, CA). Rabbit anti-APP monoclonal antibody Y188 (ab32136), rabbit anti-phospho-T668 monoclonal antibody EPR7074(N) (ab206297), rabbit anti-Fe65 [EPR3538] monoclonal antibody (ab91650) and rabbit anti-RanBP9 monoclonal antibody (ab140627) were from Abcam (Cambridge, MA). Rabbit anti-BACE1 monoclonal antibody D10E5 (5606) was from Cell Signaling Technology (Danvers MA). Rabbit anti-HSP90AB1 polyclonal antibody (11405-1-AP), mouse anti-PDIA3 monoclonal antibody (66423-1-Ig), rabbit polyclonal anti-TIP60 (10827-1-AP), rabbit anti-Moesin polyclonal antibody (16495-1-AP), rabbit anti-PPIA/cyclophilin A antibody (10720-1-AP), rabbit anti-PDIA4 polyclonal antibody (14712-1-AP), mouse anti-Hsp90AA1 monoclonal antibody (60318-1-AP)

and mouse anti-GAPDH monoclonal antibody (60004-1-Ig) were from Proteintech (Rosemont, IL). Mouse anti-APP monoclonal antibody 22C11 **(**14-9749-82), rabbit anti-DYKDDDDK (Flag) recombinant polyclonal antibody (740001), goat anti-mouse-Alexa 488 polyclonal antibody (A11029), goat anti-Rabbit Alexa 488 polyclonal antibody (A1034), goat anti-Mouse Cy3 polyclonal antibody (A10521), goat anti-rabbit Cy3 polyclonal antibody (A10520) and Fluoromount-G mounting medium with DAPI (00-4959-52) were from ThermoFisher Scientific (Waltham, MA). Rabbit anti-Enolase 1 and (GTX101803) and rabbit anti-annexin A1 (GTX101070) polyclonal antibodies were from Genetex (Irvine, CA). Mouse EEA1 mouse monoclonal antibody 14/EEA1 (610456) was from BD Biosciences (San Jose, CA). Goat anti-rabbit and goat anti-mouse horseradish peroxidase (HRP)-conjugated secondary antibodies were from Jackson ImmunoResearch Laboratories (West Grove, PA). Mouse anti-BACE1 monoclonal antibody (sc-33711), rabbit anti-JIP1 polyclonal antibody (sc-153530) and mouse anti-Mint1 monoclonal antibody (sc-137022) were from Santa Cruz Biotechnology (Dallas, TX).

Synthesis of LpCDP-DB and LpCDP-DB-COOH. LpCDP-DB and LpCDP-DB-COOH (containing CH_2COOH attached to the nitrogen of the phospho-Thr in the 6-membered ring of pCDP-DB) used in this study were custom synthesized by Viva Biotech Ltd. (Shanghai, China) and purchased through Trillience (Toronto, Ontario).

Synthesis of biotinylated LpCDP-DB. A solution of the precursor molecule LpCDP-COOH (10 mg, 0.0194mmol) dissolved in dry DCM (6 mL) was combined with PEG-Biotin (10.77 mg, 0.0233mmol), EDC (4.47 mg, 0.0291mmol) and DMAP (0.23 mg, 0.0019mmol) and the solution was stirred for 16h at room temperature. TLC analysis

showed the absence of free LpCDP-DB-COOH indicating the reaction had gone to completion. The reaction solution was diluted with DCM (30 mL) and washed sequentially by separation with 0.5 N HCl (4 mL), saturated $NaHCO_3$ (2 mL) and Brine (5 mL), dried on anhydrous Na_2SO_4, filtered and solution was evaporated. The crude product was purified on a silica column, eluted with (DCM:MeOH=10:1) and fractions were analyzed by TLC and LC-MS to determine purity. Purified biotinylated-LpCDP-DB (>96%) was dried as a white solid and stored at -20°C. (LC-MS calculated: mass is 961.07; actual 962.34 (M+H).

Preparation L-pCDP-DB and biotinylated-LpCDP-DB solutions. L-pCDP-DB and biotinylated-LpCDP-DB were solubilized in DMSO to a stock concentration of 100 mM and 50mM respectively and stored at -20°C. Equal concentrations of DMSO were used as a control for CDP treatments (0.4% for immunofluorescence and APP processing; <2% for SILAC experiments).

Cell culture. H4 neuroglioma cell lines were routinely propagated in monolayer culture in complete growth medium (F10) consisting of DMEM supplemented with 10% fetal bovine serum and 100 IU /100 μg/ml penicillin/streptomycin at 37°C in a humidified atmosphere (90%) containing 10% CO_2 unless otherwise indicated. Cells were isolated by trypsinization for routine passaging and plating for experiments as described in the Methods below and/or in the figure legends. Quantitation of cells was carried out using a TC20 automated cell counter (BioRad, Hercules, California). DMSO concentrations were maintained at 0.4% for all cell culture experiments requiring treatment with CDPs.

Generation of H4 neuroglioma clonal cell lines over-expressing non-tagged APP695 or BACE1 proteins. Cell lines constitutively over-expressing human APP695

(H4-APP695) or human BACE1 (H4-BACE1) proteins were created by co-transfecting H4 neuroglioma cells with either pCAX-AβPP695 or pCMV6-XL5- BACE1 with the G418 resistance plasmid pSV2neo (10:1 ratio) using Lipofectamine 2000 according to the manufacturer's instructions. Forty-eight hours after transfection, cells were split into complete growth medium supplemented with 500 μg/mL of G418 and after 2–3 weeks G418 resistant colonies were expanded and screened by immunoblotting for APP or BACE1 over-expression. Several positive clones of each were re-selected to generate clonal lines which were maintained in growth medium containing 200 μg/mL G418 until frozen.

Generation of H4 neuroglioma mass cultures over-expressing Flag-tagged WT and mutant APP695 proteins. Cell lines constitutively expressing Flag-tagged WT or mutant APP proteins were generated by co-transfecting individual pCAX plasmids and pSV2neo as described above. After selection with G418 the resulting mass cultures were maintained in growth medium containing 200 μg/mL G418 until frozen. Cells were used without further reselection.

Endocytosis of endogenous APP. H4 neuroglioma cells were plated in 35mm dishes (20k cells/dish) containing 12mm glass coverslips in F10. After 72h cells were washed two times with 2ml DMEM and refed with 2ml F10 containing either 400mM LpCDP-DB or DMSO (0.4%) as a control. After 26h cells were washed three times with DMEM, refed with 2ml DMEM/10mM Hepes pH7.2 containing either LpCDP-DB or DMSO and incubated for 30m at 37°C in 10% CO_2. Media was removed, replaced with 2ml DMEM/Hepes containing 1mg/ml of the N-terminal APP antibody 22C11 and incubated for 12m at 37°C in 10% CO_2 to allow APP-antibody complexes to be

endocytosed. Cells were then washed two times with PBS to remove unbound antibody, fixed, washed with PBS and processed for analysis by indirect immunofluorescence as described below.

Endocytosis of ectopically expressed Flag-tagged WT and mutant APP proteins. Mass cultures of H4 neuroglioma cells constitutively expressing WT or mutant forms of Flag-tagged APP were plated in 60mm dishes (40k cells/dish) containing 18mm glass coverslips in F10 plus 200mg/ml G418. After 72h one dish of cells for each time point was incubated on ice for 20m, refed with 3ml fresh cold F10 containing 1mg/ml of anti-Flag antibody and incubated on ice for an additional 20m to facilitate antibody binding. For the zero time point (no endocytosis) cells were washed one time with PBS at room temperature, fixed with paraformaldehyde, washed 3 times with PBS and set aside. For additional time points cells were treated as described above except that antibody containing medium was removed, cells were washed one time with PBS to remove excess antibody, refed with fresh pre-warmed F10 and incubated at 37°C to facilitate endocytosis of the antibody:APP complex. After 5m and 10m respectively cells were fixed, washed with PBS and processed for analysis by indirect immunofluorescence as described below.

Effects of LpCDP-DB on the subcellular localization of APP and potential binding partners. For co-localization studies, cells were plated in 100mm dishes containing 18mm glass coverslips in 15ml of F10 and allowed to grow for 48-72h. Cells were washed two times with 5ml DMEM, refed with 5ml fresh F10 containing either 400mM L-pCDP-DB or DMSO (0.4%) and incubated for an additional 24-26h. Cells were fixed and processed for analysis by indirect immunofluorescence as described below.

Preparation of cells for indirect immunofluorescence. Following the specific treatments of cells as outlined in previous sections cells were processed further at room temperature. Cells were fixed for 10min with 4% paraformaldehyde in PBS, washed three times with PBS, permeabilized for 10min with 0.1% Triton X-100 in PBS, washed three times with PBS and then subjected to immunostaining. All antibodies were diluted in PBS containing 1% BSA. Coverslips were inverted into solutions (20ul) containing primary antibodies (mouse or rabbit) and incubated for one hour, washed three times with PBS and incubated for an additional one hour with secondary antibodies (anti-mouse or anti-rabbit) conjugated to the Alexa 488 or Cy3 fluorophore. Coverslips were washed three times with PBS, rinsed with water, inverted onto glass slides with mounting medium containing DAPI and edges were sealed with clear nail polish. Specific primary and secondary combinations are indicated in the legend for each experiment. Images were collected by confocal microscopy as described below.

Imaging Analysis. To assess H4 cells with various fluorescent antibodies, confocal microscopy was carried out in Cornell's Biotechnology Resource Center. Images were acquired on a Zeiss LSM 710 Confocal Fluorescence Microscope using Zen Software (Zeiss). Alexa 488 and DAPI channels were excited at 488nm and 405nm, respectively and emissions were collected using filters at 490-558nm for Alexa 488 and 415-471nm for DAPI and 566-681nm for Cy3. Original images (.czi) were opened in Image J (FiJi) for analysis and saved (.tif). For presentations use only the brightness and contrast on the images (slice or z-stack images)were adjusted to display fluorescent antibodies. Individual and merged images are shown (composite). Scale bars were measured for each individual cell (μm). All images were originally collected

and subsequently adjusted based on the lowest detectable amount of fluorescent signal in order to have identical conditions for each fluorophore. EzColocalization analysis software was used to obtain the Pearson correlation coefficient (PCC) between the various antibodies between untreated and treated cells(48).

The work was partially supported through a Cornell University Institute of Biotechnology's Center for Advanced Technology (CAT) grant, funded through New York State Division of Science, Technology, and Innovation (NYSTAR): NYS contract C150124. Acknowledgement: Cornell University Biotechnology Resource Center (BRC**)** NIH S10RR025502 for data collected on the *Zeiss LSM 710 Confocal.*

http://www.biotech.cornell.edu/brc/brc/services/terms-and-policies

Analysis of APP processing in H4 neuroglioma cells. For comparison of the effects of flag-tagged WT and APP mutants on APP processing, cells were plated at a density of 2×105 cells per well in six-well cluster dishes in 5mL of F10 supplemented with 200ug/ml and grown for 48 hours. Cells were washed two times with 2ml of DMEM, re-fed with 1 mL of fresh F10 (without G418) and incubated an additional 24h. To evaluate the effect of LpCDP-DB on APP processing cells were treated as described above except that either 400mM L-pCDP-DB (final concentration) or DMSO (0.4%) was included in the 1ml of F10. For all experiments, conditioned media (CM) containing the secreted forms of APP was collected and placed on ice, the cell monolayer was washed two times with ice cold PBS and both fractions were processed as described below.

Preparation of conditioned media and whole cell lysates. Conditioned media from the APP processing experiments described above were centrifuged at 12,000 × g for 20

minutes at 4°C to remove cellular debris and aliquots of the resulting supernatants were combined with 4X Laemmli SDS-sample buffer containing 25mM DTT. The washed cell monolayers were lysed on the plate in 200–250 µL of lysis buffer (50 mM HEPES, pH 7.2, 150 mM NaCl, 2mM EDTA, 1% Triton X-100, 1mM sodium orthovanadate, 50 mM sodium fluoride, 10 mM β-glycerophosphate, 500 µM AEBSF, 10 µg /mL Aprotinin, 10 µg/mL Leupeptin, and 5 µg/mL Pepstatin) for 30min at 4°C with rocking. Whole cell lysates (WCL) were collected, centrifuged at 28,000 × g for 20 minutes at 4°C to remove cellular debris, protein concentrations were quantified using the DC Protein Assay with BSA as a standard and aliquots were combined with 4X sample buffer containing 25 mM DTT. Fresh LB and F10 were combined with sample buffer for use as a diluent for the protein standards and for normalization of sample volumes. WCLs and CM were subjected to SDS-PAGE and immunoblotting as described below.

SDS-PAGE and Immunoblotting. Aliquots of whole cell lysates (2mg), conditioned media (20ml) and pre-stained standards (5ml) were resolved in 4-20% Tris-Glycine SDS-PAGE gels and transferred to PVDF membrane according to Towbin (67) (but without methanol) using a Biorad Trans Blot system with constant cooling. Membranes were blocked with TBST (25 mM Tris-HCl pH 7.2, 150 mM NaCl, and 0.1% Tween 20) containing 5% milk for at least one hour at RT. Membranes were rinsed with water and incubated overnight at 4°C with primary antibodies (diluted in TBST containing 1% BSA) with gentle agitation. At room temperature, membranes were washed 3-4 times with TBST, incubated for 2h with the appropriate HRP-conjugated secondary antibody (diluted in TBST containing 1% milk) and washed 3-4 times with TBST. Signals were generated by enhanced chemiluminescence using either the Pierce ECL

Western Blotting substrate (all antibodies except anti-sAPPb) or the more sensitive Pierce SuperSignal West Pico Plus Chemiluminescent Substrate (sAβPPβ antibody only) and results were visualized by exposure to X-ray film. Band intensities were quantified by ImageJ following the subtraction of a background area of equivalent size within each lane and intensities were normalized. Primary antibody dilutions: anti-Flag (1:2000), anti-sAPPb (1:30,000), anti-sAPPa 6E10 (1:4,000), anti-APP pT668 (1/4:000) and anti-GAPDH (1:30,000).

SILAC Analysis (Stable Isotope Labeling by Amino Acids in Cell Culture) and Nano LC−MS/MS Analysis. SILAC analysis was carried out essentially as described by Zhang et al. (2018)(49,68). Two complimentary SILAC approaches were utilized to identify potential binding partners for the C-terminal tail of APP using biotinylated-LpCDP-DB as an affinity probe. "Heavy" cells were cultured in DMEM with [$^{13}C_6$, $^{15}N_2$]-L-lysine, [$^{13}C_6$, $^{15}N_4$]-L-arginine, and 10% dialyzed FBS for 5 generations. "Light" cells were cultured in DMEM with normal L-lysine, L-arginine, and 10% dialyzed FBS for 5 generations. The "heavy" and "light" cells were harvested separately, centrifuged for 5 min at 500×g at 4˚C, washed one time with ice-cold PBS and lysed in SILAC lysis buffer (25 mM Tris-HCl pH 7.4, 150 mM NaCl, 10% glycerol and 1% Nonidet P-40 containing protease and phosphatase cocktails) for 30min on ice followed by centrifugation for 10min at 15,000g at 4°C to remove debris. Protein concentrations were determined using the BCA assay kit and the resulting lysates (adjusted to about 2mg/ml) were used to set up the reciprocal forward and reverse sets of reactions (3mg cell lysate per reaction) as described below.

Non-competitive approach: ***Forward SILAC (DB_H):*** Heavy cell lysates were combined with 1mM biotinylated-LpCDP-DB and light cell lysates were combined with equal volume of DMSO. ***Reverse SILAC (DB_L):*** Light cell lysates were combined with 1mM biotinylated-LpCDP-DB and heavy cell lysates were combined with equal volume of DMSO. Cell lysates were pre-incubated for 4h at 4°C with rocking. High capacity streptavidin-agarose beads (20ml) were added to each sample, incubated overnight at 4°C with rocking and beads were washed three times with 1ml SILAC wash buffer (25 mM Tris-HCl pH 7.4, 150 mM NaCl, 10% glycerol and 0.2% Nonidet P-40 without inhibitors). Heavy and light beads for each set were combined, washed four times with 1ml cold PBS and beads were dried by pipetting with loading tips. DMSO concentrations were maintained below 2%.

Competitive approach: ***Forward SILAC (DB_H_competitive):*** "Heavy" cell lysates were combined with excess 2mM LpCDP-DB and "light" cell lysates were combined with same volume of DMSO. ***Reverse SILAC (DB_L_competitive):*** "Light" cell lysates were combined with excess 2mM LpCDP-DB and heavy cell lysates were combined with equal volume of DMSO. After mixing, 400uM biotinylated-LpCDP-DB was added to all lysates, incubated for 4h at 4°C. combined with beads and samples processed as described above for the non-competitive approach. Immobilized proteins from SILAC above were subjected to on-beads trypsin digestion and the resulting peptides were analyzed by LC−MS/MS analysis (LTQ-Orbitrap Elite mass spectrometer coupled with nanoLC). Dried beads were incubated in 6M urea, 10mM DTT, 50mM Tris (pH8) at room temperature for 1h to reduce disulfide bond and denature proteins followed by alkylation with iodoacetamide at room temperature for 1h in the dark.

Iodoacetamide was neutralized by incubation at room temperature for 1 hour with DTT. Samples were diluted 7 times with 50 mM Tris-HCl pH 8.0 and 1 mM CaCl2 and the solutions were transferred to fresh tubes. Trypsin (Pierce, #90058) was added to each sample and incubated at 37°C for 18 hours. Trifluoroacetic acid (0.1% in water) was added to quench the trypsin digestion, followed by desalting using a Sep-Pak C18 cartridge and lyophilization. Samples were then subjected to LC–MS/MS analysis (LTQ-Orbitrap Elite mass spectrometer coupled with nanoLC). Lyophilized peptides were dissolved in 2% acetonitrile (ACN) with 0.5% formic acid (FA) and injected into an Acclaim PepMap nano Viper C18 trap column (5 μm, 100 μm × 2 cm, Thermo Dionex) and separated in a C18 RP nano column (5 μm, 75 μm × 50 cm, Magic C18, Bruker) at a flow rate of 0.3 μL/min. The gradient was set as follows: 5–38% ACN with 0.1% FA (0–120 min), 38–95% ACN with 0.1% FA (120–127 min), 95% ACN with 0.1% FA (127–135 min). Positive ion mode was used in an LTQ-Orbitrap Elite mass spectrometer (spray voltage 1.6 kV, source temperature 275 °C). The precursor ions scan from m/z 375 to 1800 at resolution 120,000 using an FT mass analyzer. Collision-induced dissociation (CID) was used for the MS/MS scan at resolution 15,000 on the 10 most intensive peaks, isolation width was set as 2.0 m/z, and normalized collision energy was set as 35%. Xcalibur 2.2 operation software was used for collecting the data. The MS data was further processed using Sequest HT in Proteome Discoverer 2.2 (Thermo Scientific). Only proteins with heavy/light (H/L) ratios >1.5 in the forward experiment and < 0.67 in the reverse experiment were considered as possible LpCDP-DB interacting proteins.

REFERENCES

1. Travis, J. (2005) Saving the mind faces high hurdles. *Science* **309**, 731
2. Association, A. s. (2019) 2019 Alzheimer's disease facts and figures. *Alzheimer's & Dementia* **15**, 321-387
3. Scheuner, D., Eckman, C., Jensen, M., Song, X., Citron, M., Suzuki, N., Bird, T., Hardy, J., Hutton, M., and Kukull, W. (1996) Secreted amyloid β–protein similar to that in the senile plaques of Alzheimer's disease is increased in vivo by the presenilin 1 and 2 and APP mutations linked to familial Alzheimer's disease. *Nature medicine* **2**, 864-870
4. Armstrong, R. A. (2009) The molecular biology of senile plaques and neurofibrillary tangles in Alzheimer's disease. *Folia Neuropathol* **47**, 289-299
5. Mullane, K., and Williams, M. (2019) Preclinical Models of Alzheimer's Disease: Relevance and Translational Validity. *Curr Protoc Pharmacol* **84**, e57
6. Mullan, M., Crawford, F., Axelman, K., Houlden, H., Lilius, L., Winblad, B., and Lannfelt, L. (1992) A pathogenic mutation for probable Alzheimer's disease in the APP gene at the N-terminus of beta-amyloid. *Nat Genet* **1**, 345-347
7. Goate, A., Chartier-Harlin, M. C., Mullan, M., Brown, J., Crawford, F., Fidani, L., Giuffra, L., Haynes, A., Irving, N., James, L., and et al. (1991) Segregation of a missense mutation in the amyloid precursor protein gene with familial Alzheimer's disease. *Nature* **349**, 704-706
8. Di Fede, G., Catania, M., Morbin, M., Rossi, G., Suardi, S., Mazzoleni, G., Merlin, M., Giovagnoli, A. R., Prioni, S., Erbetta, A., Falcone, C., Gobbi, M., Colombo, L., Bastone, A., Beeg, M., Manzoni, C., Francescucci, B., Spagnoli, A., Cantù, L., Del Favero, E., Levy, E., Salmona, M., and Tagliavini, F. (2009) A recessive mutation in the APP gene with dominant-negative effect on amyloidogenesis. *Science* **323**, 1473-1477
9. Haass, C., and Selkoe, D. J. (2007) Soluble protein oligomers in neurodegeneration: lessons from the Alzheimer's amyloid beta-peptide. *Nat Rev Mol Cell Biol* **8**, 101-112
10. Gao, Y., and Pimplikar, S. W. (2001) The γ-secretase-cleaved C-terminal fragment of amyloid precursor protein mediates signaling to the nucleus. *Proceedings of the National Academy of Sciences* **98**, 14979-14984
11. Hartmann, D., Tournoy, J., Saftig, P., Annaert, W., and De Strooper, B. (2001) Implication of APP secretases in notch signaling. *J Mol Neurosci* **17**, 171-181
12. Landman, N., and Kim, T. (2004) Got RIP? Presenilin-dependent intramembrane proteolysis in growth factor receptor signaling. *Cytokine & growth factor reviews* **15 5**, 337-351
13. Li, T., Ma, G., Cai, H., Price, D. L., and Wong, P. C. (2003) Nicastrin Is Required for Assembly of Presenilin/γ-Secretase Complexes to Mediate Notch Signaling and for Processing and Trafficking of β-Amyloid Precursor Protein in Mammals. *The Journal of Neuroscience* **23**, 3272-3277
14. Müller, T., Meyer, H. E., Egensperger, R., and Marcus, K. (2008) The amyloid precursor protein intracellular domain (AICD) as modulator of gene

expression, apoptosis, and cytoskeletal dynamics-relevance for Alzheimer's disease. *Prog Neurobiol* **85**, 393-406
15. Kang, J., Lemaire, H.-G., Unterbeck, A., Salbaum, J. M., Masters, C. L., Grzeschik, K.-H., Multhaup, G., Beyreuther, K., and Müller-Hill, B. (1987) The precursor of Alzheimer's disease amyloid A4 protein resembles a cell-surface receptor. *Nature* **325**, 733-736
16. De Strooper, B., and Annaert, W. (2000) Proteolytic processing and cell biological functions of the amyloid precursor protein. *J Cell Sci* **113 (Pt 11)**, 1857-1870
17. Esch, F. S., Keim, P. S., Beattie, E. C., Blacher, R. W., Culwell, A. R., Oltersdorf, T., McClure, D., and Ward, P. J. (1990) Cleavage of amyloid beta peptide during constitutive processing of its precursor. *Science* **248**, 1122-1124
18. Sinha, S., Anderson, J. P., Barbour, R., Basi, G. S., Caccavello, R., Davis, D., Doan, M., Dovey, H. F., Frigon, N., Hong, J., Jacobson-Croak, K., Jewett, N., Keim, P., Knops, J., Lieberburg, I., Power, M., Tan, H., Tatsuno, G., Tung, J., Schenk, D., Seubert, P., Suomensaari, S. M., Wang, S., Walker, D., Zhao, J., McConlogue, L., and John, V. (1999) Purification and cloning of amyloid precursor protein β-secretase from human brain. *Nature* **402**, 537-540
19. Selkoe, D. J., Yamazaki, T., Citron, M., Podlisny, M. B., Koo, E. H., Teplow, D. B., and Haass, C. (1996) The role of APP processing and trafficking pathways in the formation of amyloid beta-protein. *Ann N Y Acad Sci* **777**, 57-64
20. Esler, W. P., and Wolfe, M. S. (2001) A portrait of Alzheimer secretases--new features and familiar faces. *Science* **293**, 1449-1454
21. Hardy, J., and Selkoe, D. J. (2002) The amyloid hypothesis of Alzheimer's disease: progress and problems on the road to therapeutics. *Science* **297**, 353-356
22. Mattson, M. P. (2004) Pathways towards and away from Alzheimer's disease. *Nature* **430**, 631-639
23. Sun, J., and Roy, S. (2018) The physical approximation of APP and BACE-1: A key event in alzheimer's disease pathogenesis. *Dev Neurobiol* **78**, 340-347
24. van der Kant, R., and Goldstein, Lawrence S. B. (2015) Cellular Functions of the Amyloid Precursor Protein from Development to Dementia. *Developmental Cell* **32**, 502-515
25. Asai, M., Iwata, N., Yoshikawa, A., Aizaki, Y., Ishiura, S., Saido, T. C., and Maruyama, K. (2007) Berberine alters the processing of Alzheimer's amyloid precursor protein to decrease Abeta secretion. *Biochem Biophys Res Commun* **352**, 498-502
26. Chasseigneaux, S., and Allinquant, B. (2012) Functions of Aβ, sAPPα and sAPPβ : similarities and differences. *Journal of Neurochemistry* **120**, 99-108
27. Huotari, J., and Helenius, A. (2011) Endosome maturation. *Embo j* **30**, 3481-3500
28. Kinoshita, A., Fukumoto, H., Shah, T., Whelan, C. M., Irizarry, M. C., and Hyman, B. T. (2003) Demonstration by FRET of BACE interaction with the

amyloid precursor protein at the cell surface and in early endosomes. *J Cell Sci* **116**, 3339-3346
29. Kobayashi, H., and Fukuda, M. (2013) Arf6, Rab11 and transferrin receptor define distinct populations of recycling endosomes. *Commun Integr Biol* **6**, e25036-e25036
30. Fisher, C. L., Resnick, R. J., De, S., Acevedo, L. A., Lu, K. P., Schroeder, F. C., and Nicholson, L. K. (2017) Cyclic cis-Locked Phospho-Dipeptides Reduce Entry of AβPP into Amyloidogenic Processing Pathway. *J Alzheimers Dis* **55**, 391-410
31. Koo, E. H., and Squazzo, S. L. (1994). *J. Biol. Chem.* **269**, 17386
32. Zhang, H., Ma, Q., Zhang, Y.-w., and Xu, H. (2012) Proteolytic processing of Alzheimer's β-amyloid precursor protein. *Journal of Neurochemistry* **120**, 9-21
33. Lee, M. S., Kao, S. C., Lemere, C. A., Xia, W., Tseng, H. C., Zhou, Y., Neve, R., Ahlijanian, M. K., and Tsai, L. H. (2003) APP processing is regulated by cytoplasmic phosphorylation. *J Cell Biol* **163**, 83-95
34. Ramelot, T. A., and Nicholson, L. K. (2001) Phosphorylation-induced structural changes in the amyloid precursor protein cytoplasmic tail detected by NMR. *J Mol Biol* **307**, 871-884
35. Ramelot, T. A., Gentile, L. N., and Nicholson, L. K. (2000) Transient Structure of the Amyloid Precursor Protein Cytoplasmic Tail Indicates Preordering of Structure for Binding to Cytosolic Factors. *Biochemistry* **39**, 2714-2725
36. Greenwood, A. I., Rogals, M. J., De, S., Lu, K. P., Kovrigin, E. L., and Nicholson, L. K. (2011) Complete determination of the Pin1 catalytic domain thermodynamic cycle by NMR lineshape analysis. *J Biomol NMR* **51**, 21-34
37. Pastorino, L., and Lu, K. P. (2006) Pathogenic mechanisms in Alzheimer's disease. *European Journal of Pharmacology* **545**, 29-38
38. Liu, J., Brahimi, F., Saragovi, H. U., and Burgess, K. (2010) Bivalent diketopiperazine-based tropomysin receptor kinase C (TrkC) antagonists. *J Med Chem* **53**, 5044-5048
39. Yamaguchi, S., Ito, S., Masuda, T., Couraud, P.-O., and Ohtsuki, S. (2020) Novel cyclic peptides facilitating transcellular blood-brain barrier transport of macromolecules in vitro and in vivo. *Journal of Controlled Release* **321**, 744-755
40. Oller-Salvia, B., Sánchez-Navarro, M., Giralt, E., and Teixidó, M. (2016) Blood–brain barrier shuttle peptides: an emerging paradigm for brain delivery. *Chemical Society Reviews* **45**, 4690-4707
41. Dursun, E., Gezen-Ak, D., and Yilmazer, S. (2011) A novel perspective for Alzheimer's disease: vitamin D receptor suppression by amyloid-beta and preventing the amyloid-beta induced alterations by vitamin D in cortical neurons. *J. Alzheimer's Dis.* **23**, 207
42. Arnstein, P., Taylor, D. O., Nelson-Rees, W. A., Huebner, R. J., and Lennette, E. H. (1974) Propagation of human tumors in antithymocyte serum-treated mice. *J Natl Cancer Inst* **52**, 71-84

43. Day, R. S., 3rd, and Ziolkowski, C. H. (1979) Human brain tumour cell strains with deficient host-cell reactivation of N-methyl-N'-nitro-N-nitrosoguanidine-damaged adenovirus 5. *Nature* **279**, 797-799
44. Krex, D., Mohr, B., Hauses, M., Ehninger, G., Schackert, H. K., and Schackert, G. (2001) Identification of Uncommon Chromosomal Aberrations in the Neuroglioma Cell Line H4 by Spectral Karyotyping. *Journal of Neuro-Oncology* **52**, 119-128
45. Holsinger, R. M., McLean, C. A., Beyreuther, K., Masters, C. L., and Evin, G. (2002) Increased expression of the amyloid precursor beta-secretase in Alzheimer's disease. *Ann Neurol* **51**, 783-786
46. Wisniewski, K., Howe, J., Williams, D. G., and Wisniewski, H. M. (1978) Precocious aging and dementia in patients with Down's syndrome. *Biol Psychiatry* **13**, 619-627
47. Patki, V., Virbasius, J., Lane, W. S., Toh, B.-H., Shpetner, H. S., and Corvera, S. (1997) Identification of an early endosomal protein regulated by phosphatidylinositol 3-kinase. *Proceedings of the National Academy of Sciences* **94**, 7326-7330
48. Stauffer, W., Sheng, H., and Lim, H. N. (2018) EzColocalization: An ImageJ plugin for visualizing and measuring colocalization in cells and organisms. *Sci Rep* **8**, 15764
49. Zhang, Q., Ma, C., Gearing, M., Wang, P. G., Chin, L. S., and Li, L. (2018) Integrated proteomics and network analysis identifies protein hubs and network alterations in Alzheimer's disease. *Acta Neuropathol Commun* **6**, 19
50. Borg, J. P., Ooi, J., Levy, E., and Margolis, B. (1996) The phosphotyrosine interaction domains of X11 and FE65 bind to distinct sites on the YENPTY motif of amyloid precursor protein. *Mol Cell Biol* **16**, 6229-6241
51. Taru, H., Iijima, K., Hase, M., Kirino, Y., Yagi, Y., and Suzuki, T. (2002) Interaction of Alzheimer's beta -amyloid precursor family proteins with scaffold proteins of the JNK signaling cascade. *J Biol Chem* **277**, 20070-20078
52. Eggert, S., Gonzalez, A. C., Thomas, C., Schilling, S., Schwarz, S. M., Tischer, C., Adam, V., Strecker, P., Schmidt, V., Willnow, T. E., Hermey, G., Pietrzik, C. U., Koo, E. H., and Kins, S. (2018) Dimerization leads to changes in APP (amyloid precursor protein) trafficking mediated by LRP1 and SorLA. *Cell Mol Life Sci* **75**, 301-322
53. Tan, J. Z. A., Fourriere, L., Wang, J., Perez, F., Boncompain, G., and Gleeson, P. A. (2020) Distinct anterograde trafficking pathways of BACE1 and amyloid precursor protein from the TGN and the regulation of amyloid-β production. *Mol Biol Cell* **31**, 27-44
54. Yan, R., Han, P., Miao, H., Greengard, P., and Xu, H. (2001) The transmembrane domain of the Alzheimer's β-secretase (BACE1) determines its late Golgi localization and access to β-amyloid precursor protein (APP) substrate. *Journal of Biological Chemistry* **276**, 36788-36796
55. Guénette, S., Strecker, P., and Kins, S. (2017) APP Protein Family Signaling at the Synapse: Insights from Intracellular APP-Binding Proteins. *Frontiers in Molecular Neuroscience* **10**

56. Haass, C., Kaether, C., Thinakaran, G., and Sisodia, S. (2012) Trafficking and proteolytic processing of APP. *Cold Spring Harb Perspect Med* **2**, a006270
57. Tam, J. M., Josephson, L., Pilozzi, A. R., and Huang, X. (2020) A Novel Dual Fluorochrome Near-Infrared Imaging Probe for Potential Alzheimer's Enzyme Biomarkers-BACE1 and Cathepsin D. *Molecules* **25**
58. Kaushik, S., and Cuervo, A. M. (2018) The coming of age of chaperone-mediated autophagy. *Nature Reviews Molecular Cell Biology* **19**, 365-381
59. De Duve, C., and Wattiaux, R. (1966) Functions of lysosomes. *Annu Rev Physiol* **28**, 435-492
60. Butterfield, D. A., and Lange, M. L. B. (2009) Multifunctional roles of enolase in Alzheimer's disease brain: beyond altered glucose metabolism. *Journal of Neurochemistry* **111**, 915-933
61. Stolz, A., Ernst, A., and Dikic, I. (2014) Cargo recognition and trafficking in selective autophagy. *Nat Cell Biol* **16**, 495-501
62. Nixon, R. A., Cataldo, A. M., and Mathews, P. M. (2000) The Endosomal-Lysosomal System of Neurons in Alzheimer's Disease Pathogenesis: A Review. *Neurochemical Research* **25**, 1161-1172
63. Tohda, C., Urano, T., Umezaki, M., Nemere, I., and Kuboyama, T. (2012) Diosgenin is an exogenous activator of 1,25D_3-MARRS/Pdia3/ERp57 and improves Alzheimer's disease pathologies in 5XFAD mice. *Sci Rep* **2**, 535-535
64. Zhang, M., Cai, F., Zhang, S., Zhang, S., and Song, W. (2014) Overexpression of ubiquitin carboxyl-terminal hydrolase L1 (UCHL1) delays Alzheimer's progression in vivo. *Sci Rep* **4**, 7298
65. Erickson, R. R., Dunning, L. M., Olson, D. A., Cohen, S. J., Davis, A. T., Wood, W. G., Kratzke, R. A., and Holtzman, J. L. (2005) In cerebrospinal fluid ER chaperones ERp57 and calreticulin bind β-amyloid. *Biochemical and Biophysical Research Communications* **332**, 50-57
66. Cai, Y., Arikkath, J., Yang, L., Guo, M.-L., Periyasamy, P., and Buch, S. (2016) Interplay of endoplasmic reticulum stress and autophagy in neurodegenerative disorders. *Autophagy* **12**, 225-244
67. Towbin, H., Özbey, Ö., and Zingel, O. (2001) An immunoblotting method for high-resolution isoelectric focusing of protein isoforms on immobilized pH gradients. *ELECTROPHORESIS* **22**, 1887-1893
68. Zhang, X., Cao, J., Miller, S. P., Jing, H., and Lin, H. (2018) Comparative Nucleotide-Dependent Interactome Analysis Reveals Shared and Differential Properties of KRas4a and KRas4b. *ACS Cent Sci* **4**, 71-80
69. Acevedo, L. A., Korson, N. E., Williams, J. M., and Nicholson, L. K. (2019) Tuning a timing device that regulates lateral root development in rice. *Journal of biomolecular NMR* **73**, 493-507
70. Wang, R., Zhang, Y., Kieffer, M., Yu, H., Kepinski, S., and Estelle, M. (2016) HSP90 regulates temperature-dependent seedling growth in Arabidopsis by stabilizing the auxin co-receptor F-box protein TIR1. *Nature Communications* **7**, 10269

CHAPTER 5

CONCLUSIONS AND FUTURE DIRECTIONS

My dissertation has investigated the roles of cis-specific binding events in two separate biological systems, development and disease. The first is related to the action of a prolyl isomerase enzyme on a substrate essential for lateral root initiation in rice. The second focuses on a cis-locked small molecule that mimics two Pro-containing sequence motifs in the amyloid precursor protein (APP), and the effect of this molecule on the proteolytic processing, endocytosis and intracellular trafficking of APP. In these investigations of both systems, key roles of heat shock protein 90 (Hsp90) have emerged which suggests specific connections between Hsp90 and cis-specific binding events. These studies in two distinct systems highlight the ability of the cis-isomer to impact critical molecular mechanisms.

In the first study, our experimental results strengthen the idea that rice shoot protoplasts can be used as a tool to investigate and quantify the expression of a given protein of interest *in vivo* (Chapter 3). I confirmed our plasmid OsIAA11-mVenus was localized to the nucleus in rice shoot protoplasts grown in the light and dark. I found that nuclear proteins bodies of Aux/IAA proteins OsIAA11, OsIAA17 and OsIAA31 in rice shoot protoplasts were the result of the fluorescent protein VENUS dimerizing in the nucleus. I found that the mVenus fluorescent protein is stably expressed in rice shoot protoplasts. Importantly, when we performed a cycloheximide chase of OsIAA11-mVenus and LRT2-mCherry, we observed that the degradation rate of OsIAA11 was not accelerated by the presence of LRT2. These results are consistent with our previous

work indicating that LRT2 is optimally tuned for degradation of OsIAA11 by the proteasome machinery in the cell (69). Additionally, we tested the impact of temperature and found that the degradation rate of OsIAA11-mVenus in many protoplasts was increased when the temperature was controlled in the range of 28-30°C. The results of this study are consistent with that of Wang (2016), which found Hsp90 expression to be increased in this temperature range and that Hsp90 is required for auxin signaling in *Arabidopsis* (70). The findings reported here shed new light on temperature having a significant impact in the degradation of OsIAA11 in rice shoot protoplasts.

In Chapter 3, we also tested whether the time elapsed between post-transfection and imaging influences the detection of OsIAA11-mVenus degradation in rice shoot protoplasts. Interestingly, we found that the post-transfection time did affect the detection of OsIAA11-mVenus degradation. I speculate that this is because of the amount of OsIAA11-mVenus using the constitutive promoter has overloaded the proteasomal machinery. One way to address the build-up of OsIAA11-mVenus would be to quantify the intensity of fluorescence versus time over a 12 hour – 20 hour period. Another way would be to image OsIAA11-mVenus before post-transfection time of 14hours. However, the protoplasts are still dependent on additional factors being present and function in the cell. This study suggest that transiently transfected rice shoot protoplasts should not be imaged later than 14 hours post-transfection. Further investigation and experimentation into elapsed post-transfection time on other constitutively promoted Aux/IAA proteins is strongly recommended.

To further understand the degradation of OsIAA11-mVenus in rice shoot protoplasts, confocal microscopy studies of the endogenous promoter of OsIAA11 in

the presence of auxin should be continued. The endogenous promoter of OsIAA11-mVenus will provide parameters for modeling the auxin circuit dynamics. Additionally, OsIAA11mVenus should be transiently transfected in root protoplasts in order to compare the degradation rate of OsIAA11in shoot protoplasts, which may or may not be the same rate.

The present study lays the groundwork for future research utilizing rice shoot protoplasts and transiently transfecting OsIAA11. Further work needs to be carried out co-transfecting OsIAA11, LRT2, OsSGT1, and OsHsp90 in rice shoot protoplasts in order to confirm Hsp90's role in our temperature controlled cycloheximide chase experiments. Several questions still remain to be answered regarding the role of OsSGT1 and OsHsp90 involvement in the degradation of OsIAA11. Further experimental investigations, such as RNAseq experiments should be done to compare rice shoot and root protoplasts to ask; what auxin responsive genes are already present in the shoots compared to the roots. More broadly, small interfering RNA (siRNA) and approaches to generate transgenic knock-out and mutant plants should be done in rice to test the essential role of specific factors that are involved in the auxin circuit.

In this dissertation, we also investigated a 100% locked "cis-locked" small molecule, phospho-Cyclic Dipeptide, Di-Benzyl (pCDP-DB), impacting the amyloid precursor protein's (APP) proteolytic processing (30). Existing research recognizes the critical role played by the transient structure of the 47-residue APP cytoplasmic domain (APPc residues 649-695), which has been studied in depth by the Nicholson lab (33,36). Previous studies evaluating pT668 accumulating in AD brains have hypothesized that the cis isomer could serve as a molecular signal for Aβ producing pathway(42,55).

In Chapter 4, we investigate treatment with pCDP-DB in H4 neuroglioma cells where it is shown to decrease the amount of sAPPβ. The results of this study show that treatment with pCDP-DB does not inhibit the endocytosis of APP. Additionally, treatment with our small molecule does not change the colocalization of APP and BACE1. These results suggest that pCDP-DB does not prevent the trafficking of APP and BACE1 into the same intracellular locations in the cell. Surprisingly, treatment with pCDP-DB was found to decrease the colocalization of an early endosome marker (EEA1) with both APP and BACE1, indicating that pCDP-DB reduces the association of APP and BACE1 with early endosomes. Moreover, preliminary data shows that treatment with pCDP-DB increases the colocalization of APP and BACE1 with Hsp90AA1 and Hsp90AB1 in cell models overexpressing APP or BACE1. Hsp90 has known roles in targeting cargo to the lysosomes. Lastly, our point mutations within the cytoplasmic tail of APP significantly impact proteolytic processing when stably expressed in H4 neuroglioma cells. It is possible to hypothesize that pCDP-DB might act by enhancing endosomal maturation and trafficking of APP to lysosomes for degradation.

These findings may help us understand how APP can be regulated by a small molecule through cell trafficking, proteolytic processing, and degradation mechanisms. Several questions remain unanswered at present. Further work is required to further investigate the proposed mechanism of APP being trafficked to the lysosomes for degradation. Specifically, further research should be undertaken to investigate longer time points in internalization assays, especially lysosomes with and without pCDP-DB treatment. To develop a full picture of pCDP-DB binding to Hsp90 causing the

trafficking of APP to the lysosomes, additional studies will be needed to investigate the trafficking of APP in the cell. A greater focus on small molecules like pCDP-DB could produce interesting findings that reveal how Aβ production is regulated and whether we can target the regulatory pathway to treat Alzheimer's disease.

REFERENCES

1. Acevedo, L.A., et al., *Tuning a timing device that regulates lateral root development in rice*. Journal of biomolecular NMR, 2019. **73**(8-9): p. 493-507.
2. Wang, R., et al., *HSP90 regulates temperature-dependent seedling growth in Arabidopsis by stabilizing the auxin co-receptor F-box protein TIR1*. Nature Communications, 2016. **7**(1): p. 10269.
3. Fisher, C.L., et al., *Cyclic cis-Locked Phospho-Dipeptides Reduce Entry of AβPP into Amyloidogenic Processing Pathway*. Journal of Alzheimer's disease : JAD, 2017. **55**(1): p. 391-410.
4. Lee, M.S., et al., *APP processing is regulated by cytoplasmic phosphorylation*. J Cell Biol, 2003. **163**(1): p. 83-95.
5. Greenwood, A.I., et al., *Complete determination of the Pin1 catalytic domain thermodynamic cycle by NMR lineshape analysis*. J Biomol NMR, 2011. **51**(1-2): p. 21-34.
6. Guénette, S., P. Strecker, and S. Kins, *APP Protein Family Signaling at the Synapse: Insights from Intracellular APP-Binding Proteins*. Frontiers in Molecular Neuroscience, 2017. **10**(87).
7. Arnstein, P., et al., *Propagation of human tumors in antithymocyte serum-treated mice*. J Natl Cancer Inst, 1974. **52**(1): p. 71-84.

APPENDIX

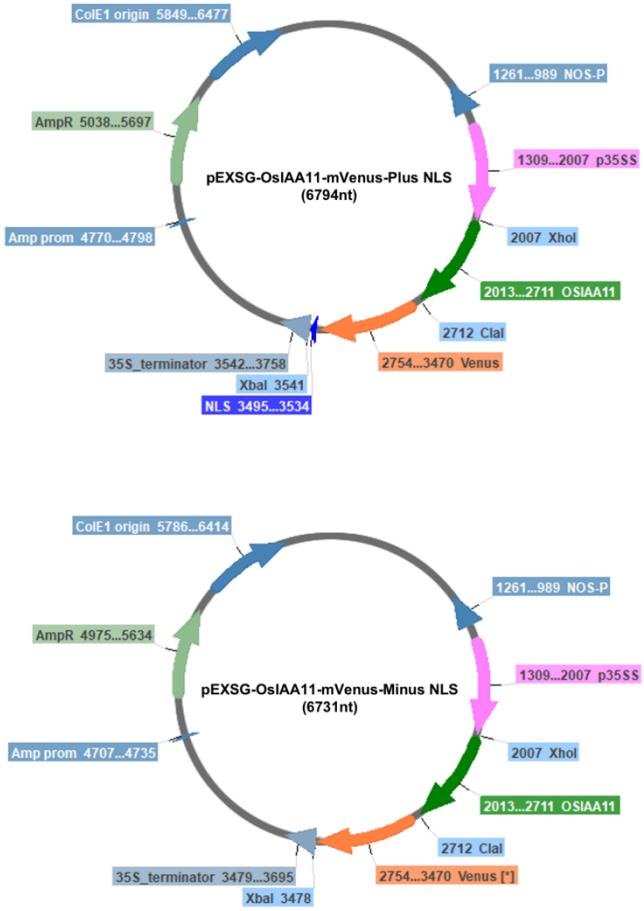

Appendix Figure 2.1: Plasmid vectors map of OsIAA11-mVenus with and without the nuclear localization signal (NLS). The pSLIK-Venus vector was used as a template for PCR to generate the Venus gene containing the terminal ClaI and XbaI restriction sites and the resulting fragment was used to replace eYFP to generate the pEXSG-OsIAA11-Venus plasmid. Site-directed mutagenesis was used to insert the C-terminal nuclear localization signal (NLS; KKKRKVPKKKRKV) and introduce the A206K point mutation into Venus to generate mVenus (the monomeric version) and create the pEXSG-OsIAA11-mVenus and pEXSG-OsIAA11-mVenus-NLS expression vectors.

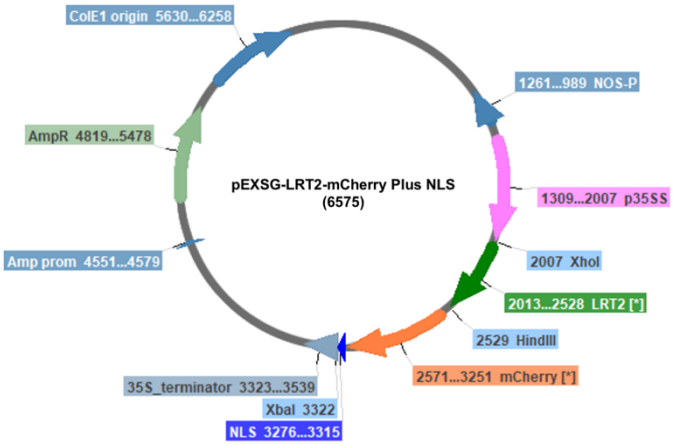

Appendix Figure 2.2: Plasmid vectors map of LRT2-mCherry without the nuclear localization signal (NLS). The genes for LRT2 and the mCherry were individually subjected to PCR to generate fragments containing the terminal XhoI/HindIII and HindIII/XbaI restriction sites respectively and used to sequentially replace OsIAA11 and mVenus to create the pEXSG-LRT2-mCherry-NLS expression vector. All vectors contained a GAGAGAGAGAGP spacer between the Rice gene and the fluorescent tag and a GAGAGAGP spacer between the fluorescent tag and the NLS where applicable

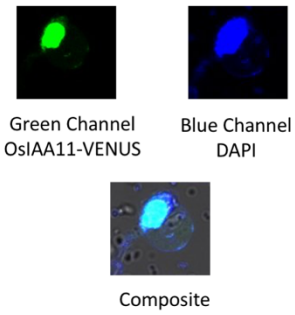

Appendix Figure 3.1: DAPI stain showing OsIAA11-Venus is localized to the nucleus. Image of OsIAA11-mVenus in protoplasts from plants grown in the dark at a post-transfection time of >24hours. Addition of DAPI (5mg/ml) in a protoplasts dish with 2 ml of WI buffer.

A

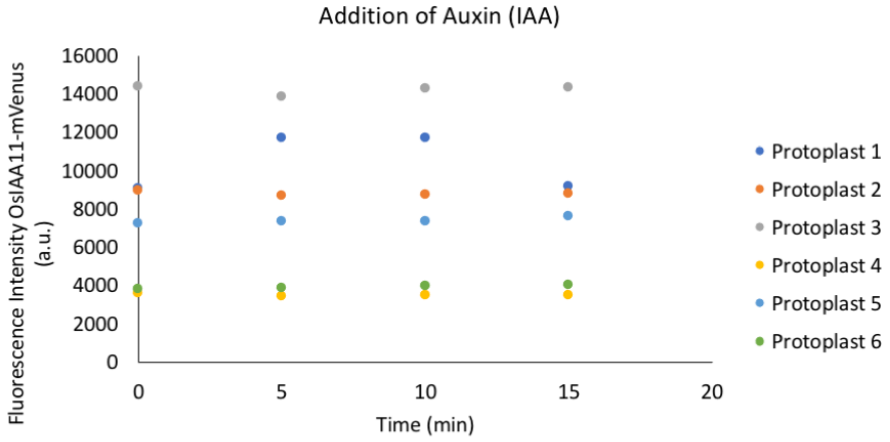

B

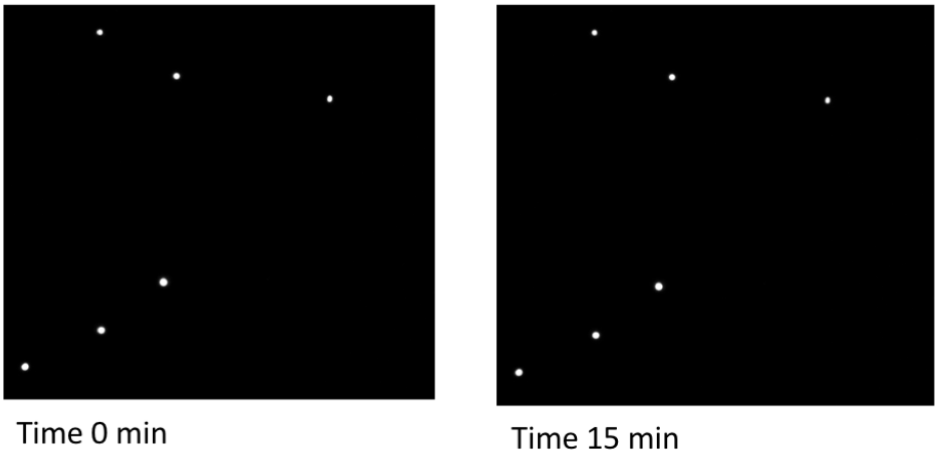

Appendix Figure 3.2: Addition of Auxin does not decrease the fluorescence of OsIAA11-mVenus. **(A)** Scatterplot shows the addition of auxin at time zero does not exponentially decrease the fluorescence of OsIAA11-mVenus. **(B)** Confocal fluorescence microscopy image of protoplast at t=0 (the time at which 20μM Auxin (IAA) was added) and 15minutes (min). OsIAA11-Venus (green) channels were excited at 488nm and 520nm, respectively.

A

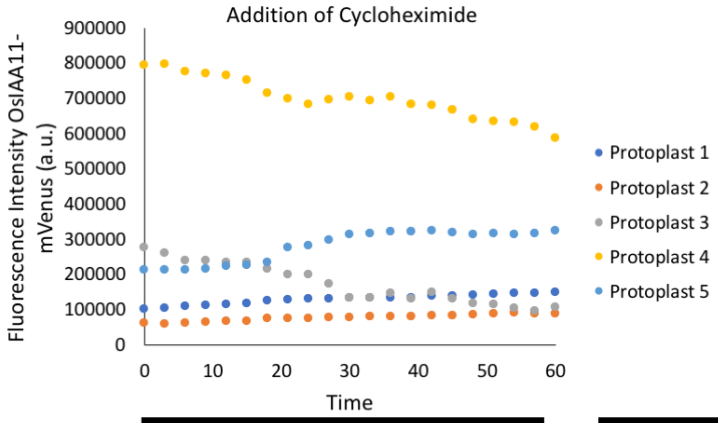

B

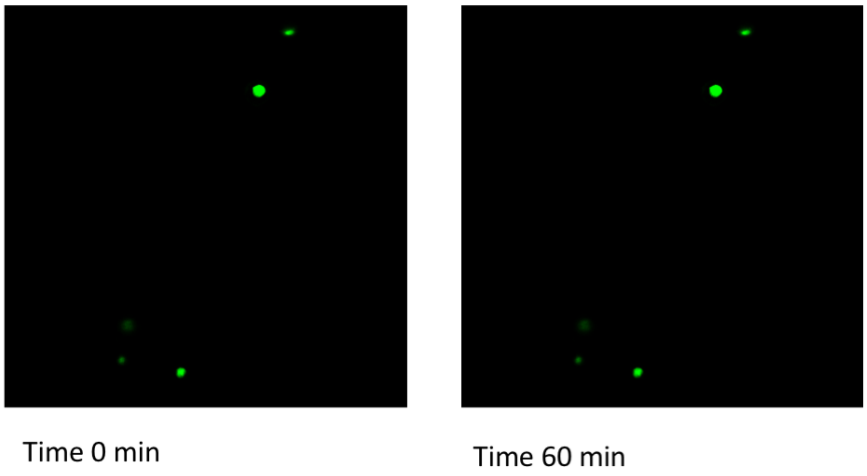

Appendix *Figure* 3.3 : Addition of Cycloheximide (CHX) does not exponentially decrease the fluorescence of OsIAA11-mVenus. (A) Scatterplot shows the addition of CHX at time zero does not exponentially decrease the fluorescence of OsIAA11-mVenus. **(B)** Confocal fluorescence microscopy image of protoplast at t=0 (the time at which 50μM CHX was added) and 60minutes (min). OsIAA11-Venus (green) channels were excited at 488nm and 520nm, respectively.

Appendix Table 3.4 Post-transfection time of OsIAA11-mVenus. The elapsed time post-transfection effects the fluorescence intensity of OsIAA11-mVenus. Each time course had the same imaging conditions and had the addition of auxin (20μM) and CHX (50μM), please see text for more information**.**

Timecourse #1:							
Post-Transfection Time	13-14 hours						
		Fluorescence Intensity (a.u.)				Fluorescence Intensity (a.u.)	
Protoplasts	Time	mVenus	mCherry	Protoplasts	Time	mVenus	mCherry
1	0 mins	5994662	-80564	1	90 mins	1376452	74662
2	0 mins	2712366	93800	2	90 mins	850228	92358
3	0 mins	29081916	1337852	3	90 mins	7780280	1426292
4	0 mins	63739280	4025608	4	90 mins	13948832	3012856
Timecourse #2:							
Post-Transfection Time	15-16 hours						
		Fluorescence Intensity (a.u.)				Fluorescence Intensity (a.u.)	
Protoplasts	Time	mVenus	mCherry	Protoplasts	Time	mVenus	mCherry
1	0 mins	65901804	448112	1	70 mins	46835772	308752
2	0 mins	29438101	478032	2	70 mins	19375957	404808
3	0 mins	39815433	191096	3	70 mins	26966025	33736
4	0 mins	12363838.5	-194440	4	70 mins	11286550.5	-121856
Timecourse #3:							
Post-Transfection Time	17-18 hours						
		Fluorescence Intensity (a.u.)				Fluorescence Intensity (a.u.)	
Protoplasts	Time	mVenus	mCherry	Protoplasts	Time	mVenus	mCherry
1	0 mins	87778474.7	943984	1	45 mins	38219018.7	804560
2	0 mins	37040610	27136	2	45 mins	22809490	86432
Timecourse #4:							
Post-Transfection Time	19-20 hours			Addition:			
		Fluorescence Intensity (a.u.)				Fluorescence Intensity (a.u.)	
Protoplasts	Time	mVenus	mCherry	Protoplasts	Time	mVenus	mCherry
1	0 mins	36851496	2247340	1	46 mins	22836848	1915168
2	0 mins	15186968	521500	2	46 mins	7909448	392476
3	0 mins	23359888	2199792	3	46 mins	15741760	1977164
4	0 mins	26362472	1229036	4	46 mins	15358904	1100496
5	0 mins	13885380	1311652	5	46 mins	2376960	820980

Appendix Table 4.1: Proline Mutants T-test (two-tail) P-Values. 1. T-test between WT cells at time 0, 5, and 10 mins. 2. T-test between WT and Group 1 (P669A), Group 2(P685A), and Group 3(FFAA). *p<0.05, ** is p<0.01 and *** is p<0.001.

T Test:	WT				Group1	P669A			
	Variable1	Variable2				Variable1	Variable2		
1	WT 0min	WT5min	P(T<=t) two-tail	1.2703E-13		Group 0min	Group 5min	P(T<=t) two-tail	1.4231E-15
2	WT 5min	WT 10min	P(T<=t) two-tail	0.07441484		Group 5min	Group10min	P(T<=t) two-tail	3.7668E-06
					Group2	P685A			
Time 0min						Variable1	Variable2		
3	WT 1	Group1	P(T<=t) two-tail	0.00121997		0min	5min	P(T<=t) two-tail	2.8497E-05
4	WT1	Group2	P(T<=t) two-tail	0.00146644		5min	10min	P(T<=t) two-tail	0.03577441
5	WT1	Group3	P(T<=t) two-tail	0.00661263					
Time 5min									
3	WT 1	Group1	P(T<=t) two-tail	0.07797095					
4	WT1	Group2	P(T<=t) two-tail	0.00065219					
5	WT1	Group3	P(T<=t) two-tail	0.47712809					
Time 10min					Group3	FFAA			
3	WT 1	Group1	P(T<=t) two-tail	1.5714E-05		Variable1	Variable2		
4	WT1	Group2	P(T<=t) two-tail	0.43698768		0min	5min	P(T<=t) two-tail	6.085E-13
5	WT1	Group3	P(T<=t) two-tail	0.04404251		5min	10min	P(T<=t) two-tail	0.42637303

Appendix Table 4.2: Potential pCDP-DB interactors. Listed proteins have H/L > 2 (<0.5 in reverse SILAC), and protein score >15.

Gene Symbol	Annotation	Gene Symbol	Annotation
ACAT1	Acetyl-CoA acetyltransferase, mitochondrial	IPO4	Importin-4
ACO2	Aconitate hydratase, mitochondrial	KIF4A	Chromosome-associated kinesin KIF4A
ACOT9	Acyl-coenzyme A thioesterase 9, mitochondrial	KRT10	Keratin, type I cytoskeletal 10; Keratins, type I
AHCY	Adenosylhomocysteinase	LARS	Leucine--tRNA ligase, cytoplasmic
ALDH18A1	Delta-1-pyrroline-5-carboxylate synthase	LDHA	Lactate dehydrogenase A
ALDOA	Fructose-bisphosphate aldolase A	LDHB	Lactate dehydrogenase B
ANXA1	Annexin A1	MCCC2	Methylcrotonoyl-CoA carboxylase beta chain, mitochond
APOBEC3C	DNA dC->dU-editing enzyme APOBEC-3C	MCM4	DNA replication licensing factor MCM4
ATP1A1	Sodium/potassium-transporting ATPase subunit alpha-1	MCM7	DNA replication licensing factor MCM7
ATP5B	ATP synthase subunit beta, mitochondrial	MDH2	Malate dehydrogenase, mitochondrial
BTF3	Transcription factor BTF3	MSN	Moesin
CALR	Calreticulin	MYOF	Myoferlin; Involved in endocytic recycling.
CANX	Calnexin	NAA15	N-alpha-acetyltransferase 15, NatA auxiliary subunit
CCAR2	Cell cycle and apoptosis regulator protein 2	NAP1L1	Nucleosome assembly protein 1-like 1
CCT2	T-complex protein 1 subunit beta	NME2	Nucleoside diphosphate kinase
CCT3	T-complex protein 1 subunit gamma	NONO	Non-POU domain-containing octamer-binding protein
CCT4	T-complex protein 1 subunit delta	NUP205	Nuclear pore complex protein Nup205
CD44	CD44 antigen; Receptor for hyaluronic acid (HA).	NUP98	Nuclear pore complex protein Nup98-Nup96
CLIC1	Chloride intracellular channel protein 1	OAT	Ornithine aminotransferase, mitochondrial
CTSD	Cathepsin D	P4HB	Protein disulfide-isomerase
CYB5R3	NADH-cytochrome b5 reductase 3	PAFAH1B1	Platelet-activating factor acetylhydrolase IB subunit alph
DCTN1	Dynactin subunit 1	PDG	D-3-phosphoglycerate dehydrogenase
DHX16	Pre-mRNA-splicing factor ATP-dependent RNA helicase	PDIA3	Protein disulfide-isomerase A3
DNAAF5	Dynein assembly factor 5, axonemal	PDIA4	Protein disulfide-isomerase A4
DYNC1LI1	Cytoplasmic dynein 1 light intermediate chain 1	PDIA6	Protein disulfide-isomerase A6
ECHS1	Enoyl-CoA hydratase, mitochondrial	PDLIM7	PDZ and LIM domain protein 7
EEF1B2	Elongation factor 1-beta	PFN1	Profilin-1
EEF1D	Elongation factor 1-delta	PHB	Prohibitin
EEF1G	Elongation factor 1-gamma	PHB2	Prohibitin-2
EIF3A	Eukaryotic translation initiation factor 3 subunit A	PKM	Pyruvate kinase PKM
EIF3B	Eukaryotic translation initiation factor 3 subunit B	PLOD3	Procollagen-lysine,2-oxoglutarate 5-dioxygenase 3
EIF3F	Eukaryotic translation initiation factor 3 subunit F	PPIA	Peptidyl-prolyl cis-trans isomerase A
EIF3L	Eukaryotic translation initiation factor 3 subunit L	PRDX3	Thioredoxin-dependent peroxide reductase, mitochondri
EIF4A1	Eukaryotic initiation factor 4A-I	PSAT1	Phosphoserine aminotransferase
EIF4A3	Eukaryotic initiation factor 4A-III	PSMA7	Proteasome subunit alpha type-7
EIF5A	Eukaryotic translation initiation factor 5A-1	PSMC2	26S proteasome regulatory subunit 7
ELAC2	Zinc phosphodiesterase ELAC protein 2	PSMC3	26S proteasome regulatory subunit 6A
ENO1	Alpha-enolase	PTRH2	Peptidyl-tRNA hydrolase 2, mitochondrial
FEN1	Flap endonuclease 1	RAB5C	Ras-related protein Rab-5C
G6PD	Glucose-6-phosphate 1-dehydrogenase	RAN	GTP-binding nuclear protein Ran
GALNT2	Polypeptide N-acetylgalactosaminyltransferase 2	RTN4	Reticulon-4
GANAB	Neutral alpha-glucosidase AB	SERPINH1	Serpin H1; Binds specifically to collagen
GAPDH	Glyceraldehyde-3-phosphate dehydrogenase	SFPQ	Splicing factor, proline- and glutamine-rich
GLUD1	Glutamate dehydrogenase 1, mitochondrial	SHMT2	Serine hydroxymethyltransferase, mitochondrial
GPI	Glucose-6-phosphate isomerase	SMARCC2	SWI/SNF complex subunit SMARCC2
GSTP1	Glutathione S-transferase P	SMC2	Structural maintenance of chromosomes protein 2
HECTD1	E3 ubiquitin-protein ligase HECTD1	TAGLN2	Transgelin-2; Transgelin 2
HEXIM1	Protein HEXIM1	TFRC	Transferrin receptor protein 1
HIP1R	Huntingtin-interacting protein 1-related protein	TKT	Transketolase
HIST2H3A	Histone H3.2	TPI1	Triosephosphate isomerase 1
HIST2H3C	Histone cluster 2 H3 family member c	TRAP1	Heat shock protein 75 kDa, mitochondrial
HIST2H3D	Histone cluster 2 H3 family member d	TXNDC5	Thioredoxin domain-containing protein 5
HLA-A	HLA class I histocompatibility antigen, A-3 alpha chain	UBA1	Ubiquitin-like modifier-activating enzyme 1
HSP90AA1	Heat shock protein HSP 90-alpha	UCHL1	Ubiquitin carboxyl-terminal hydrolase isozyme L1
HSP90AB1	Heat shock protein HSP 90-beta	UQCRC2	Cytochrome b-c1 complex subunit 2, mitochondrial
HSP90B1	Endoplasmin (HSP90B1)	VARS	Valine--tRNA ligase
HSPD1	60 kDa heat shock protein, mitochondrial	VCP	Transitional endoplasmic reticulum ATPase
HYOU1	Hypoxia up-regulated protein 1	VDAC1	Voltage-dependent anion-selective channel protein 1

Appendix Table 4.3: Colocalization analysis of selected SILAC potential pCDP-DB interactors. B18 cells are overexpressing BACE1 and WT7 cells are overexpressing APP. Summarized data shows the Pearson Correlation Coefficient (PCC). *p<0.05, ** is p<0.01 and *** is p<0.001.

Cell Line	Number of Cells Analyzed	Antibodies Hsp90 AA1	Treatment pCDP	PCC (average)	Stdev	T-test (P-Value)
	7		No	0.35	0.0705	0.000139
B18	8		Yes	0.63	0.1604	
	9		No	0.136	0.0174	0.0269
WT7	6		Yes	0.207	0.0593	
		Hsp90AB1				
B18	5		No	0.541	0.0171	0.0309
	6		Yes	0.5114	0.0532	
WT7	6		No	0.7236	0.0582	0.0023
	12		Yes	0.603	0.0268	
		Eno1				
B18	10		No	0.467	0.0259	0.798
	8		Yes	0.392	0.0282	
WT7	10		No	0.569	0.0511	0.921
	10		Yes	0.591	0.0403	
		Moesin				
B18	10		No	0.433	0.0585	0.194
	6		Yes	0.396	0.062	
WT7	4		No	0.157	0.0316	0.108
	4		Yes	0.216	0.0211	
		PPIA				
B18	7		No	0.435	0.0536	0.662
	4		Yes	0.475	0.062	
WT7	4		No	0.283	0.0226	0.0785
	4		Yes	0.358	0.0375	
		PDIA4				
B18	8		No	0.56	0.076	0.266
	6		Yes	0.501	0.118	
WT7	4		No	0.255	0.0481	0.962
	4		Yes	0.255	0.0261	
		PDIA3				
B18	11		No	0.328	0.0298	0.798
	11		Yes	0.333	0.0198	
WT7	11		No	0.601	0.0233	0.00165
	10		Yes	0.715	0.0446	
		Annexin A1				
B18	8		No	0.421	0.0395	0.378
	6		Yes	0.391	0.0274	

Appendix Table 4.4: Investigating the colocalization of known APP interactor proteins found in the literature with pCDP-DB treatment. B18 cells are overexpressing BACE1 and WT7 cells are overexpressing APP. Summarized data shows the Pearson Correlation Coefficient (PCC). *p<0.05, ** is p<0.01 and *** is p<0.001.

Cell Line	Number of Cells Analyzed:	Antibodies EEA1	Treatment pCDP	PCC (average)	Stdev	T-test (P-Value)
B18	8		No	0.546	0.0678	0.00449
	15		Yes	0.453	0.0505	
WT7	7		No	0.429	0.135	0.00127
	9		Yes	0.205	0.0436	
		TIP60				
B18	16		No	0.239	0.0448	0.000303
	21		Yes	0.153	0.0193	
		JIP1				
B18	18		No	0.237	0.052	0.935
	12		Yes	0.24	0.0287	
		Fe65				
B18	12		No	0.182	0.0234	0.379
	11		Yes	0.169	0.0286753	
		RanBP9				
B18	13		No	0.175	0.0468	0.729
	19		Yes	0.181	0.0193	
		Mint1				
B18	11		No	0.317	0.0148	0.054
	10		Yes	0.251	0.0317	
WT7	10		No	0.457	0.0276	0.851
	10		Yes	0.456	0.0336	
B18	10	**APP Y188**	No	0.641	0.0324	0.0743
APP Y188	11	**Bace1 (alphaCT)**	Yes	0.684	0.0409	
B18	6	**APP C1/6.1**	No	0.48	0.037	0.737
APP C1/6.1	6	**Bace1**	Yes	0.473	0.0581	